SYNTHESIS AND INVESTIGATION OF ZIRCONIUM METAL-ORGANIC FRAMEWORKS FOR ADSORPTION APPLICATION

Thesis

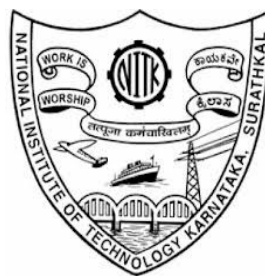Submitted in partial fulfilment of the requirements for the degree of

DOCTOR OF PHILOSOPHY

by

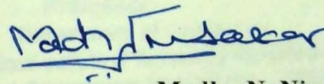## MADHU N. NIMBALKAR

(Reg. No.155037CY15P01)

DEPARTMENT OF CHEMISTRY

NATIONAL INSTITUTE OF TECHNOLOGY KARNATAKA,

SURATHKAL, MANGALORE – 575025

August, 2022

DECLARATION

I hereby *declare* that the Research Thesis entitled "**Synthesis and Investigation of Zirconium Metal-organic frameworks for Adsorption Application**" which is being submitted to the **National Institute of Technology Karnataka, Surathkal** in partial fulfilment of the requirements for the award of the Degree of **Doctor of Philosophy** in **Chemistry** is a *bonafide report of the research work carried out by me*. The material contained in this Research Thesis has not been submitted to any University or Institution for the award of any degree.

Madhu N. Nimbalkar
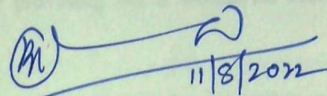
Reg. No. 155037CY15P01
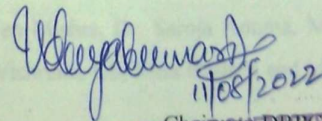
Department of Chemistry

Place: NITK-Surathkal

Date: 11\08\2022

CERTIFICATE

This is to *certify* that the Research Thesis entitled "**Synthesis and Investigation of Zirconium Metal-organic frameworks for Adsorption Application**" submitted by **Madhu N. Nimbalkar (Register Number: 155037CY15P01)** as the record of the research work carried out by him, is *accepted as the Research Thesis submission* in partial fulfilment of the requirements for the award of degree of **Doctor of Philosophy.**

11/8/2022

Dr. B. RAMACHANDRA BHAT
Professor
Department of Chemistry
National Institute of Technology Karnataka
Surathkal, Srinivasnagar, MANGALORE - 575 025

Research Guide

11/08/2022

HEAD, DEPARTMENT OF CHEMISTRY
National Institute of Technology Karnataka
Surathkal, Srinivasnagar
MANGALORE- 575 025, D.K.

Chairman DRPC

ACKNOWLEDGEMENT

ABSTRACT

The thesis titled **"Synthesis and Investigation of Zirconium Metal-Organic Frameworks for adsorption Application"** comprehend the work on synthesis of functionalised zirconium based UiO-66 type metal-organic framework for the adsorptive removal of contaminants from water. A green method for the synthesis of stable, free carboxylic functionalised MOF is developed. The promising outcomes of the strategies employed are confirmed by the characterization of the MOF. The MOF is utilised in the simultaneous adsorption of methylene blue dye and heavy metal ions (Lead and Cadmium) from aqueous solution. Under optimised condition the removal capacity of the MOF for cadmium, lead and methylene blue are found to be 37 mg g^{-1}, 100 mg g^{-1} and 169 mg g^{-1} respectively. The maximum adsorption of MB dye among the other adsorbates is due to strong ionic interaction between MOF adsorbent and cationic MB dye. Lead adsorbs fairly better than cadmium because of its smaller size and the interaction with free carboxylic group present in the MOF. A fluorescence active zirconium based MOF synthesised from mixed ligand strategy displayed sensitive detection ability for p-nitrophenol along with rapid adsorption. In-house synthesised fluorescence active trifunctional ligand namely H$_3$ntb (4,4',4''-Nitrilotrisbenzoic acid) and BDC (1,4-Benzenedicarboxylic acid) are used in various proportions to synthesize MOF. PXRD studies affirmed the formation of crystalline phase and TGA revealed the effect of structural defects on framework integrity. The trifunctional ligand imparted the defects in the framework due to its inability in forming continuous array for crystalline network. As a result, increase in the proportion of trifunctional ligand during synthesis induced more defects in the framework and lesser stability to the MOF. The fluorescence active MOF is able to detect p-nitrophenol at low concentration and obeys Langmuir isotherm for adsorption with maximum adsorption capacity of 62 mg g^{-1}. The work presented in this thesis illustrate the efficacious synthesis and application of zirconium metal-organic frameworks for adsorptive removal of contaminants from water.

Key words: Metal-organic frameworks, Multi solute adsorption, Green synthesis, Fluorescence active MOF.

TABLE OF CONTENTS

CHAPTER-3

SIMULTANEOUS ADSORPTION OF METHYLENE BLUE AND HEAVY METALS FROM WATER USING Zr-MOF HAVING FREE CARBOXYLIC GROUP

CHAPTER-4

SYNTHESIS AND APPLICATION OF Zr-MOF FOR SIMULTANEOUS DETECTION AND RAPID ADSORPTION OF p-NITROPHENOL FROM WATER

LIST OF FIGURES

LIST OF TABLES

LIST OF ABBREVIATIONS

3D : Three Dimensional

ABDC : 2-aminobenzene-1,4-dicarboxylic acid

AWWA : American Water Works Association

BDC : 1,4-benzendicarboxylic acid, Terephthalic acid

BET : Brunauer-Emmett-Teller

BETC : 1,2,4,5-Benzene-tetra-carboxylic acid

cdc : trans-1,4-Cyclohexanedicarboxylic acid:

CN : Coordination Number

Cnuc : Critical concentration of nucleation

Csat : Concentration at Saturation

DMF : Dimethyl formamide

DMSO : Dimethyl sulfoxide

EDTA : Ethylenediaminetetraacetic acid

EDX : Energy-dispersive X-ray spectroscopy

ERRSQ : Sum of the squares of the errors

FCC : Face-centred cubic

FTIR : Fourier Transform Infrared Spectroscopy

H3ntb : 4,4',4''-Nitrilotrisbenzoic acid

HKSUT : Hong Kong University of Science and Technology

HPLC : High Pressure Liquid Chromatography

HSAB : hard and soft acids and bases

IPD : Intraparticle diffusion model

MB : Methylene Blue

MOF : Metal-organic framework

MPSD : Marquardt's percent standard deviation

N-donor : Nitrogen Donor

PCN : Porous Coordination Network

PXRD : Powder X-ray Diffraction

RMSE : residual root mean square error

SALE : Solvent Assisted Ligand Exchange

SBU   : Secondary Building Unit

SEM   : Scanning Electron Microscopy

SLI   : Sequential Linker Installation

TGA   : Thermogravimetric analysis

TLC   : Thin layer chromatography

UiO-66 : Universitetet i Oslo

USEPA : United States Environmental Protection Agency

UV-vis : Ultra Violet -Visible Spectroscopy

WHO   : World Health Organization

XPS   : X-ray Photoelectron Spectroscopy

XRD   : X-ray Diffraction

CHAPTER-1

INTRODUCTION

Abstract: This chapter provides brief introduction about metal-organic frameworks. Significance of zirconium MOF is highlighted and principles of adsorption relevance to MOFs are outlined.

1.1 INTRODUCTION TO POROUS MATERIALS

"Nature abhors vacuum" stated by Aristotle believing every space needs to be filled with something and creating a vacuum space is highly unfavourable. Likewise, in connection to the material science, synthetically creating a void at molecular level was seems to be inexpedient for scientific community until 19th century, although porous materials are known from ancient times, as Hindus and Egyptians used charcoal for water purification and medicinal purposes.

The occurrence of porosity in natural structures indicates the importance of porous architecture in the biosphere. Furthermore, porous nature of the natural substance is sometimes a result of optimized reciprocation under constrained conditions mainly to increase the surface area of the total mass. For example, consider the coconut sprout (Figure 1), the germination of the coconut seed occurs up to 3 to 4 months after detaching from the coconut plant.

Figure 1.1. Porous coconut sprout covering the inner core

During this period, the seed is completely isolated from the external sources. Once seed starts to grow, it produces highly porous spherical sponge-like cotyledons. This covers

the whole inner volume and takes nutrients from the inner core of the coconut and grows. Similarly, porous materials are integral part of many applications in the modern field of technology, from energy to the environment and electronics (like in porous materials with low k dielectrics and heat sinks). In these applications, the porous materials are engineered to the desired requirement to deliver specific performances. This tailoring of the pore structures is progressing tremendously and created a vast array of highly structured advanced porous materials.
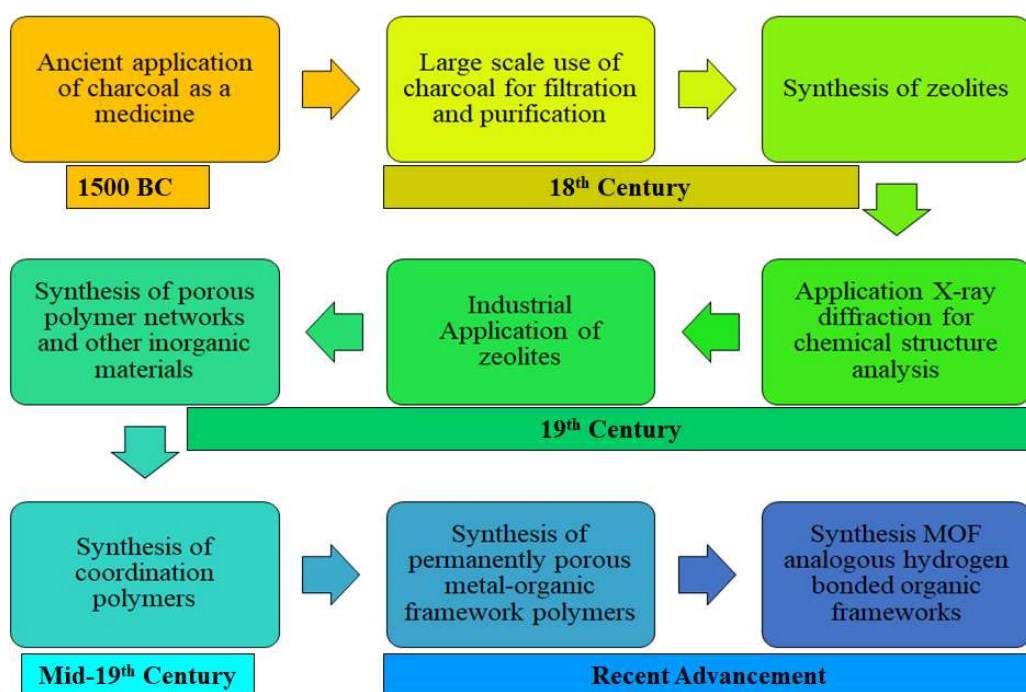
Figure 1.2. Advancement of porous materials

Porosity is the main criterion for material to be called as an adsorbent and these materials have occupied a significant part in solid–state materials domain. The functionalization improves potential applications of porous materials which made them as integral part in our day to day life. Hence, it is of great interest to investigate the advanced porous materials for their ubiquity and significance in today's world. Activated carbon, zeolites and activated alumina are few examples of porous materials used traditionally. The history of charcoal outspread from ancient times to the recent and played vital role as porous adsorbent till World War I (Figure 1.2). Activated

carbon materials usually prepared by pyrolysis of carbon materials, have high surface area and displayed high adsorption capacities. But main drawback of these materials are, it does not possess ordered structure and difficult to introduce functionality in the pore structure. Despite this disadvantage activated carbon materials are extensively used in separation, recovery process and water purification. Apart from these antique carbonaceous materials, porous materials segment witnessed another class of niche family called zeolites. Zeolites are another sort of porous materials which have ordered framework structure made by inorganic backbone. Zeolites are most important and largely used group of porous materials. With the discovery of X-rays for structural determination, research over synthesis and application of natural and synthetic zeolites was escalated to another level and zeolites has become an integral part of many chemical processes from adsorption to catalysis. The main use of zeolites is in petroleum refinement, catalysis and ion exchange applications. The advantage of zeolites over activated carbons lies in their ionic nature and accessible periodic channels and cavities. Even with these superiority zeolites applications are limited because of their atomic composition, restricted pore size in addition to limited functionality. As the advancement of technology progressed researchers envisaged the building of nano porous materials and manipulating the pore structure with the augmentation of functionality. This resulted discovery of microporous structures made of coordination complexes or coordination polymers called metal-organic frameworks (MOF) with well-known geometrical forms.

From last few decades there has been exponential development in organic–inorganic hybrid materials such as metal-organic framework materials. These materials are formed by coordination network of organic ligands having repeating units and extending in two or three dimension, generating permanent voids with stable framework structure. These new class of highly crystalline porous solids, metal-organic frameworks (MOFs) demonstrated superior performances in adsorptive separation and purification. Compared to other coordination polymers, MOFs are crystalline in nature while others are amorphous. This crystallinity even after removing solvent from pore structure made it easier to understand and study the framework to know the exact position of each atom and connection between them. This will help in designing new

3

kind of MOFs with enhanced properties. Tuning the pore size and incorporation of functional groups to obtain desired properties in the framework are the extra flexibilities of MOFs when compared to conventional porous materials such as activated carbon and zeolites.
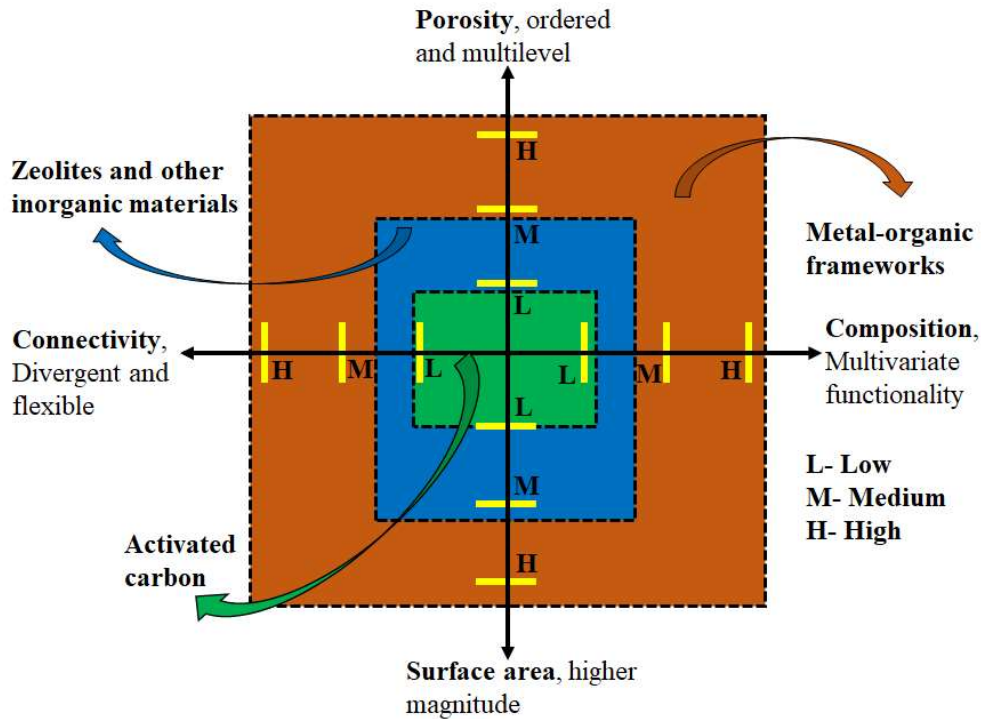
Figure 1.3. Hierarchal superiority of MOFs over conventional porous materials

There are four main important parameters which differentiate MOFs from conventional porous materials and place them in hierarchal superiority (Figure 3).

1. Composition; MOFs have multivariate functionality
2. Porosity; They have highly ordered porous structure and can possess multilevel porosity
3. Connectivity; MOFs are made of flexible and divergent connections
4. Surface area; MOFs displayed highest surface area as compared to traditional porous materials.

Furthermore, highly crystalline nature and mild synthesis techniques along with superior surface area of MOFs made them as prime member of porous adsorbents.

4

Zirconium-based metal-organic frameworks considered to be most attracted MOFs to scientific community due to their highly stable framework and versatile application areas. High charge on zirconium and its affinity towards oxygen donor ligands brings excellent chemical and mechanical stability to the framework (Kim and Cohen 2012). UiO-66 is one of the most researched zirconium metal-organic frameworks since its first synthesis, mainly due to its extraordinary stability towards moisture (Cavaka et al. 2008).

1.2 MOFs BACKGROUND

In 1990s Hoskins' and Robson's proposed new design principle for constructing polymeric network structure containing tetrahedral and octahedral metal centre with organic ligands as molecular rods to join them forming molecular framework as represented in the figure 1.4. Initially it was envisioned to design the framework to produce larger pores by using sufficiently rigid ligand in the structure and the functionalization of ligand molecule to intensify the properties of MOF such as catalytic activities, molecular sieving, thermal and mechanical stabilities. When these metal centres are constructed even by smaller links, they are capable of producing array of voids of appreciable size. The structure of the framework was guided by the way metal centre were bonded to linking organic molecule. When the synthesise was meticulously designed with metal centres and rod like ligands, which resulted in spontaneous formation of polymeric framework as that of cross linked polymers. But presence of order structure disparate it from cross linked polymers making them acquiescent for X-ray crystallographic studies, which will be used explicitly to understand and to control the framework domain. This ordered nature of MOF resembles the features of zeolites, which have enormous interest due to their application in catalyst and as molecular sieves. But MOFs offers more flexibility in designing bigger cavities and incorporating numerous and diversified functionalization of framework over cross linked polymers or zeolites. It was appeared that these infinite molecular framework structure have promising properties and suitable functionalization in the framework could enhance the features for versatile applications (Hoskins and Robson 1989). During the initial stages, rod like ligands used for the

construction of MOFs are mainly using N-donor coordination chemistry such as cyanide and Aromatic-N ligands. 4,4-bipyridine and its derivatives served as best suitable candidates by possessing monodentate nitrogen atoms at the opposite sides of the molecules coordinating similar as that of cyanide ion. Variety of MOFs structure were synthesised by regulating various factors such as metal ligand ratio, counter ions and coordination geometry of the metal ions. 4,4-bipyridine molecule is being a liner ligand made it simple to determine the MOFs topology because it's now depends only on coordination geometry of the metal ion.

Despite the possibility of designing and synthesizing these infinite molecular structures attaining permanent porosity in the framework structure was barely achieved. This is because flexibility of metal nitrogen bond made them to lose their crystallinity once the solvent was removed. Prerequisite for the presence of counter ions caused another problem for developing robust MOFs for factual applications. These limitations of N-donor ligands have made researcher to look for more versatile ligands for the construction of MOFs. During the mid-1990s polytopic carboxylic based ligands were explored and employed in developing resilient MOFs candidates.
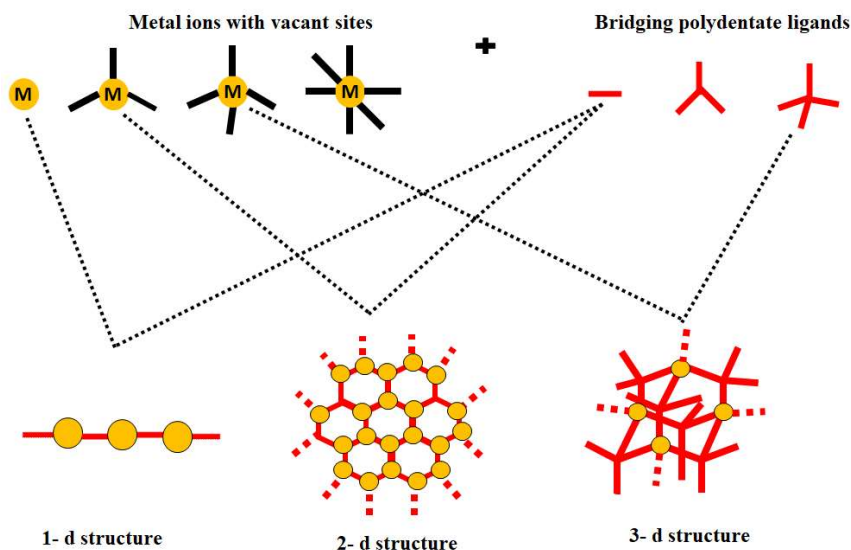
Figure 1.4. Building blocks for constructing coordination polymers

A remarkable milestone was achieved in 1998 when Yagi and co-workers published first permanently porous metal-organic framework MOF-2 (Figure 1.5, a-b). This MOF was constructed by using a dicarboxylic ligand Terephthalic acid and Zinc metal ion. Terephthalic acid being linear ditopic ligand and its carboxylic acid group coordinates bis-monodentate fashion to two square pyramidal Zn^{2+} ions forming 4-connected dinuclear metal-carboxylate cluster (square paddle wheel structure). Initially the structured formed was two dimensional but each layer was held together by hydrogen bonds formed between aqua ligands attached to metal ion at axial position of one layer and carboxylate oxygen of the adjacent layer. The structure was stable even after removing water molecules because of the formation of bonds between open metal atom sites and carboxylate oxygen of neighbouring layer. This substantial progress in synthesizing stable, permanently porous MOFs has commenced new era especially for carboxylate based linkers in developing robust and tailor made materials. These clusters formed from carboxylate and metal centres has intrigued MOFs scientific community to amplify the research to understand the various combination of metal nodes and linker ligands for constructing 3D frameworks. It also understood that the uncoordinated open metal sites can be utilised for diverse applications like catalytic activities and gas storage.
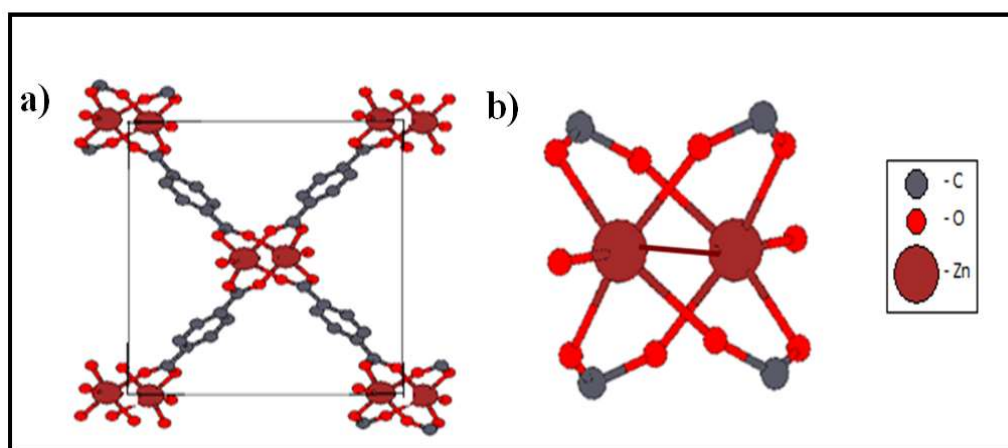
Figure 1.5. (a) Unit cell of MOF-2 viewed from 100 projections and (b) paddle wheel building unit of the MOF-2 [Hydrogen atoms are not shown for the sake of clarity, images created using. cif file of MOF-2 and Topospro program.]
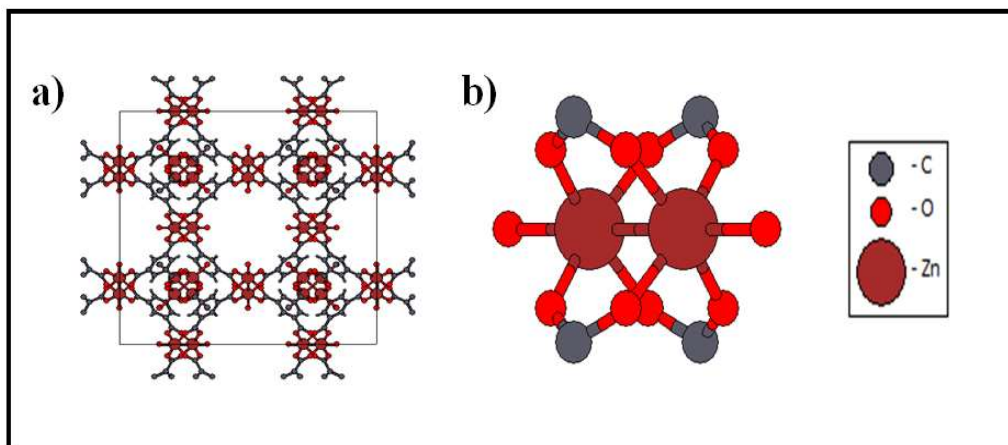
Figure 1.6. (a) Unit cell of HKSUT viewed from 001 projections. and (b) SBU of HKSUT -1 MOF [Hydrogen atoms are not shown for the sake of clarity, images created using. cif file of HKSUT-1 and Topospro program.]

Based on polytopic carboxylate and metal-carboxylate cluster two new prime MOFs were reported in 1999. One of them was synthesised by using square paddle wheel copper-oxygen clusters formed from trimesic acid and named as HKUST-1(Chui et al. 1990). The BET surface area of this MOF was 692.2 m^2 g^{-1} and whose pore size was in par with zeolites. As in the case of MOF-2, here too the aqua ligand situated at the axial position can be removed on heating to have open metal site or replaced by other ligands without compromising on framework structure.

The other metal organic framework MOF-5 (Li et al. 1999), was synthesised using zinc and Terephthalic acid forming basic zinc acetate cluster for constructing 3d framework and become the archetypical MOF having open cubic-like network topology (Figure 1.7.). Even though metal-carboxylate cluster based MOFs showed permanent porosity, their unstable nature towards moisture snagged their practical application interest. Chemical and thermal stability are the two main properties which count the superiority of any advanced materials over their counterparts. The fragile nature of MOF on exposing to moisture depends on ligand metal bonds strength. Transition metal ions

with d^{10} electronic configuration possess no ligand field energy hence its ligand field environment controlled only by steric aspects.
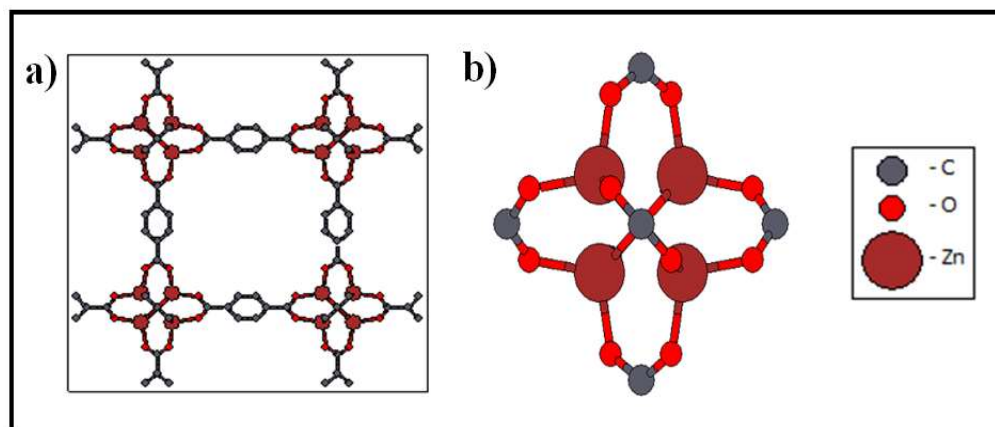
Figure 1.7. (a) Unit cell of MOF-5 viewed from 001 Projection and (b) SBU of MOF-5 [Hydrogen atoms are not shown for the sake of clarity, images created using. cif file of MOF-5 and Topospro program.]

These features make the ligand exchangeability easy, leading to framework collapse. But this kind of lability of ligand-metal bond helps in the formation of crystalline framework allowing to synthesise single crystals for precise determination structure from single crystal XRD. Regardless how big crystals are formed; the easy exchangeability of the ligands makes water molecule to displace carboxylate ligands leading to structure disintegration. Despite the high bond strength, if ligand exchange barrier is low, MOFs are susceptible to decompose. Hence to increase the stability, metal ion with high valance are investigated. With equal coordination environment, metal having higher charge decreases the ligand exchangeability by escalating electrostatic interaction between ligand and metal ions. The concept of metal-ligand stability is also explained by HSAB principle. Low-oxidation state soft metal ions Zn^{2+} forms less stable bonds with hard base like carboxylate ions. Whereas highly charged smaller hard ions like Cr^{3+} and Zr^{4+} makes strong bonds. In 2009 Cavaka and co-workers synthesised a highly water and thermal stable hexanuclear zirconium based metal organic framework UiO-66, which possesses 12-connected Zr_6O_8 SBU (Secondary building unit) (Figure 1.8. a & b).

9
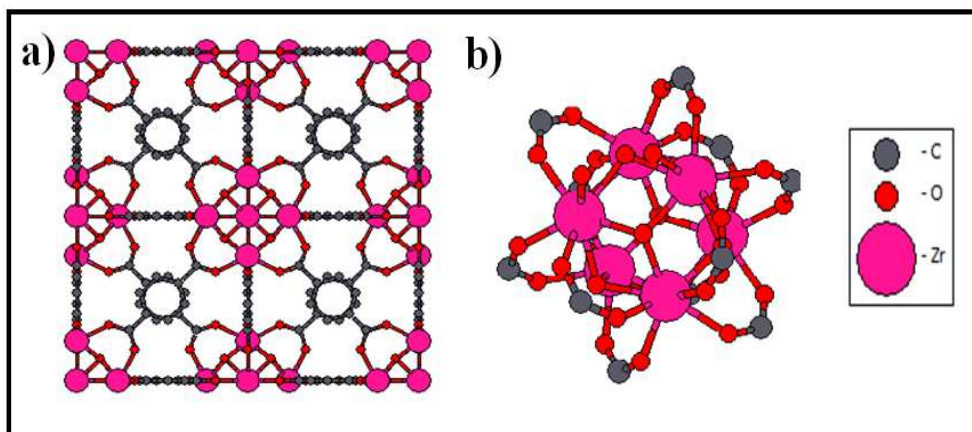
Figure 1.8. (a) Unit cell of Uio-66 and (b) SBU of Uio-66 [Hydrogen atoms are not shown for the sake of clarity, images created using. cif file of UiO-66 and Topospro program.]

1.2.1 Zirconium based MOFs

Zirconium is the 18th most abundant element available on earth crust, more abundant than copper and zinc (Figure 1.9.). Zirconium silicates has been known to mankind since long time as gem stones, in fact uncoloured specimens looks like diamonds. However, in the modern day major buyer of zirconium metal are nuclear industries. Because of resistant to corrosion at high temperature and being transparent to neutrons, zirconium-tin alloy, Zircaloy is used as cladding for uranium oxide fuel. Interestingly, both of these major materials used in nuclear industry, zirconium and uranium are discovered by Martin Heinrich Klaproth in the same year of 1789.

Apart from its major use in nuclear power stations as an alloy, zirconium finds its application in corrosion resistance coatings, production of strong ceramics and pigment industry. Being a fourth group element, it interacts strongly with oxygen, forming rigid bonds. This is in agreement with HSAB concept explained earlier.
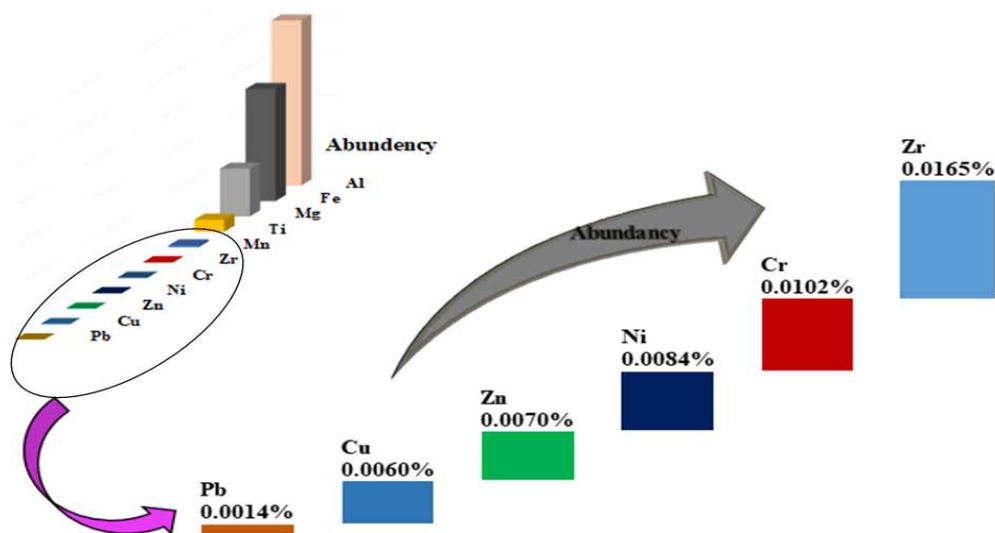
Figure 1.9. Abundance of zirconium metal available on the earth crust over other industrially important metals

Moreover, zirconium based materials has another excellent advantage to become the prime candidate as an adsorbent for water purification process, because of its biocompatibility. Zirconium has no known role in biological toxicity, hence used in surgical implants and prosthetic devices. Since its non-toxicity, environmentally amiable and abundancy, the use of zirconium in the future is continue to grow. After the first report of UiO-66 MOF, immense research has been going on in the area of development and application of this highly stable MOF (Figure 1.10).

The geometry of two-, three-, four-, and six-coordinated metal complexes are well known. In these metal complexes, the structure depends mainly on size and charge of the central metal ion. Large size and high charge of the metal ion and smaller size of the ligands, favours high coordination number. In case of the larger size ligands, highly charged metal cations influences the polarizability of the ligand and makes overlap of the electron cloud their by increasing the covalent character of the bond, resulting stability of the complex. When chemically identical ligands approaches, the central metal ions choose a particular coordination polyhedron for bonding.
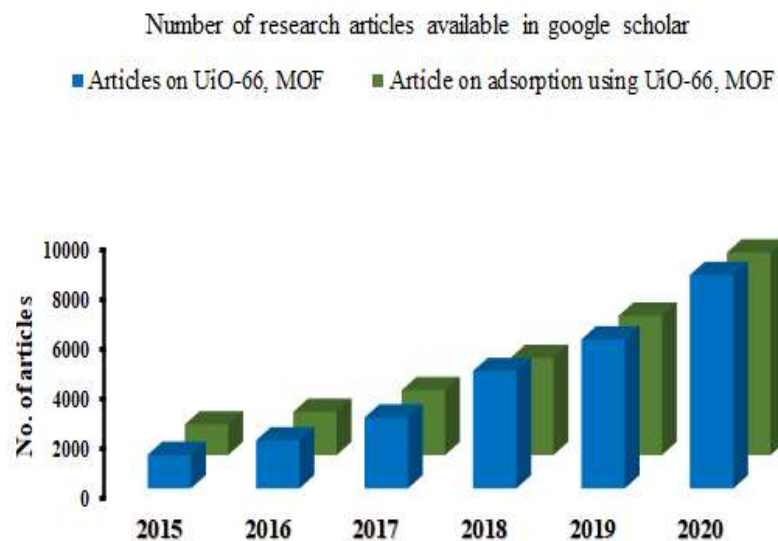
Figure 1.10. Number of research articles of UiO-66 MOF, available on google scholar as of 2021

Zirconium (Zr^{4+}) uses sp^3d^4 hybridisation for eight coordination number complex. For eight coordination number there are four possible polyhedron arrangement are possible (as given in the Table 1. 1).

Table 1.1. Coordination number and their polyhedron

CN	Polyhedron	CN	Polyhedron
3	equilateral triangle	8	dodecahedron
4	tetrahedron square		square antiprism bicapped trigonal prism cube
5	trigonal bipyramid	9	tricapped trigonal prism monocapped square antiprism
6	octahedron trigonal prism	10	bicapped square antiprism
7	monocapped octahedron monocapped trigonal prism pentagonal bipyramid	12	icosahedron cuboctahedron
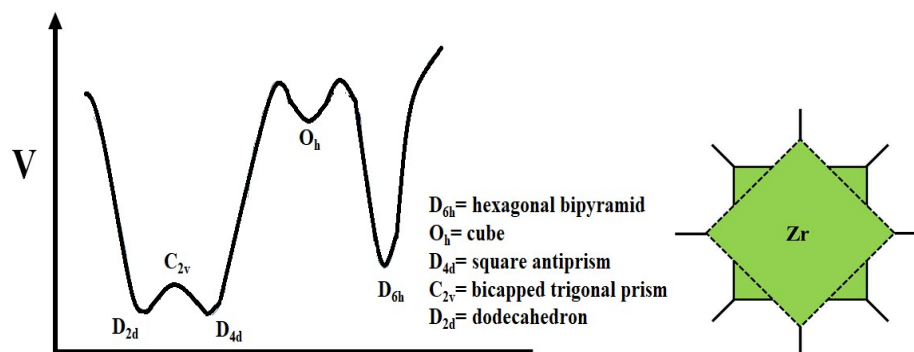
Figure 1.11. Representation of number of possible polyhedral for eight coordination related to its energy of formation. (Green) Square antiprism structure of the eight coordinated zirconium
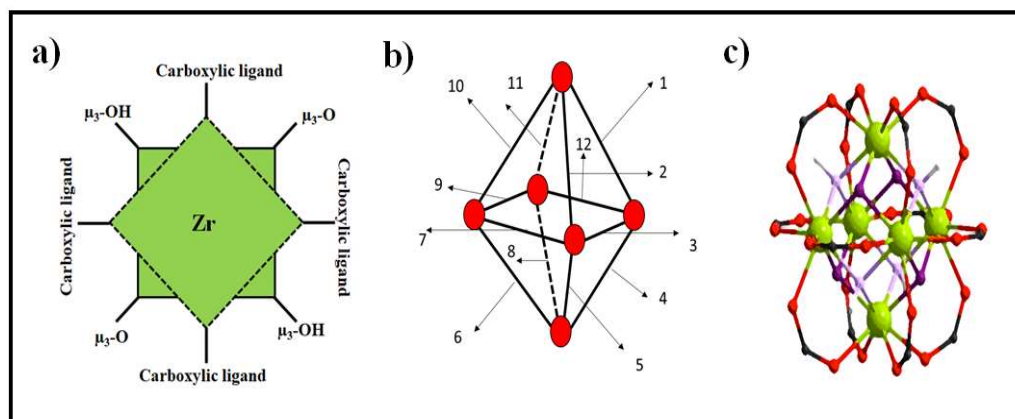
Figure 1.12. (a) Square antiprism arrangement of zirconium, , (b) Representation of vertex as bonding directing points in UiO-66 zirconium octahedron, (c) Zirconium octahedron structure in UiO-66

A plot of potential energy verses various possible geometric forms of eight-coordinated shows that only the square antiprism formation has the lowest energy (Figure 1.11.). Zirconium forms the square antiprismatic structure to form the bonding with oxygen ligands. One of the square face of antiprismatic structure is connected by oxygen atoms of the carboxylate ligands and the other one by oxygen atoms of the μ_3-O and μ_3-OH groups.

13

This leads to the formation of octahedral $Zr_6O_4(OH)_4(CO_2)_{12}$ cluster which is the inorganic brick for UiO-66 structure. This octahedral cluster act as nodes and directs the crystal grow from its vertex resulting a FCC crystalline framework (Figure 1.12.).

1.3 SYNTHESIS OF MOFS

As the name suggests, MOFs are made of two important components, metal centre and organic linkers. Transition metal ions and cluster act as nodes connecting multi ligands together in constructing MOF structures. These metal centre and ligands are together called as secondary building units (SBUs) (Eddaoudi et al. 2001). These SBUs helps to visualize MOF structures in terms of simplified geometric schemes. Figure 1.13. shows schemes of metal ions or clusters as connectors and ligands as linkers and figure 1.14 few of the organic ligands used in the design of MOF structures (Kitagawa et al. 2004).
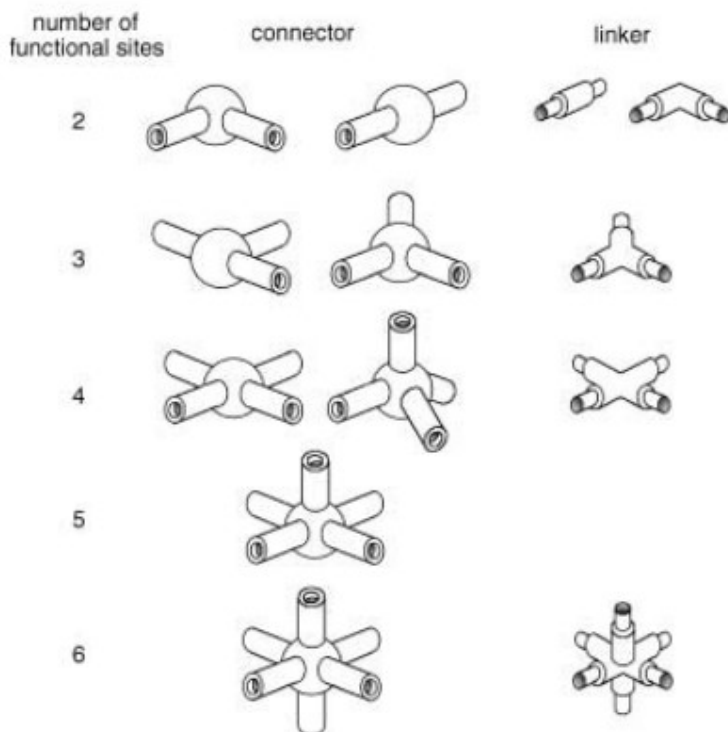
Fig 1.13. Schematic representation of metal ions or clusters as connectors and ligands as linkers (Kitagawa et al. 2004).

14

(a) inorganic ligands

Halides (F, Cl, Br, and I)   Cyanometallate ([M(CN)$_x$]$^{n+}$)

CN$^-$ SCN$^-$

(b) neutral organic ligands

(c) anionic organic ligands

(d) cationic organic ligands
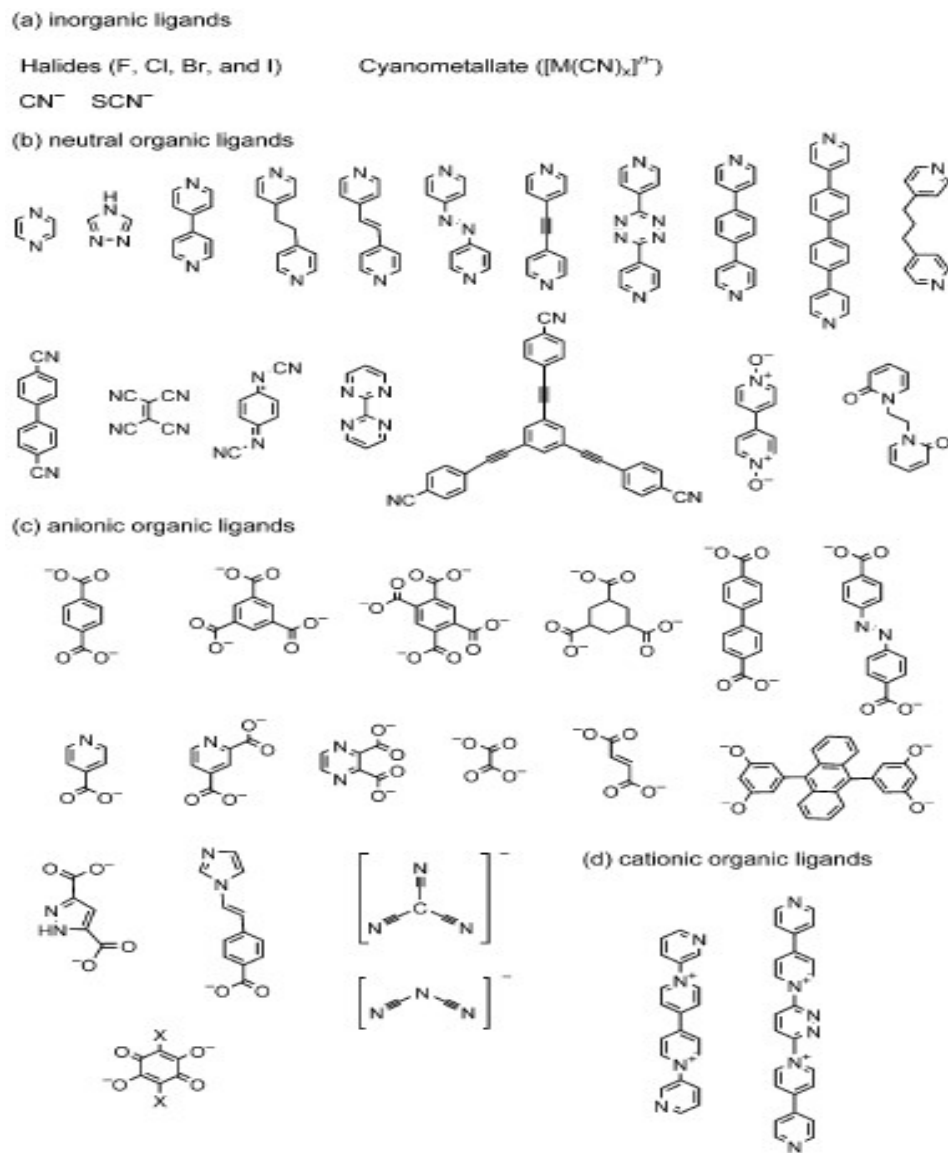
Figure 1.14. The organic ligands used for constructing MOFs (Kitagawa et al. 2004).

MOFs are formed by the assemblage of organic and inorganic functional building units. This results in greatly diversified structural formation and applications areas of MOFs. Due to the background of the varied applications, the interdisciplinary scientific community has made numerous approaches for the synthesis of MOFs. Principles governing the crystallization process significantly influence the synthesis conditions and give command over the morphology of the crystals.

In the beginning, coordination chemists from the field of crystal engineering conceptualized the formation of MOFs in the form of molecular interactions and tried to build the porous structure from the assemblage of organic and inorganic building units. The reaction conditions were kept mild, as weak interactions between the building units are expected (Hoskins and Robson 1990). While on the other hand, researchers from zeolite-related materials background envisaged organic entities not only as structure directing agents but also as reactants having strong interactions with the inorganic units in building framework (Cheetam et al. 1999). Hence, to form strong bonds between the building units' higher temperature reaction conditions were employed. This elucidates the diverse approaches used by the researchers to synthesize the MOFs.

The reaction temperature is one of the main parameters and plays a vital role along with time in the synthesis of MOFs. It was understood that, increase in temperature helps to form –M-O-M- linkages and –M-O-M- clusters due to an entropy driven dehydration process (Forster et al. 2005 & Mahatha et al. 2008). This indicates that formation of MOFs as a function of temperature could be thermodynamically controlled. Whereas zeolites and other traditional framework materials are kinetically controlled.

A conventional electric heating instrument is used for heating the reaction mixture and the temperature range determines, whether the process is solvothermal or nonsolvothermal. The reaction conditions which take place in a closed vessel under autogenous pressure above the boiling point of the solvent are referred as solvothermal (as given in the figure 1.15.). Whereas reactions below or at the boiling point and under ambient pressure are called nonsolvothermal (Stock and Biswas 2012).
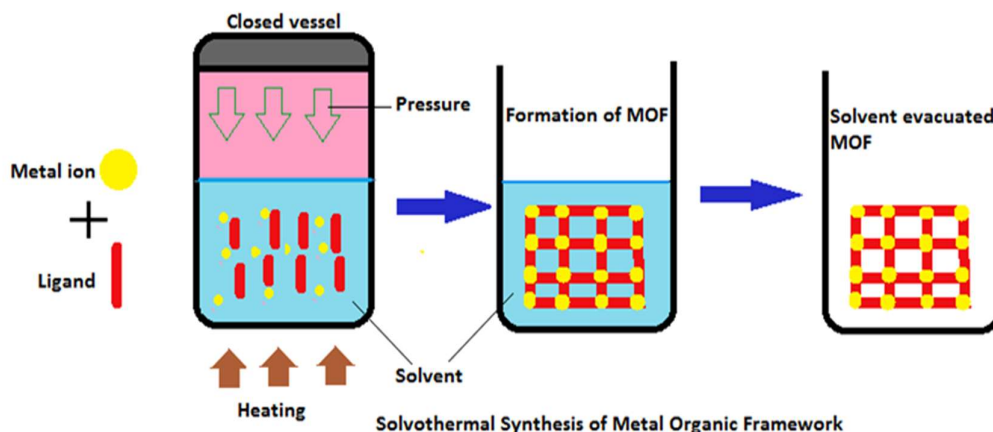
Fig 1.15. Schematic representation of solvothermal synthesis

A crystal is formed by two-step process, initially combination of reactants to nucleation and followed by the crystal growth (LaMer model) (LaMer, and Dinegar 1950). Nucleation is the process where ions or molecules come together and form a cluster. Until the critical size, the cluster is not stable and re-dissolves. When the cluster attains the minimum size (in nm range) it is thermodynamically stable and is called nucleus. This attainment of minimum size and formation of nucleus occurs only when the concentration exceeds the critical concentration of nucleation (*Cnuc*). Due this process the concentration of reactants decreases and the system reaches an equilibrium (*Csat*). The crystal growth occurs at concentration between *Csat* and *Cnuc* (Feng et al 2019) the process is depicted in the below figure 1.16.

In general crystallization process can be considered as an equilibrium reaction between dissolved organic, inorganic units and solid crystals of MOF. At constant pressure the thermodynamics of this process is described by Gibbs-Helmholtz equation.

$$\Delta G = \Delta H - T\Delta S$$
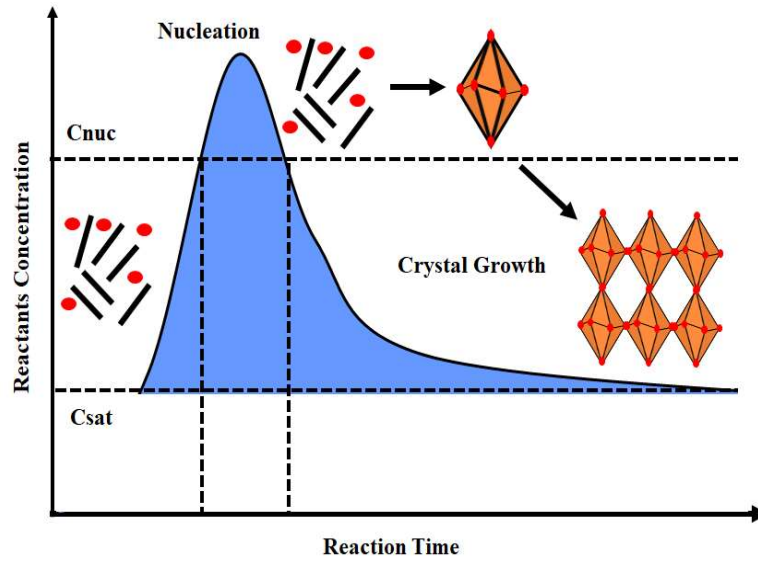
Figure 1.16. La Mers model of crystallization

The Gibbs free energy of crystallization is composed of two entities, interfacial energy and volume free energy as represented in the above figure (Figure 1.17) and equation below,

$$\Delta G = \frac{4}{3} \pi r^3 \Delta G_v + 4\pi r^2 \gamma \qquad (1.1)$$
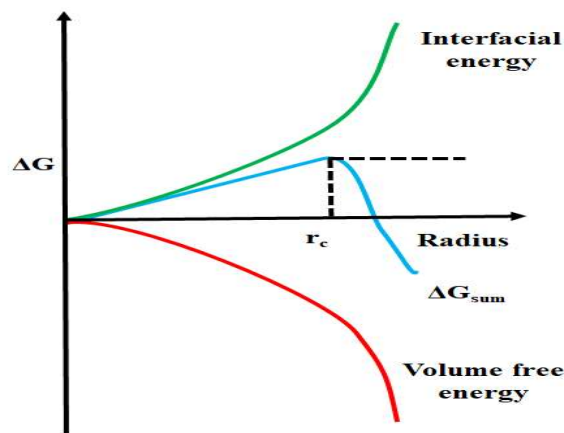
Figure 1. 17. Thermodynamics of crystallization

18

Where ΔGv is the free energy related to volume and is negative and driving force for nucleus formation. The surface free energy γ is always positive and acts against the nucleus formation. When the particle size reaches critical size r_c, ΔG decreases rapidly and the growth of the crystals becomes exergonic process.

For the successful commercialization of MOFs, it is important to find facile, inexpensive, rapid synthesis techniques. Also the desired property of the MOFs depends on its physical and chemical nature such as morphology, porosity, stability-which again depends on the way it is synthesized. In search of this, research group around the globe has investigated the application of various techniques on the synthesis of MOFs.

It is obvious that chemical reactions require energy in terms of temperature to proceed. As it was stated earlier, the synthesis of MOFs could occur in the range from room temperature to around 250 °C. Conventionally the energy in terms of temperature was given by electrical heating, such as oven, heating mantle through convection. However, the energy can also be supplied by other means like electric potential, electromagnetic radiation, and mechanical waves. Each of these techniques affect strongly on the product formation and its morphology.

Modulated synthesis is a strategy to control the formation and size of the metal-organic framework. Generally, modulators used in the synthesis will be monotopic ligands present in excess quantity and have higher solubility in the reaction media (Tsurukoa et al. 2009). During the reaction course, these modulators compete with the bridging ligands and alters the crystal growth, facilitating the framework formation. Development of green synthetic methods are the another important aspect of MOF synthesis.

Solvents used in the synthesis of MOFs also affects and regulate the coordination environment. In most cases solvent acts as structure directing agents or a medium for the crystal growth process. In case of carboxylate linkers dissolved in DMF solvent (the condition where most of zirconium MOF synthesised), it was explored that (Hausdorf

et al. 2007), DMF decomposes under acidic condition to form basic dimethylamine (Figure 1.18.), which deprotonates and then the carboxylate anion is free to attack metal centre.
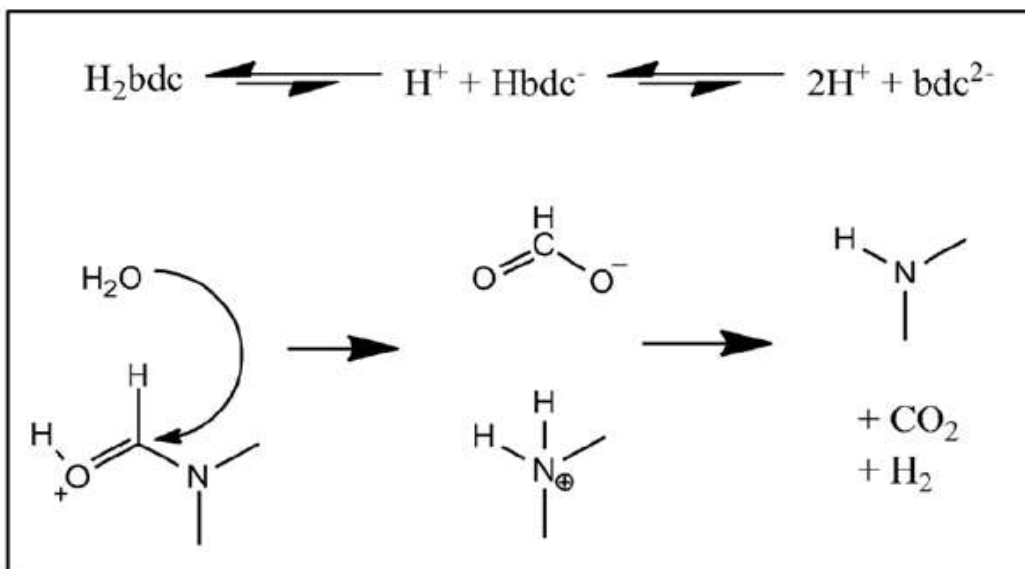
Fig 1.18. Decomposition of DMF during MOF synthesis (Hausdorf et al. 2007)

Table 1.2. Various synthesis techniques of MOF

Synthesis techniques	Principle	Outcomes
Microwave synthesis	Heating is generated by the interaction of electromagnetic waves with mobile electric charges such as polar solvent molecules, ions in solution or electrons, ions in the solid causing increased temperature, due to resistance of the solid.	Highly efficient heating due to high heating rate and homogeneous heating throughout the sample. This results in accelerated nucleation leading to smaller crystals.

20

Electrochemical synthesis	Continues introduction of metal ions through anodic dissolution to the solution containing linker molecules and a conducting salt.	Formation of concerned anions such as nitrate, perchlorate and chloride ions at industrial scale can be eliminated by avoiding the metal salt for synthesis. Products obtained by electrochemical method are lesser quality as compared to conventional solvothermal synthesis mainly due the incorporation of linker and conductive salt during crystallization.
Mechnochemical synthesis	Chemical reactions induced by mechanical force, reactions are carried out by without or with slight amount of solvent.	Environment friendly because no use of solvents and shorter period of time for synthesis.
Sonochemical synthesis	The reactions that takes place upon application of high-energy ultrasound to a reaction mixture.	Short synthesis time at ambient room temperature and higher yields.

1.4 APPLICATION OF MOFs

The construction of metal-organic framework architectures has developed enormously, so that we can first formulate the hypothesis on the structural requirements to obtain best performance for a particular application and then synthesize MOFs. Since these materials are crystalline, exact position of the atoms and their relation with the structure can be predicted to validate the hypothesis. These MOFs can be used for variety of applications. In our study we are more focused on the application of zirconium based MOFs for removing contaminants from water and its allied applications.

1.4.1 Adsorption

Adsorption can be defined as the enrichment of a species on the interface of the solid phase from a fluid phase. Transfer of one or many species from one phase to another occurs during the process of adsorption, hence it can be regarded as a phase transfer process (Figure 1.19.). Industrially adsorption is the most desired process specifically when it comes to environment-related treatment operations because of its low operation cost and low energy consumption.
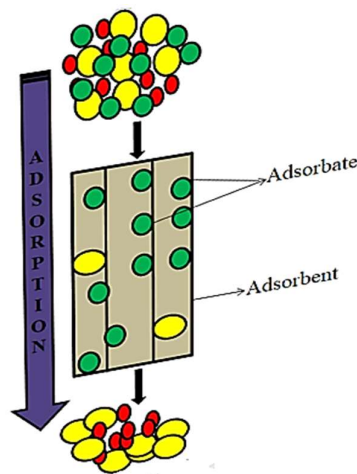
Figure 1.19. Representation of adsorption process

Many chemical, physical and biological processes take place through the adsorption phenomenon. Basically, a solid surface is comprising of active energy (binding energy) sites distributed all over the surface, which are capable to interact with solute species from the fluid phase (Figure 1.20). The electronic and spatial arrangement of the active sites helps to draw the solute particle towards themselves. The energy for the attraction depends on the local environment of the active site. Depends on the energy distribution, the surface can be energetically heterogeneous or homogeneous (Figure 1.21). The interaction between the adsorbate and adsorbent also depends on the concentration of the adsorbent. By definition the phase which provides surface for adsorption is called as adsorbent and the species which gets adsorbed is known as adsorbate. By altering the condition, the adsorption process can be reversed, known as desorption. The

characterization of absorption process is done by modelling the number of sites and their interaction ability in terms of binding energy with the adsorbed species.

The process of adsorption can be expressed chemisorption or physisorption process based on interaction ability between the adsorbate and adsorbent. Physisorption is reversible, occurs through easily breakable weak electrostatic interactions such as London forces, Dipole-diploe and Van der Waals interactions. Through physisorption multilayer formation of adsorbate over adsorbent can takes place and occurs at low temperature. In chemisorption, formation of strong chemical bond happens between adsorbate and adsorbent and once these bonding sites are over further no interaction occurs between adsorbate and adsorbent, hence only monolayer forms in chemisorption.

The adsorption process can be expressed as,

$$Surface\ concentration = \frac{\text{The amount of solute adsorbed}}{\text{The adsorbent surface area}} \qquad (1.2)$$

Since it is difficult to know exactly the surface area of the adsorbent, adsorbent mass is used in determining the surface concentration typically known as adsorbent loading.

$$Surface\ concentration = \frac{\text{The amount of solute adsorbed}}{\text{The adsorbent mass}} \qquad (1.3)$$

The dependency of the solute particles to get adsorbed on the surface of the adsorbent is needs to be evaluated and underlying theoretical basis should be described in order to practically apply the adsorption process. The study and understanding of adsorption equilibrium and adsorption kinetics are the two main steps to guide the practical utility of the adsorbent materials. It can be assumed that all the adsorbent surface will have some kind of heterogeneity because of the presence of various binding energy sites.
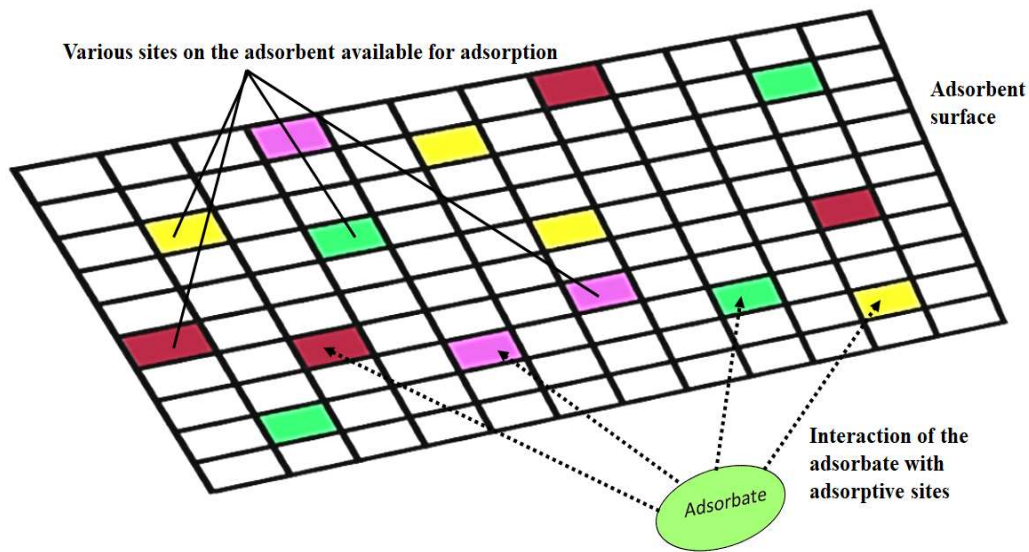
Figure 1.20. Adsorbent surface with various sites for adsorption

In the case of metal-organic frameworks the pore structure is uniform throughout the structure still it poses different types of adsorption sites for the adsorbate. Adsorption can be because of Van der Waals interaction in the narrow passage of the adsorbent, with interaction with the metal ion or with the interaction of the functional group present in the framework. Adsorption isotherms are developed on the basis of this interaction of the adsorbent and its binding energy capacity with the adsorbate molecules. The necessity of advanced porous materials will come into picture in the situation where it is supposed to remove a particular pollutant from contaminant system below statutory level. Conventional adsorbent does not process specific sites having higher binding energy so that they can remove the pollutant even in the low concentration, hence the application of conventional adsorbent is suitable in situations where pollutant concentration is high. In case of advanced porous materials such as metal-organic frameworks, possess higher surface area hence more number of absorption sites (specific functional groups) which are having higher binding energy interact strongly with the pollutant molecule even in low concentration and bring its level in the effluent to the desired level.
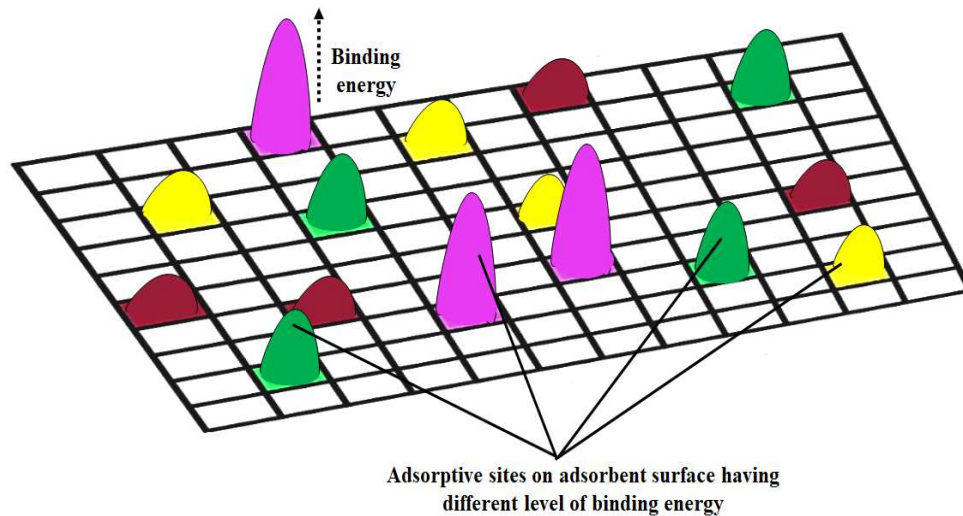
Figure 1.21. Adsorbent surface with various binding sites having different binding energies

1.4.2 Adsorption equilibrium

Consider a situation where an adsorbent having a binding site with a binding energy e_1 and with another binding site having binding energy lower than the e_1, called as e_{1-x}. When at infinite dilution it is assumed that, the adsorbate species experiences same amount of attractive energy and the chances of getting at either of the adsorption site is same. Whereas the increase in the concentration of the adsorbate in the fluid system causes adsorption to increase. If the energy of the one the site is sufficiently increased, even at infinite dilutions this specific site can bring the adsorbate species into adsorbed phase from the bulk phase (Figure 1.22). The low energy site can also do the same at higher adsorbate concentrations (Figure 1.23). From the thermodynamic point of view, a system of high concentration is having lower entropy in the bulk phase than the system with lower concentration of adsorbate. Hence, the energy required to move the adsorbate species from bulk phase to adsorbed phase is lower in the former case.

Interaction of adsorbate with adsorptive sites having higher
binding energy at lower concentration of adsorbate
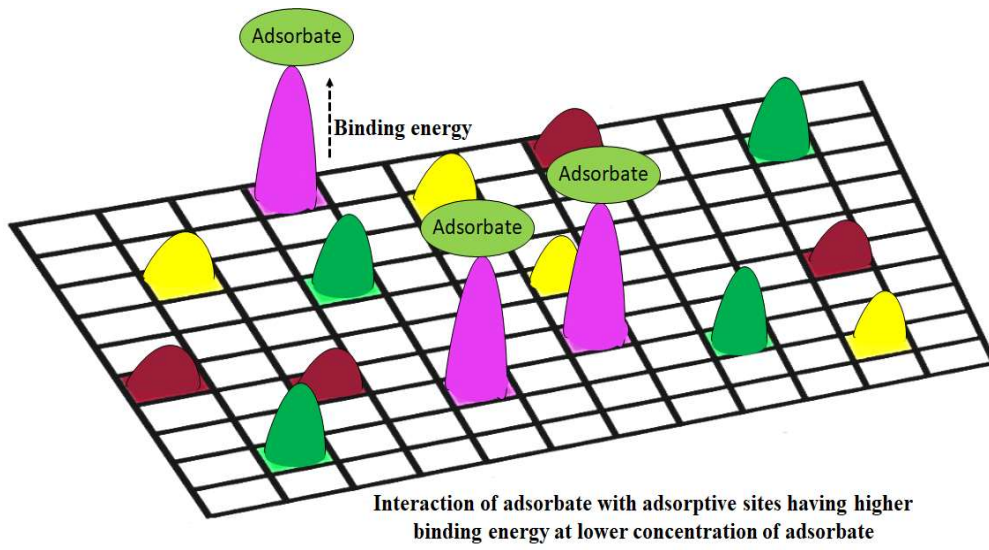
Figure 1.22. Interaction of adsorbates with binding sites present in the adsorbent at lower adsorbates concentration

Interaction of adsorbate with adsorptive sites at higher
concentration of adsorbate
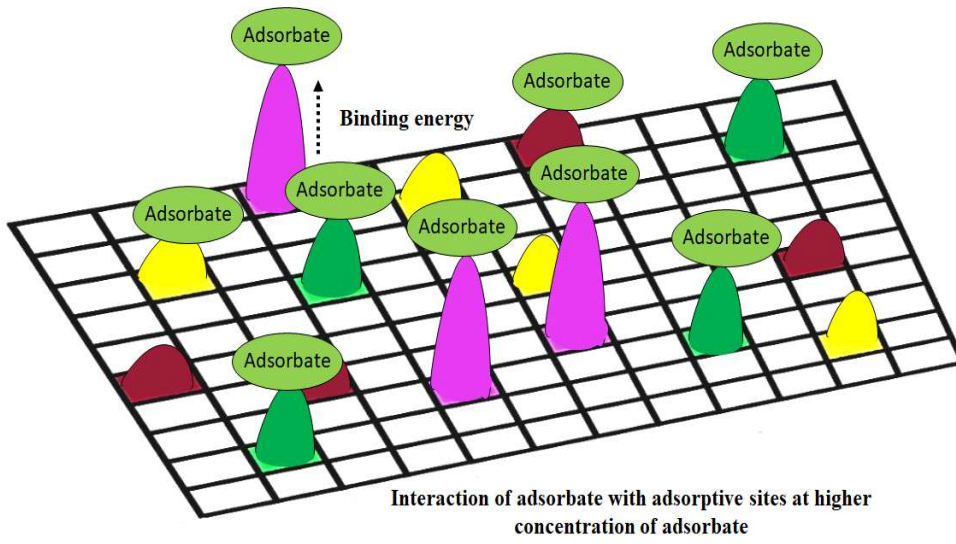
Figure 1.23. Interaction of adsorbates with binding sites present in the adsorbent at higher adsorbates concentration

Under homogeneous adsorption, decrease in entropy and binding energy are in equilibrium making the adsorption to occur at equal binding energy level. In this situation, the expression for the amount adsorbed is given by

$$q_h = N e_n C_e \qquad (1.4)$$

26

Where, q_h is the amount adsorbed in a homogeneous adsorbent, N, is the number of adsorption sites having binding energy e_n and C_e is the concentration of the adsorbate molecule at equilibrium. In practical situations the relationship is not simple as described above and it is influenced by number of variables. Approximation of the number of adsorption sites obtained by running experiments and modelling the experimental results with the theoretical adsorption isotherms. The theoretical adsorption isotherms join the variable parameters such as number of adsorption sites, their binding energy and their distribution on the adsorbent surface.
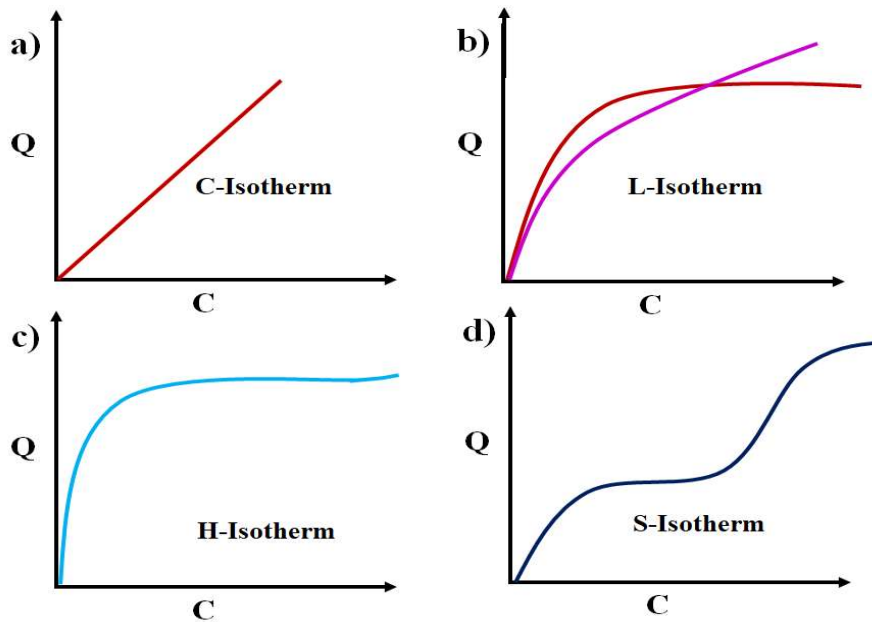
Figure 1.24. Various adsorption isotherm models

1.4.3 Modelling of adsorption isotherms

Based on the interaction between adsorbate and adsorbent system four types of isotherm modelling can be constructed. Which are described below,

a. The "C" isotherm

As represented in the figure 1.24a, in this case the ratio of the concentration of the adsorbate remaining in bulk phase and in adsorbed phase is same at any concentration.

The ratio is called distribution coefficient or partition coefficient, the reason why it is called C isotherm because of this constant partition.

  b. The "L" isotherm

Here, the ratio between the concentration of the adsorbate in bulk phase and in adsorbed phase decreases as the adsorbate concentration increases leading to concave curve (Figure 1.24b). This suggest the continuous saturation of the adsorbent. There are two types of outcomes are possible in this type of isotherm. One associated with a strict plateau implying the adsorbent has a limited adsorption capacity and another not having strict plateau indicating the adsorbent do not have clear limited adsorption capacity. Most of the theoretical isotherms such Langmuir (reason this isotherm called "L"), Freundlich, Redlich-Peterson, Sips and other used in our study are based on this kind of isotherm (Isotherms and their expression are given table 1.3.).

 Langmuir isotherm model is a theoretical equilibrium model and assumes that adsorption occurs at a finite delocalized sites forming monolayer adsorption of the sorbent molecule (Langmuir 1916). Freundlich isotherm is an empirical, widely used isotherm for heterogeneous adsorption (Foo and Hameed 2010). Redlich-Peterson is a hybrid of Langmuir and Freundlich isotherms, it can be applied to homogenous and heterogeneous adsorption systems. It approaches Freundlich model at high concentration (as g tends to zero) and at low concentration to Langmuir isotherm (as g tends to one) (Redlich and Peterson 1959). Sips isotherm is combined form of Langmuir and Freundlich isotherms model used for predicting heterogeneous adsorption systems and Sips model exponent gives nature of adsorption (Sips 1948). Dubinin-Radushkevich isotherm gives insight into whether the adsorption is physical or chemical in nature (Hu and Zhang 2019). The mean free energy (E) was calculated by the equation (3) below and tells the nature of adsorption.

$$E = \frac{1}{\sqrt{2k_{ad}}} \qquad\qquad (3)$$

The value of E < 8 kJ/mol indicates physical and 8 to 16 kJ/mol indicate chemical interaction of adsorbate with the adsorbent.

c. The "H" isotherm

This is high affinity isotherm (reason H), where the adsorbate has a very high affinity towards adsorbent. It is a particular case of L isotherm (Figure 1.24c).

d. The "S" isotherm

This isotherm represents the sigmoidal curve for the ratio of adsorbate in bulk and adsorbed phase. This generally exists where two kinds of mechanisms are involved in the adsorption and occurs one after another (Figure 1.24d)

Table 1.3. Adsorption isotherms models and their expressions

	Isotherm	Expression	
1	Langmuir	$q_e = \dfrac{Q_o b C_e}{1 + b C_e}$	Q_o- Maximum adsorption capacity (mg g^{-1}) b- Langmuir equilibrium constant (L mg^{-1})
2	Freundlich	$q_e = K_F C_e^{\frac{1}{n}}$	K_F-Fruendlich constant (L g^{-1}) n- Fruendlich exponent
3	Redlich-Peterson	$q_e = \dfrac{K_R C_e}{1 + a_R C_e^g}$	K_R-Redlich-Peterson isotherm constant (L g^{-1}) a_R- Redlich-Peterson constant L mg^{-1} g- Redlich-Peterson model exponent
4	Dubinin-Radushkevich	$q_e = q_s e^{-k_{ad}\varepsilon^2}$	q_s- Dubinin-Radushkevich model constant (mg/g) k_{ad}- Dubinin-Radushkevich model constant (mol^2 kJ^{-2}) E- mean free energy (kJ mol^{-1})
5	Sips	$q_e = \dfrac{K_s C_e^{\beta_s}}{1 + a_s C_e^{\beta_s}}$	K_s- Sips model isotherm constant (L g^{-1}) a_s- Sips model constant (L mg^{-1}) β_s- Sips model exponent

The isotherm and their expression used for the modelling of adsorbates are given in following chapters.

1.4.4 Adsorption Kinetics

Adsoprtion being a surface phenonmenon proceeds through diffrrent stages,

a. Transportation of adsorbates from bulk phase to the surafce of the adsorbent called as film diffusion.
b. Transporation from the surface of the adsorbent to exteranal surface by pore diffusion.
c. Surafce reaction between adsorbate and adsorbent , attachment of adsorbate.
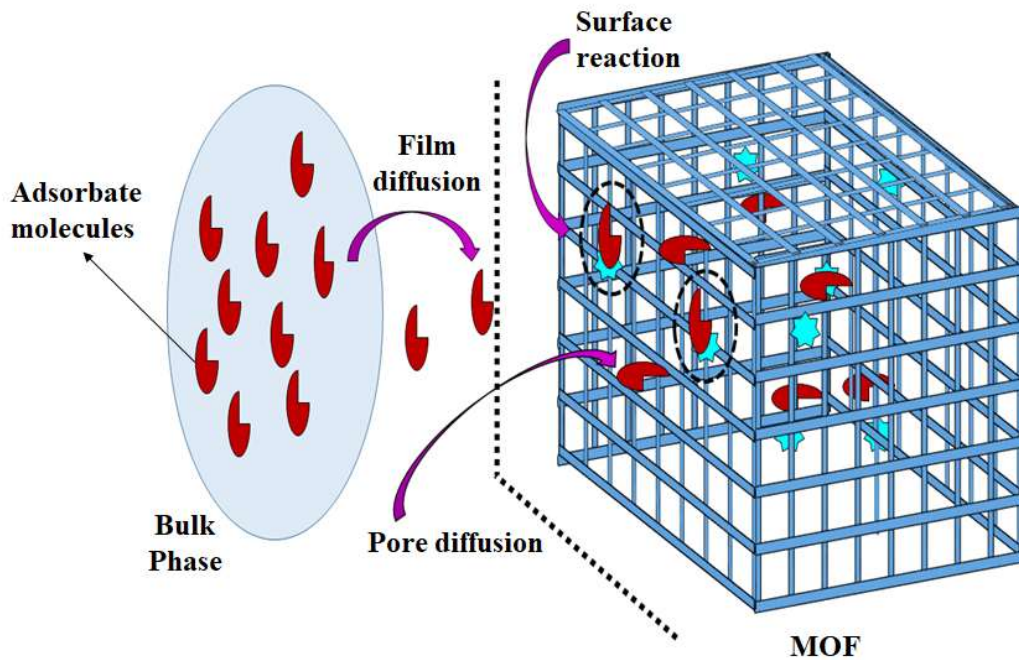
Figure 1.25. Adsorption kinetics mechanism

All the process are dicpted in the figure 1.25., transportaion steps posses higher resistance to the adsoprtion compared to surafce reaction , which typically rapid and cause negilazable resistance. The overall rate of the adsorption is the total resitance produced by the all the stages. If one of them contributed more resistance towards

adsorption then the step is called the rate controlling step. Usually the adsorption process is carried out batch operation or continues operation in a column packed with adsorbent, in such situation mass transfer effects are inevitable. Kintics studies of an adsorption experiments revels the underlying mechansm and describe the rate limiting step. Kinatc models are diveded bassed on the rate controling step such as diffusion models and reaction models. In this study both kind of models (Table 1.4) are fitted with experimental data in order to explore the extent and rate of the adsorption process.

Table 1.4. Adsorption kinatc model and their expressions

	Kinetic model	Expression		Reference
1	Pseudo first order kinetics	$q = q_e(1 - e^{-k_1 t})$	k_1-Rate of adsorption (min^{-1})	(Kumar 2006)
2	Pseudo second order kinetics	$q = \dfrac{k_2 q_e^2 t}{1 + k_2 q_e t}$	k_2- Rate of adsorption (g mg^{-1} min^{-1})	(Kumar 2006)
3	Elovich model	$q = \left(\dfrac{1}{\beta}\right)\ln(1 + \alpha\beta t)$	α- Initial sorption rate (mg g^{-1} min^{-1}) β- related to the extent of surface coverage and activation energy for chemisorption (g mg^{-1})	(Tan and Hameed 2017)
4	Weber- moris model	$q = k_{id}\sqrt{t} + B$	k_{id}-rate coefficient (mg g^{-1} min$^{-1/2}$) B-thickness of the boundary layer	Weber- moris model

1.4.5 Error evaluations in adsorption isotherm and kinetics

Earlier adsorption isotherm data were fitted by using linearized equations and coefficient of determination (R^2) was chosen as the goodness of fit. By doing so non-linear equations are converted to linear form, which will result in disturbing error values

making hard to find the best fitting isotherm. In addition to this, linear regression analysis is not suitable to use for the isotherms more than two parameters, hence non-linear regression analysis was opted to determine the isotherm parameters.

Commonly there are two types of error associated in expressing adsorption studies. First one is the experimental error, which is the difference between the experimental value and the true value. This kind of errors can be reduced by increasing higher accuracy in system and using standard reagents and equipment. Second type of error is fitting error, which transpire when practical data was correlated with theoretically calculated isotherm model data.

Optimization of fitting error involves, evaluating the fit of isotherm model parameters with experimental values by an error function. Generally, it is considered that, coefficient of determination equal to unity and lower error values of error functions indicates the best fitting isotherm. Five type of error functions (as given in the table 1.5) are used to evaluate the goodness of fit. This error functions and statistical comparison were done by using solver add-in with Microsoft excel spreadsheet.

Table 1.5. Error functions and their expressions

Error function	Expression	Reference
1. The Coefficient of determination (R^2)	$$R^2 = \frac{\sum(q_{e,meas} - q_{e,calc})^2}{\sum(q_{e,meas} - q_{e,calc})^2 \sum(q_{e,meas} - q_{e,calc})^2}$$	(Nebaghe et al. 2016)
2. Nonlinear chi-square test (χ2)	$$\chi^2 = \sum_{i=n}^{n} \frac{(q_{e,meas} - q_{e,calc})^2}{q_{e,meas}}$$	(Boulinguiez et al. 2008)
3. Residual root mean square error (RMSE)	$$RMSE = \sqrt{\frac{1}{n} \sum_{i=n}^{n} (q_{e,meas} - q_{e,calc})^2}$$	(Foo and Hameed 2010
4. Marquardt's percent standard Deviation (MPSD)	$$MPSD = 100 \sqrt{\frac{1}{n-p} \sum_{i=n}^{n} \left(\frac{q_{e,meas} - q_{e,calc}}{q_{e,meas}} \right)^2}$$	(Saadi et al. 2015)
5. Sum squares errors (ERRSQ)	$$ERRSQ = \sum_{i=1}^{n} (q_{e,mea} \quad q_{e,calc})^2$$	(Foo and Hameed 2010

CHAPTER-2

LITERATURE SURVEY AND CURRENT ASPECTS OF MOFs SYNTHESIS

This page is intentionally left blank

Abstract: This chapter provides the summary of current aspects of MOFs synthesis emphasizing more on zirconium based MOFs and its application in adsorbing undesired constituents from aqueous solution.

2.1 LITERATURE SURVEY

MOFs are developed by carefully designing and choosing precise mixture of metal ions and ligands. Apart from these, other compositional parameters such as pH, solvent, substituent present in the ligand, counter ions and process parameters like temperature, pressure and time can also affect the framework formation. Hence, recognizing the interdependency and influence of these parameters on one another is crucial for designing MOFs for practical application.

2.1.1 Synthesis of MOFs

Bernard F. Hoskins and Richard Robson, (1989) introduced the idea of connecting tetrahedral or octahedral nodes to rod like ligands resulting polymeric infinite crystalline structure. Reported the use of copper metal ion as the tetrahedral site along with 4,4',4",4"'-tetracyanotetraphenylmethane ligand to synthesize crystal framework having adamantane like cavities. X-ray analysis of the mother liquor taken in Lindeman tube confirms the formation of crystalline framework correlating interatomic distances, bond angels and inherent placement of all the species in the crystal. The obtained structure is in accordance with the intended structure. Inspired from the previously reported synthesis on extended polymeric crystalline network, Gable et al. (1990) used a linear bidentate ligand 4,4'-bipyridine along with zinc metal ion for the construction of the infinite framework. The formation of square grid structure containing sheets of zinc bridged by 4,4'-bipyridine stacked on top of one another was confirmed by X-ray diffraction studies.

Li et al. (1998) constructed the first permanently porous metal-organic framework, synthesized by slow diffusion of reagents to the solution of zinc nitrate and benzene dicarboxylate yielding stable framework structure. Apart from the conformation of monoclinic crystal structure from XRD, for the first time nitrogen sorption isotherm

studies were conducted on this permanently porous metal-organic framework. The Langmuir surface area of this MOF is 270 m^2 g^{-1}, micro pore volume of 0. 094 cm^3g^{-1}. The weight loss due to the removal of guest molecules from framework obtained from TGA studies and during activation of the MOF for nitrogen sorption isotherm are both in complete agreement. Realizing the importance of bond strength between metal ion and the ligand, Cavaka et al. (2008) synthesised a highly stable MOF from zirconium and Terephthalic acid. The synthesized MOF was highly stable, even in the presence of moisture. The XRD analysis confirmed the FCC crystalline structure, having 12 connected Zr_6 cluster. The Langmuir surface area was found to be 1187 m^2 g^{-1} and the framework revealed openings of windows 6,8,10 Å.

Hexing et al. (2010) synthesized the MOF with multivariate functionalities, by introducing various derivatives of 1-4 benzene dicarboxylic acid together. Nitro, amine, fluoro, bromo, chloro, methyl and methoxy functionalities were incorporated in the framework. The framework structure was not changed by the use of mixture ligands but the arrangements of functional groups are not in ordered. Multiple increase in the characteristic features of the MOF observed when compared to the linear sum of pure compounds. Morries et al. (2012) synthesized zirconium based MOF having ftw and csq topology with porphyrin ligands (MOF-525 and 545). The strategy used was to control the coordination in the zirconium cluster by blocking the coordination site (12 connections to 8 connection). MOFs are stable in water at neutral and acidic pH. The MOFs obtained exhibited a surface area MOF-525 and MOF-545 2620 m^2 g^{-1} and 2260 m^2 g^{-1} respectively and pore diameter 20 and 36 Å respectively.

Feng et al. (2013) reported the synthesis of highly stable zirconium MOFs (PCN-224) with metalloporphoyrins ligands (no metal, Ni, Co, Fe) by using linker elimination strategy. These MOFs displayed highest BET surface area of 2600 m^2 g^{-1} with a pore diameter 19 Å and stable pH=0 to pH=11. Suresh et al. (2014) described the synthesis of permanently porous MOF having large three dimensional channels by using two ligands in synthesis together. Two linkers (L1 = 4,4',4'',4'''-([1,1'-biphenyl]-3,3',5,5'-tetrayltetrakis(ethyne-2,1-diyl)) tetra benzoic acid (btba)), L2 = 4,4',4'',4'''-(pyrene-1,3,6,8-tetrayltetrakis(ethyne-2,1-diyl)) tetra benzoic acid (ptba)) were used. Multilinker synthesis strategy used in this work resulted in the synthesis of MOF having

surface area over 4000 m^2 g^{-1} and hydrolytically stable structure at room temperature. These enhanced properties were not obtainable when synthesized with single linker method. Liang et al. (2014) used mono carboxylic acids (formate, acetate and propionate) along with BDC ligand for the construction of Zr$_6$ core of UiO-66 framework. The monocarboxylic acids control the pore size of the framework. As the chain length of the monocarboxylic acid increases pore size, surface area and total pore volume decreases.

Sachin et al. (2015) Synthesised of five different zirconium based MOFs by varying the mole ratio of two ligands (benzene-1,4-dicarboxylic acid and (ABDC) 2-aminobenzene-1,4-dicarboxylic acid). Utilizing MOF instability in high pH solution, the MOFs are re-dissolved in NaOH solution and 2-aminobenzene-1,4-dicarboxylic acid concentration in the solution was quantified by UV-vis spectroscopy measurements. Finally, elucidated that the porosity and thermal stability of the framework depends on the ratio of the ligands used. Yuan et al. (2015) introduced multivariate functionalities in the framework by Sequential Linker Installation (SLI) strategy. Using this strategy, zirconium MOF with eight coordinated nodes were designed to create pockets for linear dicarboxylate linkers. The obtained MOF contains multivariate functionalities with stable porous structure.

Feng et al. (2015) synthesized mesoporous zirconium based MOF (PCN-777) through topological rationalization. The MOF having largest cage size of 3.8 nm and highest pore volume of 2.8 cm^3 g^{-1} showed superior stability in aqueous conditions making it excellent candidate for incorporation of different functionalities. Bruken et al. (2017) synthesized zirconium MOF UiO-66 by utilizing a thermolabile linker trans-1,4-cyclohexane-dicarboxylate (cdc) with (BDC) benzene-1,4-dicarboxylic acid. Later this thermolabile linker was eliminated by heating, leaving defects in the framework. Characterization of the MOF revealed the homogeneous distribution of defects formed by the thermolabile linker. It was realized that the zirconium node can tolerate 4.3 missing linker defects over this, framework loses its integrity leading to collapse of the framework.

2.1.2 Applications of MOFs

Magnetic zirconium MOF composite with flexible mercapto group pendants synthesized through solvent-assisted ligand exchange process utilized for the removal of mercury ions from aqueous solution (Huang et al. 2013). The terephthalic acid in the UiO-66 cluster is replaced with mercaptoaceteic acid and framework retained its porosity and crystalline nature. This ligand exchanged MOF exhibited high adsorption capacity 282 mg g^{-1} of Hg^{2+} from aqueous solution. Carboni et al. (2013) described the synthesis and application of zirconium MOF UiO-68 for the extraction of Uranium from water. Phosphorylurea groups are incorporated to terphenyl dicarboxylate linker to increases adsorption. The resulting UiO-68 MOF derivatives exhibited high adsorption capacity of uranyl from water and sea water. An adsorption mechanism was proposed on the basis of interaction between phosphorylurea groups and uranyl cation.

Nagarakar et al. (2014) reported synthesis of fluorescent zirconium MOF with ligand 2-phenylpyridine-5,4'-dicarboxylic acid for the detection of nitro explosives in the aqueous phase. The MOF possess pore windows of 11.5 Å and 23 Å allowing the analytes to move inside the framework and keeping the analytes and MOF close for efficient fluorescent quenching. This MOF displayed selective and sensitive detection of trinitrophenol in aqueous solution.

Zhu et al. (2014) demonstrated the synthesis and application of UiO-67 for the adsorptive removal of organophosphorus compounds from water. Due to strong affinity of zirconium towards phosphate containing compounds, the synthesized MOF showed efficient adsorption of organophosphorus compounds glyphosate and glufosinate herbicides. It was understood that the terminal Zr–OH groups are the reason behind adsorption through the formation bonds between Zr-O-P.

Liu et al (2014) studied the adsorption of phenol and p-nitrophenol from aqueous solution over three MOFs namely MIL-100 (Cr, Fe) and NH$_2$-MIL-101(Al). It was found that the adsorption behaviour towards phenol was similar from all the three MOFs. However, NH$_2$-MIL-101(Al) displayed higher adsorption capacity for p-nitrophenol. This profound adsorption capacity was attributed to the hydrogen bonding between the p-nitrophenol and the amine group of the MOF.

Nagarakar et al. (2015) utilised the isoreticular expansion of zirconium MOF, UiO-68 for the detection of trinitrophenol in aqueous solution. The ligand 2′-amino-[1,1′:4′,1″-terphenyl]-4,4″-dicarboxylic acid imparted the fluorescence property to the MOF. The electrostatic interaction between the trinitrophenol and the pendent amine group of the ligand caused fluorescence quenching. It was proposed that, the recognition of trinitrophenol by the amine group can be efficiently used in sensing nitro explosives.

Zhang et al. (2015) reported the synthesis and application water stable zirconium MOF, UiO-66(Zr)–2COOH for the removal of Cu^{2+} over Ni^{2+} from aqueous solution. The presence of two free carboxyl groups facilitated the formation of unique chelation effect and because of Jahn-Teller effect, the MOF showed superior selectivity for Cu^{2+}/Ni^{2+} in aqueous solution when compare to other adsorbents.

Ahmed et al. (2015) demonstrated the application zirconium MOF, UiO-66-SO_3H for the adsorption of indole and quinolone. As the –SO_3H content in the MOF increased so is the adsorption of indole, this effect is might be due to the hydrogen bonding between oxygen of the –SO_3H group and hydrogen of the indole. Application zirconium MOF, UiO-66 for the adsorption of arsenic from aqueous solution was reported by Wang et al. (2015). UiO-66, MOF showed high adsorption capacity 303 mg g^{-1} over a broad range of pH (1 to 10). This excellent uptake is attributed to porous nature and zirconium oxide cluster for providing a large contact area with plenty of active sites. The presence of hydroxyl group and benzenedicarboxylate ligand are responsible for high uptake.

Lin et al. (2015) reported the application zirconium MOF, UiO-66 and UiO-66-NH_2 for the adsorption of phosphate anions from aqueous solution. A slight increase in the uptake by UiO-66-NH_2 indicates the influence of hydrogen bonding and electrostatic interactions between phosphate group and amine. However, the major role for the adsorption is by interaction between zirconium and phosphate group. Application zirconium MOF, NU-1000 for the adsorption selenate and selenite from aqueous solution was conducted by Howarth et al. (2015) and reported the fastest uptake rates of all the zirconium MOFs. The presence of large 30 Å apertures helped for fast diffusion and labile hydroxyl and water ligand facilitated the binding of selenium oxyanions to zirconium cluster leading to higher adsorption.

Chen et al (2015) demonstrated the application of UiO-66 and UiO-66-NH$_2$ for the removal anionic and cationic dyes from the aqueous solution. It is observed that both MOFs were able to remove cationic dye (methylene blue) more effectively than anionic dye (methyl orange). This selective adsorption is because of favourable electrostatic interaction arising from intrinsic surface charge of the MOFs and the cationic dye. Lv et al. (2016) utilised the UiO-66 and UiO-66-NH$_2$ MOFs for the adsorption of nitrophenols from phenol, 4-nitrophenol, 2,4-dinitrophenol, and 2,4,6-trinitrophenol mixed solutions. The 2,4-dinitrophenol was able to adsorb more at acidic pH on both the MOFs. Hydrogen bonding and electrostatic interactions are the mechanism responsible for the adsorption.

Wang et al. (2017) used the zirconium MOF having -NH$_2$ group for the adsorption lead and cadmium ions from water and 100 % removal of lead and cadmium ions reported (at 10 ppm initial concentration). The adsorption mechanism studies confirmed the coordination interaction between NH$_2$ group and lead and cadmium ions responsible behind this superior adsorption.

Mohammadi et al (2017) described the use of UiO-66 for the adsorption of methylene blue from aqueous solution. Adsorption optimization studies revealed that the maximum adsorption occurs at pH = 9. The adsorption capacity of the MOF was found to be 91 mg g^{-1}. Jin-Min Yang (2017) reported the phosphate immobilized UiO-66 (UiO-66-P) for the application of adsorptive removal of Methylene blue from aqueous solution. This UiO-66-P composite showed superior adsorption capacity form 24.4 mg g^{-1} to 91.1 mg g^{-1} (272 %) over pristine UiO-66. Phosphate anions induced negative charge on the MOF, facilitating electrostatic interaction between methylene blue and MOF leading to higher adsorption. El-mehalmay et al. (2018) synthesised and reported the application of a composite of the amino-derivative Zr- (MOF) and silica gel for the removal of chromium. The porous silica gel helped to increase the sorbent–solute contact time. This composite exhibited an excellent chromium uptake capacity 277.4 mg g^{-1} even in the presence of other competing ions. This indicated the practical usability of the composite for the removal of chromium from water.

Synthesis and application of Amino-decorated Zr-based magnetic metal-organic frameworks (Zr-MFCs) composites for the removal organic dyes and metal ions was reported by Huang et al. (2018). The amine derivative of Zr-MFCs (Zr-MFC-N) exhibited higher adsorption capacity and faster adsorption kinetics. The maximum adsorption capacity of Zr-MFC-N for Pb^{2+} and methylene blue and methyl orange was found to 102 mg g^{-1}, 128 mg g^{-1} and 130 mg g^{-1} respectively.

Shi-wen et al. (2019) utilised the UiO-66-NH$_2$ for the removal of anionic dye (methyl orange) and cationic dye (methylene blue) simultaneously from aqueous solution. Adsorption studies indicated that at acidic pH, methyl orange adsorbed more (148 mg g^{-1}) where as in the alkaline pH methylene blue adsorption was more (549.6 mg g $^{-1}$). This exhibited the pH-dependency of the adsorption process. The simultaneous adsorption capacity at neutral for methyl orange and methylene blue was 105.2 and 144.9 mg g^{-1} respectively.

2.2 CURRENT ASPECTS OF ZIRCONIUM BASED MOF FOR ADSORPTION APPLICATION

Surface area, porosity, surface energy, mechanical strength and ability to interact chemically with the adsorbate, these are few important characteristics of an adsorbent considered essential for the successful application in adsorption. After the discovery of MOFs, an extensive research on the adsorptive application has been published. This evidences the huge potential of MOFs to become an eminent class of segment in the industrially important porous materials cluster.

The affinity of the MOF towards the target species is enhanced by the presence of certain moieties, which possess higher energy and interact specifically. The summary of the mechanism of this interaction was recently reviewed (Hasan and Jhung 2015) and given in the below figure 2.1. The following kinds of mechanism are generally expected, Electrostatic interactions, acid-base interactions, hydrogen bonding, pi-pi interactions, hydrophobic interactions and interactions due to the presence of framework metal.

The electrostatic interactions can occur only when both the MOF and adsorbate are charged, such situation often expected in aqueous solution. The adsorption of ionic dyes and charged metal species follow this type of mechanism. The presence of hydrogen bonding bearable polar groups like amine, acid, carbonyl and hydroxyl in the organic molecules supports to adsorb on the MOF, when the MOF also possess polar groups which can form hydrogen bonding. The acid-base interactions are expected between acidic and basic groups present on both adsorbate-adsorbent system, for example, acidic MOF containing carboxylic acid groups interact with an organic molecule having amine group. Interaction due to the presence of framework metal in case of lewis acid base interactions happening due to open coordination sites present in the metal to form coordinate bond with organic molecules. The pi-pi interactions are possible when favourable interaction occurs due to the presence of many pi-electrons such as aromatic rings present in the both the system.
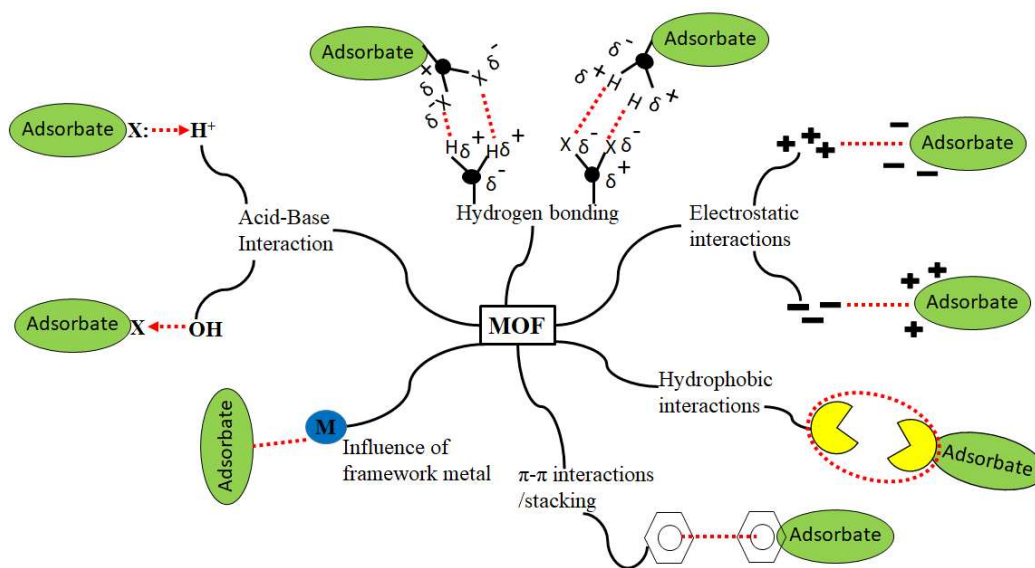
Figure 2.1. Plausible mechanism of interaction between MOF and adsorbates

As the knowledge of the possible mechanism of interactions of the MOFs with the target molecules are realized, so is the further development in the synthesis of MOF

materials for adsorption application (Figure 2.2). Functionalization of zirconium MOF is the major part where most of the research is focused. Along with functionalization of MOF, exploration on the various forms of zirconium MOFs adsorbents such as membranes, polymer matrix, composites, and nano particle immobilized composites are also under development.

The functionality in the zirconium MOF is incorporated by using dicarboxylate ligands having additional groups such as amines, halides and others (Figure 2.3, Kandiah et al. 2010).
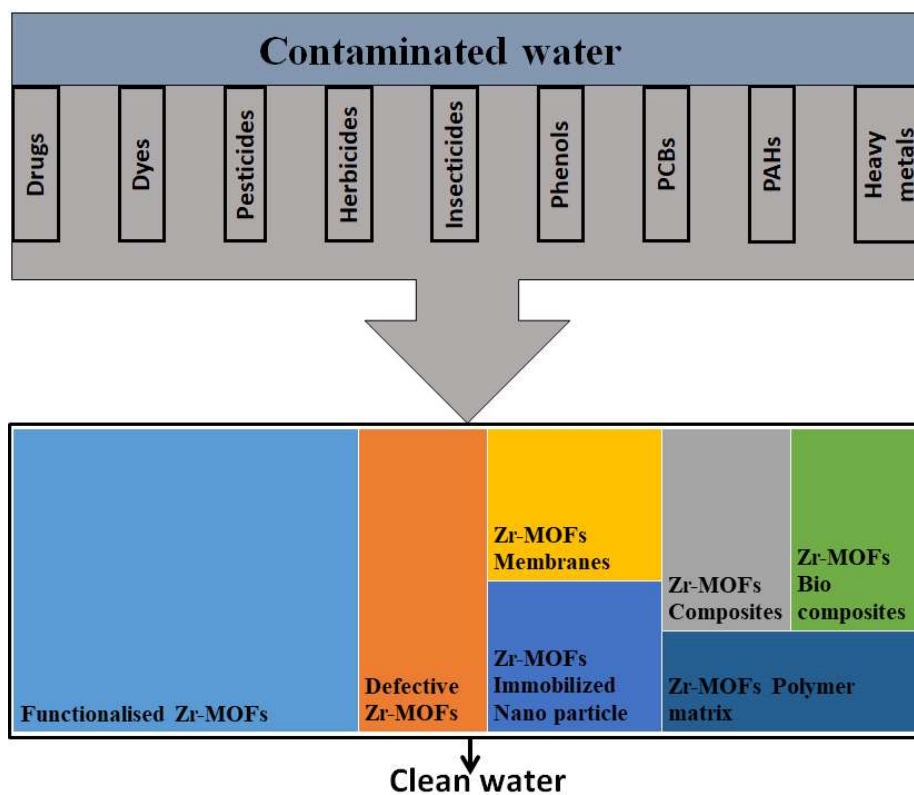
Figure 2.2. Current aspects of zirconium MOF research for adsorption of various contaminants from aqueous solution

In case where it is difficult to obtain both functional groups in same ligand, a mixed ligand strategy was used, dicarboxylic acid ligands with different functional groups are combined in a single framework (Kim and Cohen 2012).
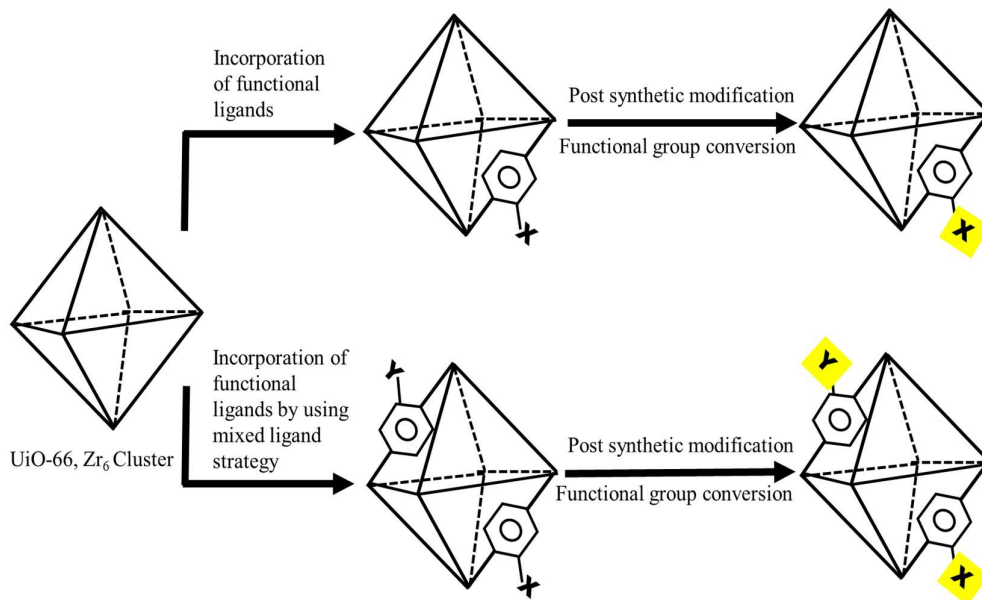
Figure 2.3. Incorporation of functional group to MOF by mixed ligand and functional group conversion

Further desired functionalities in the framework was introduced by post synthetic modification of the existing groups either using chemical conversion method like conversion of bromo to cyano (Kim et al. 2011) or by using ligand exchange method (Kim et al. 2012). These functionalized MOF show similar stability as that of UiO-66 along with superior performance features. In extension to this functionalization of zirconium framework, Daliran et al. (2020) synthesised pyridyltriazol-functionalized UiO-66 framework by three step post synthetic modification and efficiently utilised the MOF for the adsorption of palladium from aqueous solution, in addition after adsorption, the palladium adsorbed framework was also used as a catalyst for the Suzuki–Miyaura cross-coupling reaction.

Defective MOFs consists sites that locally break the regular periodic arrangement of atoms or ions of the static crystalline parent framework because of missing or dislocated atoms or ions (Fang et al. 2015). In zirconium based MOFs the defect arises due to missing linkers (ligands) generating a coordination vacancy on the adjacent zirconium metal ions. In similar way a missing cluster creates vacancy on each neighbouring

cluster. These defects help to alter the physical and chemical properties the MOFs producing positive effects.

Recently Ali et al. (2021) reported the synthesis of defect engineered UiO-66 framework by varying reactants mole ratio and reaction temperature. These MOFs showed increased absorptivity of lead ions from water indicating influence of open metal site and open framework on the adsorption of heavy metal ions. Use of monocarboxylic acid as ligands to create defects in the UiO-66 framework was reported by li et al. (2021). These monocarboxylic acid ligands increased the open site on the framework enhancing the phosphate adsorption capacity and increased the rate adsorption compared to pristine UiO-66.

MOFs synthesised in powder forms have little usability in terms of industrial application. To make them industrially prominent materials, fabrication of the MOFs to an appropriate form is necessary. Hence, making a composite with suitable another material can overcome this shortage. A composite is a multi-component material with multiple phases which has at least one continuous phase (Hoeri et al. 2003). Liu et al. (2015) first reported the fabrication of zirconium MOF on alumina hollow fibre to obtain continuous UiO-66 polycrystalline membranes for the application of desalination of water. The synthesised membrane showed good stability in saline water and promising separation performance. Cai et al. (2020) synthesised the continuous polycrystalline UiO-66(Zr)-NH$_2$ membranes on a flexible carbon cloth substrate for the separation of organic solvents through nanofiltration. The membrane showed complete rejection for dyes such as methylene blue, oil red and Nile red and moderate permanence for organic solvents (methanol and dichloromethane).

Functionalizing the MOFs by nano particle increases its intrinsic property or bestow new properties which are not inherently present in MOF. Raiely et al. (2017) proposed a classification on arrangement of nanoparticles in MOF. In the first case nano particles are deposited on the outer surface of the MOF and in second case multiple nanoparticles are randomly implanted in the MOF, finally core-shell structure with one or more nanoparticles completely encapsulated in the MOF shell represents the third category. To obtain the MOF nanoparticle composites explained before two synthetic strategies

were applied. Those are "ship in the bottle", where nano particles precursors are infiltrated into a preformed MOF matrix and form the nano particle, in the second strategy "bottle around the ship" involves building MOF around a preformed nanoparticle.

Feng et al. (2020) reported the synthesis of silver nanoparticle containing zirconium metal organic framework to remove radioactive iodine waste from nuclear plant waste. The synthesised MOF-Nanoparticle displayed high porosity and stability with exceptional adsorption capacity for Iodine (1260 mg g^{-1}). This high performance is attributed to the synergistic effect of MOF and silver nanoparticle.

Owing to their difficulties in preparing neat MOF membranes, mixed matrix membrane approach has been used for the integration of MOF with membrane. These mixed matrix membranes are composites with polymer as a continuous phase and MOFs as additive in the continuous pause. Here, the membrane essential properties are governed by the polymer such as porosity, whereas the additive (MOF) look after the adsorptive properties. In a recent study (Gutiérrez-Serpa et al. 2022) thin-films made of mixed matrix membrane of zirconium MOFs are utilised in analytical microextraction of contaminants arising from personal care product were studied. The mixed matrix membranes exhibited good adsorptive uptake behaviour of contaminants.

Jia et al. (2021) demonstrated the synthesis of porous starch-chitosan-UiO-66-COOH composite for the adsorptive application of sulphanilamide from water. The composite showed hierarchical porosity which facilitated the efficient adsorption of sulphanilamide.

It is clear that, synthesis and application of zirconium MOFs for the removal contaminants from water is progressing in a fast pace. New strategies and techniques for the improvisation of intrinsic properties and amalgamation of material science principles resulting highly advanced and performance oriented MOF materials. These materials have the ability to answer the environment remediation problems efficiently.

2.3 SUMMARY OF LITERATURE SURVEY

From the literature survey it is clear that water stable MOFs made of zirconium were extensively used to remove pollutants from aqueous systems. The adsorbing ability of the adsorbents (MOFs) was augmented by incorporating specific groups in the framework. These groups are either introduced after the formation of framework as post synthetic modification or in the beginning as a part of the framework during synthesis by mixed ligand strategy. Presence of larger pores also increases adsorption by allowing adsorbate molecule to pass through the framework channels and adsorb physically. The metal centres present in the framework shows high affinity through their unsaturated open sites for adsorption as in the case of zirconium metal centres towards phosphate containing adsorbate. Introducing fluorescence active property to the framework has an advantage of detection and adsorptive removal of pollutants at the same time. The MOF was made fluorescence active by incorporating fluorescence active ligand using alone or with the other ligands during synthesis. Over all electro static attraction, hydrogen bonding, acid base interactions of the functional groups and the metal centres present in the framework were the main mechanisms through which adsorption mainly occurs in removing pollutants from water.

Development and application of a multifunctional engineered material for effluent treatment systems have tremendous benefits in terms of treatment efficiency and cost. Having a highly porous structure, MOFs are considered as a prominent class of materials in environment remediation applications. Zirconium based MOFs are having high stability towards moisture and temperature due to the strong bonding between metal and oxygen atoms. Hence, zirconium-based MOFs form ideal materials for water-based adsorption applications.

2.4 PROPOSED WORK

2.4.1 Scope of the work

It is evident from the literature survey that the synthesis and application of MOFs has attracted many researchers worldwide for its expanding utility in the field of separation. However, application of MOFs in simultaneous adsorption of multiple contaminants

like dyes and toxic metal ions from aqueous solution seems to be limited. The industrial effluents compose multiple pollutants and developing robust adsorbent is the key in solving regulatory issues. Furthermore, it is also perceived that the development works on smart adsorbents, which can detect and adsorb pollutants simultaneously is yet to turn up. Therefore, keeping in view the advantages offered by this material, research is in progress to overcome their existing drawbacks by some suitable modifications in order to make them as an ideal application material. The possibility of enhancing the properties by introducing functional groups and improving their chemical resistance, stability towards water and temperature may help in large scale utilization of this material in the near future.

2.4.2 Aim of the work

Aim of the current work is to synthesize and maximum utilization of metal-organic framework materials. Furthermore, addressing the need to improve their chemical resistance, stability towards water and temperature. Also improving the desired properties by proper chemical modification, by introducing new chemical entities etc. This may result in augmentation in enhancing separation and detection of pollutants from the resulting MOFs.

2.4.3 Objectives

- To synthesize N, O donor ligands.
- To synthesise zirconium metal-organic frameworks using in-house synthesised ligands.
- To synthesise functionalised zirconium MOFs.
- To study the structure of ligand and MOF by various analytical techniques.
- To study the surface area and pore structure of MOFs by gas adsorption.
- To study the detection and adsorption of hazardous materials over synthesised zirconium MOFs.

CHAPTER 3

SIMULTANEOUS ADSORPTION OF METHYLENE BLUE AND HEAVY METALS FROM WATER USING Zr-MOF HAVING FREE CARBOXYLIC GROUP

Abstract: This chapter describes the greener method for the hydrothermal synthesis of UiO-66 (COOH)$_2$ MOF using easily available zirconium chloride salt with BETC ligand and acetic acid as modulator and accounts the use of hydrothermal synthesised UiO-66 (COOH)$_2$ MOF to adsorb methylene blue and heavy metals simultaneously from aqueous solution. The detailed characterization of the material has also been discussed

3.1 INTRODUCTION

The freshwater resources are under great threat because of rapid urbanization. To meet the demand of the essential products industrialization is occurring at a rapid pace, which ultimately releases a large number of hazardous pollutants of inorganic and organic wastes into the water, causing severe water pollution (Ashiq et al. 2012, Baral et al. 2009). Hence, it is required to protect the aquatic resources and supplies from these contaminations effectively and efficiently. Textile, pharmaceutical, food, tanning, and paper industry were the prevalent users of dyes and pigments which also contain toxic metals (Baral et al. 2009, Dotto et al. 2011). Methylene blue is the most common colouring agent, used mainly in dyeing leather, printing cotton, and tannin (Gupta et al. 2011). It is obligatory to remove dyes from the aquatic system because of their defiant, harmful and abiding nature (Jain at el. 2014). The existence of dyes in the water bodies reduces sunlight penetration that leads to decrease in photosynthesis and has a detrimental effect on aquatic life (Zhou et al. 2014). High toxicity and ubiquity of metal ions in water bodies such as lead, cadmium released from industrial process cause multiple organ damage, birth defects, and carcinogenic to human life. Hence environmental agencies (World Health Organisation (WHO)) and American Water Works Association (AWWA)) limit the concentration of lead and cadmium in drinking water to 0.015 mg L^{-1} and 0.005 mg L^{-1} respectively (Mohan and Singh 2002, Cuenot et al. 2005). These factors were forcing the scientific community to find newer solutions for efficient low-cost remediation of polluted water (Tchounwou et al. 2012).

The conventional methods to treat water include adsorption, coagulation, sedimentation, filtration, chemical and membrane technologies. The adsorption process

is less energy consuming and hence cost-effective applications for water treatment (Zhou et al. 2014, Gupta et al. 2000, Vinod and Anirudhan 2003). Porosity is the main criteria for material to be called an adsorbent; hence, it is of great interest to investigate the advanced porous materials for this application. A new class of highly crystalline porous solids, metal-organic frameworks (MOFs) demonstrated superior performances in adsorptive separation and purification.

The uppermost concern in treating effluents from dye-based industries is to remove colour. Adsorption has been found to be a pivot technique in removing dyes from water. Heavy metals can also be removed by an adsorption process along with other low-cost removal processes such as coagulation and sedimentation followed by filtration (Fu and Wang 2011). Advanced and efficient adsorbents are of great interest to overcome multiple effluent treatments for an effluent system containing different pollutant species like organic dyes and inorganic metal ions (Ahmad et al. 2020, Ayub et al. 2021). It is also a statutory requirement that the effluents released should be at neutral pH, hence industrially it is economical and beneficial to develop a treatment process at neutral pH and remove all the pollutants.

3.2 STRATEGY AND OBJECTIVES

As stated in the chapter 1, very few of the synthesised MOFs are stable and can hold their framework integrity in presence of water. This instability is due to weak bonding between the metal ions and ligands. Where as in the case of zirconium based MOFs, the strong affinity between Zr (IV) ion and carboxylic oxygen makes the bond stronger. In addition to this maximum coordination number of metal ion makes it difficult to external ligands to replace the existing ligand. Functionalization of this highly stable MOF opens wide opportunities in various applications. One such way is to use functionalized ligands during synthesis. Many attempts were made to use greener methods for sustainable synthesis of zirconium based MOFs but ended with poor crystallinity and repeatability. In recent years' modulator approach has been used, where ligands having one coordination sites were used during synthesis of MOF which competes with linkers to form complex with metal cations, there by altering the rate of crystal formation (Schaate et al. 2011). Acetic acid seems to be the best modulating

agent as it offers no solubility issue for hydrothermal synthesis. The solubility of the ligands in aqueous condition is the main criteria for the green synthesis of zirconium based MOFs (Schaate et al. 2011). Even with water soluble ligands it was difficult to obtain crystal solids as the reaction mass turns into amorphous solids. But the presence of water is essential for the formation of UiO-66 type MOFs, as $Zr_6(O)_4(OH)_4$ structure consists – OH and – O bridges (Valenzano et al. 2011). In fact, synthesis with BDC-NH_2 ligands requires water to obtain well-ordered single crystal (Schaate et al. 2011). Yang et al (2013) first reported the synthesis of UiO-66(COOH)$_2$ with BETC ligands under aqueous condition without using any modulators. But reproducibility often questioned by many researchers (Hu et al 2015). Ragon et al. (2015) conducted a comprehensive study on aqueous synthesis of UiO-66 (COOH)$_2$ using high throughput technique with HCl and water mixture at 100 to 150 °C. It was concluded that equimolar ratio of metal ion and ligand with optimum dosage of HCl/water is necessary for crystal formation. Excess of acid prevents deprotonation of ligands reducing the reaction rates. The rate of crystal formation increases as the temperature increased from 100 to 150 °C. Hu et al. (2015) used nitrate salt of zirconium and acetic acid as modulator along with BETC ligands to obtain nano sized crystalline UiO-66(COOH)$_2$ by hydrothermal method. Zirconium chloride was avoided which might be due to its hygroscopic nature and formation of gel like products (Bueken et al. 2017). Here, we report modified hydrothermal method for the synthesis of UiO-66(COOH)$_2$ metal-organic framework with 1,2,4,5-benzenetetracarboxylic acid and zirconium chloride as metal source.

The objective of the present study was to evaluate the usefulness of the easily synthesizable, water stable and low cost (from hydrothermal synthesis) MOF in removal of multiple contaminants simultaneously from water. The influence of various experimental factors such as contact time, pH, adsorbate initial concentration and amount of adsorbent were investigated. The sorption behaviour at optimized condition was assessed and correlated with underlying mechanism. The outcomes are compared with similar works in the literature and found favourable.

3.3 MATERIALS AND METHODS

3.3.1 Materials

Zirconium chloride ($ZrCl_4$) (99.5%, Reactor grade) was purchased from Alfa Aesar. 1,2,4,5-benzentetracarboxylic acid was purchased from Sigma Aldrich, Acetic acid were supplied by Spectrochem Pvt Ltd, India. All chemicals were used as received without further treatment.

3.3.2 Methods

The synthesis of UiO-66(COOH)$_2$ was carried out based on literature with a slight modification (Hu et al. 2015). In this process, organic ligand (~5 mmol) and $ZrCl_4$ (~5 mmol) were suspended in 50 mL of water/acetic acid mixed solvent (30 ml:20 ml), and the reaction mixture was heated to 130 °C under reflux condenser for 10 h to yield a powder product. The product was cooled to room temperature and filtered, washed with water and acetone. Then the sample was dried under vacuum at 80 °C for 12 h to yield the final product with a yield of 90% based on the overall weight of ligand and metal salt.

3.3.3 Characterization

The crystal structure of the as synthesized MOF was analysed using an X-ray diffractometer (XRD, Rigaku) with monochromatic Cu-Kα radiation (Λ = 0.154 nm) at a scan rate of 2° per minute in the range of 5-60°. The morphological features of the synthesized MOF were analysed using SEM (Carl Zesis). The nitrogen adsorption-desorption isotherms were obtained by the BET method, before the analysis, the sample was degasified for 2 h at 120 °C (BELSORP-mini II (Japan)). FTIR spectra of the sample were recorded using Perkin Elmer spectrum 100 analyser by preparing the sample and KBr pellets. Zeta potential measurement carried out by Horiba scientific (nanopartica) nanoparticle analyser at neutral pH. Metal ions concentrations were determined by GBC SavntAA atomic absorption spectrometer. Kratos XSAM800 spectrometer equipped with Al Kα source used for XPS analysis.

3.3.4. Adsorption experiments

A solution containing each adsorbate from 10 mg L^{-1} to 100 mg L^{-1} initial concentration (methylene blue and heavy metals) were taken and an optimum dosage of 0.35 g L^{-1} of adsorbent was fixed for isotherm studies. The adsorbate-adsorbent system was kept in an orbital shaker under isothermal condition for sufficient time to reach equilibrium. 0.1 N NaOH and 0.1 N HCl used for pH adjustments and the effect of various parameters on adsorption were evaluated. After each experiment, the solution was centrifuged (2000 rpm and 10 min) and the methylene blue dye concentration at equilibrium was determined by a spectrophotometer (k = 664 nm) (Qiu et al. 2017), and metal ions concentrations were determined by atomic absorption spectrometer. All the trials were replicated at identical conditions. The amount of adsorption at equilibrium, qe (mg g^{-1}), was calculated by equation (3.1) (De haro-del et al. 2017).

$$q_e = \frac{(C_o - C_e)V}{W} \qquad (3.1)$$

Where Co and Ce are the initial and equilibrium adsorbate concentration (mg L^{-1}) respectively. V is the volume of the solution (L) and W is the mass of dry adsorbent used (g). Adsorbate removal (%) was calculated by equation (3.2) (Alhassani et al. 2020).

$$\text{Adsorbate removal (\%)} = \left(1 - \frac{C_t}{C_o}\right) * 100 \qquad (3.2)$$

Where C_t is adsorbate concentrations at any time t (mg L^{-1}). Kinetic experiments were similar to those of equilibrium tests (20 mg L^{-1} initial concentration). The concentrations of dye and metal ions from the aqueous samples were measured at different time intervals. The amount of adsorption at time t, q_t (mg g^{-1}), was calculated by equation (3.3) (Al-jubouri et al. 2020).

$$q_t = \frac{(C_o - C_t)V}{W} \qquad\qquad\qquad (3.3)$$

3.4 RESULTS AND DISCUSSION

3.4.1 Characterization MOF

From literature it was found that chloride salt of zirconium was not used along with acetic acid modulator for hydrothermal synthesis. When Zirconium chloride was used in aqueous condition gel like product obtained which needs further treatment to get powder (Yang et al. 2013). This is due to the rapid reaction of metal salt with water molecule. In presence of modulator this reaction gets altered, provided the modulator is soluble in reaction condition. As the temperature of the reaction was increased this modulator was replaced by ligand molecule to from framework structure. By combining the outcome of the previous reports, it was concluded that at higher concentration of metal ions, under aqueous conditions using acetic acid as modulator and at high temperature facilitates formation of UiO-66(COOH)$_2$ crystals. The structure of UiO-66(COOH)$_2$ MOF consists of octahedron zirconium atoms. Each zirconium atom is eight-coordinated in square antiprismatic fashion with eight-oxygen atoms, where four of which from carboxylate and the other four from μ_3-O and μ_3-OH atoms. The octahedral edges are bridged by carboxylate groups from 1,2,4,5-benzentetracarboxylic acid forming three-dimensional FCC structure. The Powder XRD results confirm the crystallinity of the synthesized MOF. As shown in the figure 3.1(a), the characteristic two peaks at 7.4° and 8.5° corresponds to the plane [111] and [220] respectively indicate that the MOF synthesized was having isostructural UiO-66 framework topology (Hu et al. 2015).

The band at 1710 cm^{-1} from FTIR spectra figure 3.1(b) shows the presence of freely available COOH, which acts as anchors for holding the cationic methylene blue dye. Apart from this FTIR confirms the presence of regular bands of MOFs metal-carboxylic bonds. The band at 1420 cm^{-1} and 1580 cm^{-1} corresponds to carboxyl symmetric and asymmetric stretching bonded to zirconium. The band at 1511 cm^{-1} is from aromatic

C=C vibration of benzene ring. The bands around 820, 710, and 550 cm^{-1} are associated with C-H vibration, O-H bending and Zr-(OC) asymmetric stretching.
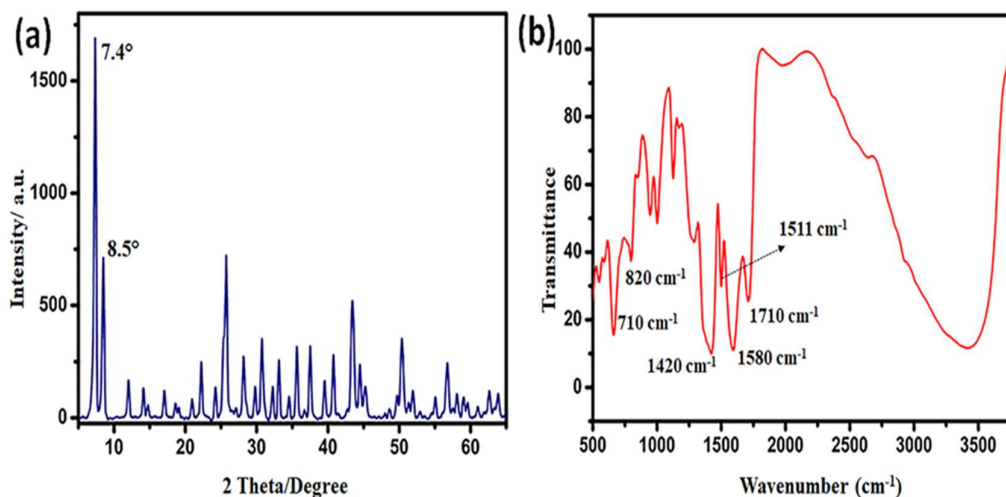
Figure 3.1. (a) PXRD spectra of synthesized MOF (b) FTIR spectra of MOF

Surface area and pore size were studied by N$_2$ sorption isotherm (Figure 3.2(a)). Which reveals a composite kind of I/IV isotherm. There is a sharp increase in the volume of gas adsorbed at p/po=1, which shows condensation of gas in mesopores formed due to the defects in MOF structure. BET Surface area is 505 m^2 g^{-1}. The pore distribution plot (inset of figure 3.2 (a)) studied by micropore method shows that the sample has micropores 0.4 to 0.7 nm and has distribution peak at (dp, peak/nm) at 0.57 nm. Hence, it can be concluded that the occurrence of hysteresis is due to condensation of N$_2$ gas in voids formed in the framework during synthesis. The SEM morphology of UiO-66(COOH)$_2$ (Figure 3.2(b)) shows relatively circular particles of size 150−300 nm, this was attributed by fast nucleation of the metal cation with water molecules at a higher temperature and different levels of molecular aggregation during synthesis. The energy dispersive X-ray spectroscopy (EDX) determines the elemental composition of the sample. EDX analysis image of MOF is given in figure 3.2 (c). The figure shows the representative elements in appropriate proportion. The major constituent is oxygen present in 59.36 atomic percent (at %) and carbon is present in 29.68 at% followed by zirconium 10.96 at%.
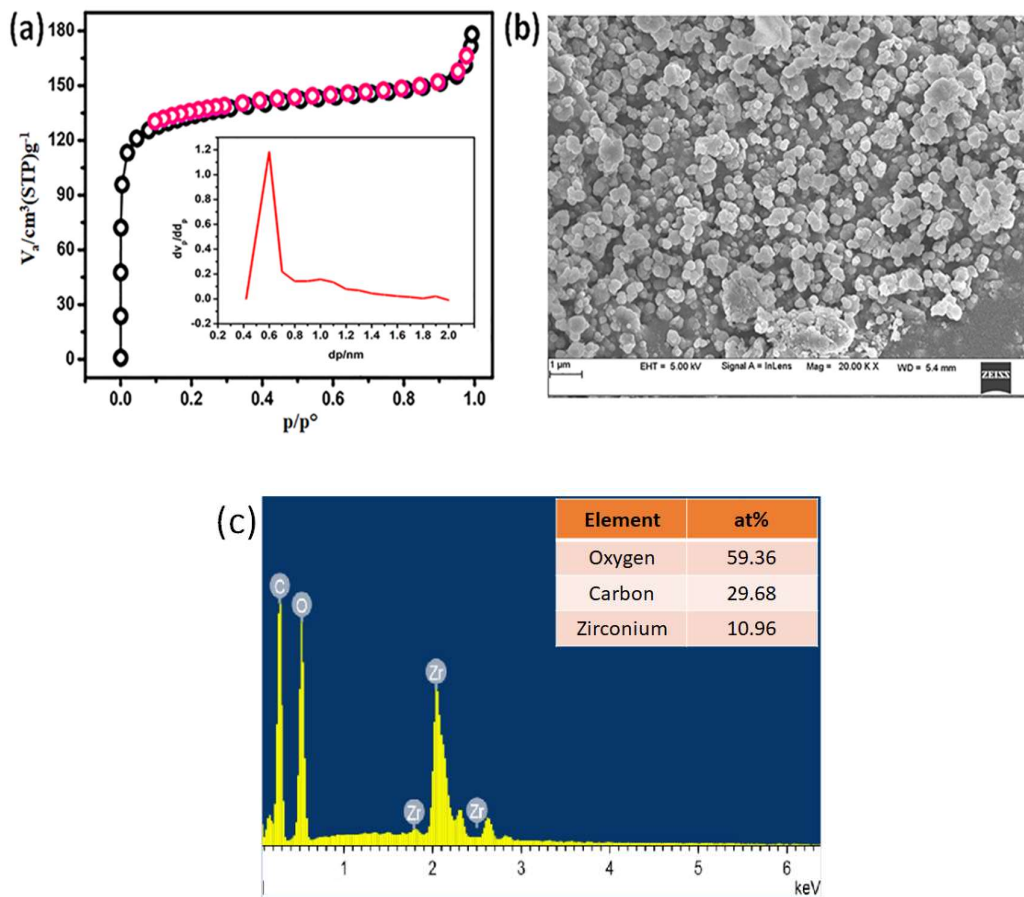
Figure 3.2. (a) Nitrogen adsorption isotherm of MOF (b) SEM image of MOF (c) EDX spectra of the MOF

3.4.2 Parameters optimised for adsorption

3.4.3 Effect of pH

Effect of pH studies was conducted at 20 mg L^{-1} concentration of dye molecules and 0.5 g L^{-1} dosage of adsorbent. As a result of free carboxylic groups, the adsorbent exhibits a different level of adsorption in the acidic and basic medium and the surface charge of the adsorbent is greatly affected by pH of the solution. Due to the ionic nature of MB, the dye adsorption on the surface of the MOF is dependent on the surface charge of the adsorbent. The degree of dissociation of dye molecules also depends on pH. At lower pH, protonation of the carboxylic group of the MOF occurs, which makes the

cationic dye to interact weakly with the MOF. This competition between hydrogen ions and dye molecules for the ionic interaction with the MOF, causes decrease in adsorption of dye molecules at low pH. However, at higher pH, though the surface charge of the MOF may be negative but the adsorption seems to be less may be due to charge neutralization of dye molecules with hydroxyl ions. This results in the reduced ionic interaction between dye molecules and the MOF. The Zeta potential value of MOF at neutral pH is -7.7 mV, a slight negative charge on the surface of the MOF, which is favourable for the cationic dye to adsorb and shows maximum adsorption at neutral pH (figure 3.3(a)). It was found that the maximum dye removing capacity of the adsorbent is at neutral pH. This advantage was considered, and decided to explore the ability of the adsorbent to remove the heavy metals at neutral pH. Furthermore, switching back and forth to pH corrections to the removal pollutants was not found to be cost-effective. Hence for the adsorption studies the pH was kept between 6.5 and 7.0., in considering the precipitation effect of heavy metals. As it was found that the insoluble precipitates of metal hydroxide such as lead and cadmium will only start to form after pH 7.0 (Hahne and Kroontje 1973).
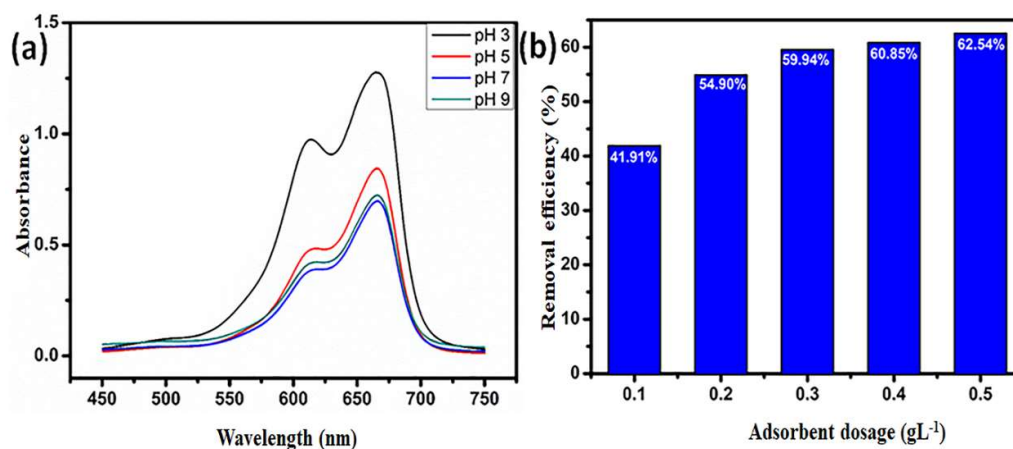
Figure 3.3. (a) Effect of pH on MB dye adsorption. (b) Effect of dosage on adsorption of MB dye molecule.

3.4.4 Variation in adsorbent dosage

In this study, it was decided to explore the potential use of the adsorbent when used in the treatment of pollutants from the dye industry. Hence the effect of pH and adsorbent dosage optimized for maximum dye adsorption, later the ability of the

adsorbent to remove lead and cadmium ions at these optimized conditions was studied. The quantity of MB adsorbed was strongly affected by adsorbent dosage. To understand this effect, a known concentration of adsorbate solution was contacted with varying concentrations of adsorbent dose from 0.1 g L^{-1} to 0.5 g L^{-1} as shown in figure 3.3(b). Initially, adsorption increases with dosage but later saturates at 0.3 g L^{-1} onwards. This is because the number of sites for adsorption over adsorbent increases with the dosage, removal efficiency also increases but there is a decrease in the density of adsorption at a higher adsorbent dose resulting lower q_e value (Vadivelan and Kumar 2005).

3.4.5 Effect of time

Figure 3.4. shows the plot of adsorption efficiency and amount of adsorbates adsorbed as a function of time, when the experiments are conducted using 20 mg L^{-1} adsorbates with 0.35 g L^{-1} of adsorbent dosage. Higher dye removal capacity at the initial stage is due to the attractive interaction between of anionic carboxylic acid and cationic methylene blue dye. As the adsorption progress, dye molecules cover the surface of the adsorbent partially or completely resulting in lower adsorption. Close experimental values were obtained when the dye/adsorbent system was in a state of adsorption equilibrium (Dotto and Pinto 2011). It can also be concluded from the figure 3.4., that the single–component adsorption with respect to a particular metal ion is more when compared to multi-component system. This shows there is a competitive adsorption phenomenon between cationic metal species but this is not the same for the dye molecules present in the solution. Because the adsorption efficiency of MB is almost same and not influenced by the metal ions present in the system. It is also clear that the adsorption efficiency of lead is selectively more when compared to cadmium. This is due to the smaller size of hydrated lead ions in water and the affinity of the electron-rich carboxylic oxygen towards lead (Yu et al. 2017). The average pore size of MOF determined from surface area measurement is around 0.5 nm whereas hydrated ionic radii of lead is almost half of the pore size hence it is easier for lead ions to move inside the pores. Another factor that favours the adsorption is the lower hydration energy, as the metal ions need to lose hydrated water before entering smaller-sized pores.
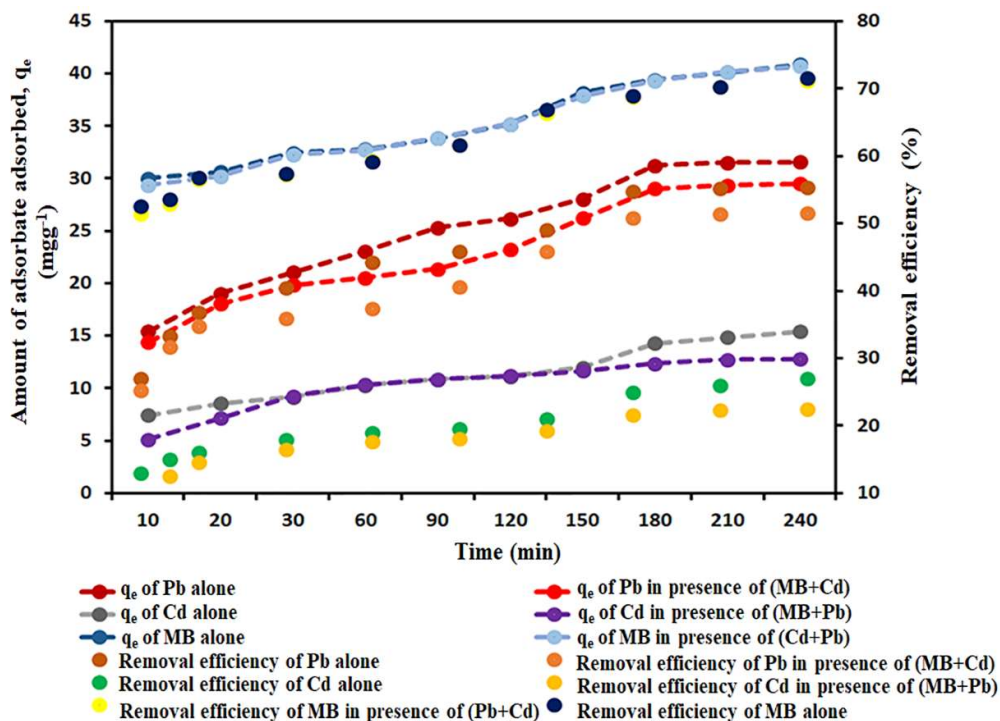
Figure 3.4. Effect of time on individual and multicomponent adsorption removal efficiency.

Therefore, from table 3.1. (Yu et al. 2017), larger ionic radius and lower hydration energy of lead favours the interaction with anionic MOF adsorbent. As the adsorption proceeds, dye molecules block the pores of MOF leading to the decrease in the diffusion rate of metal cation adsorption and forming a barrier between metal ions and electron-rich oxygen atoms. It can be concluded that when there is a competition for diffusion and surface adsorption, lead ions prevail over cadmium because of their smaller size and lower hydration energy.

The selectivity of adsorbent among the adsorbates can be analyzed from distribution coefficient (K_d (mg L^{-1})) as given in equation (3.4) (Yan et al. 2011). Where C_o and C_f (mg L^{-1}) are the initial and equilibrium concentration of adsorbates respectively. V (L) is the volume of the solution and m (g) is mass of the adsorbent. Which is used as an indicator of the selectivity of the adsorbent to the particular ion in the presence of complex matrix of interfering ions.

$$K_d = \frac{(C_o - C_f)}{C_f} \times \frac{V}{m} \qquad (3.4)$$

A selectivity coefficient α for the adsorption of specific adsorbate in the presence of competitor species can be given by equation (5).

$$\alpha = \frac{K_d(T)}{K_d(I)} \qquad (3.5)$$

In which $K_d(T)$ is the K_d value of the targeted species and $K_d(I)$ is the K_d other competing species. The calculated values of α for methylene blue is 14.18 (in presence of Cd) and 3.40 (in presence of Pb). For lead ions α values are 0.29 (in presence of MB) and 4.16 (in presence of Cd). For cadmium ions α values are 0.07 (in presence of MB) and 0.24 (in presence of Pb).

It is clear that the adsorbent has higher selectivity in the order MB > Pb > Cd.

Table 3.1. Properties of dehydrated and hydrated heavy metal ions

Metal ion	Ionic radii	Hydrated Ionic radii	Hydration energy
Cadmium	0.097 nm	0.426 nm	1755 kJ mol^{-1}
Lead	0.122 nm	0.261 nm	1425 kJ mol^{-1}

XPS analysis (Figure 3.5) was conducted to understand the mechanism between adsorbate/adsorbent interactions. The presence of Pb 4f and Cd 3d peaks confirms the loading of metal species after adsorption (Figure 3.5 (c) survey). High resolution spectra of XPS reveal the more details on metal cation interaction with anionic MOF adsorbent. The peaks 138.44 and 143.3 (Figure 3.5 (a)) corresponds to Pb $4f_{7/2}$ and Pb $4f_{5/2}$ have 1.2 eV shift towards lower binding energy compared to 144.5 eV and 139.6 eV of purified Pb(NO)$_3$ shows likeliness affinities between Pb and MOF. In case of cadmium, Cd $3d_{5/2}$ and Cd $3d_{3/2}$ (Figure 3.5 (b)) corresponds to peaks 404.9 and 411.6 has 0.3 eV shift lower when compared to 405.2 eV and 411.9 eV of standard. This implies that adsorbent affinity towards cadmium is less which was also confirmed by experimental results. Furthermore from FTIR analysis (Figure 3.5 (d)) the change of peak shape at 1400 cm^{-1} after adsorptions shows the presence of NO$_3^-$ for charge

balance. Decrease in the area of peak 1710 cm^{-1} of free carboxyl groups is due to the possible coordination interaction with metal cations.
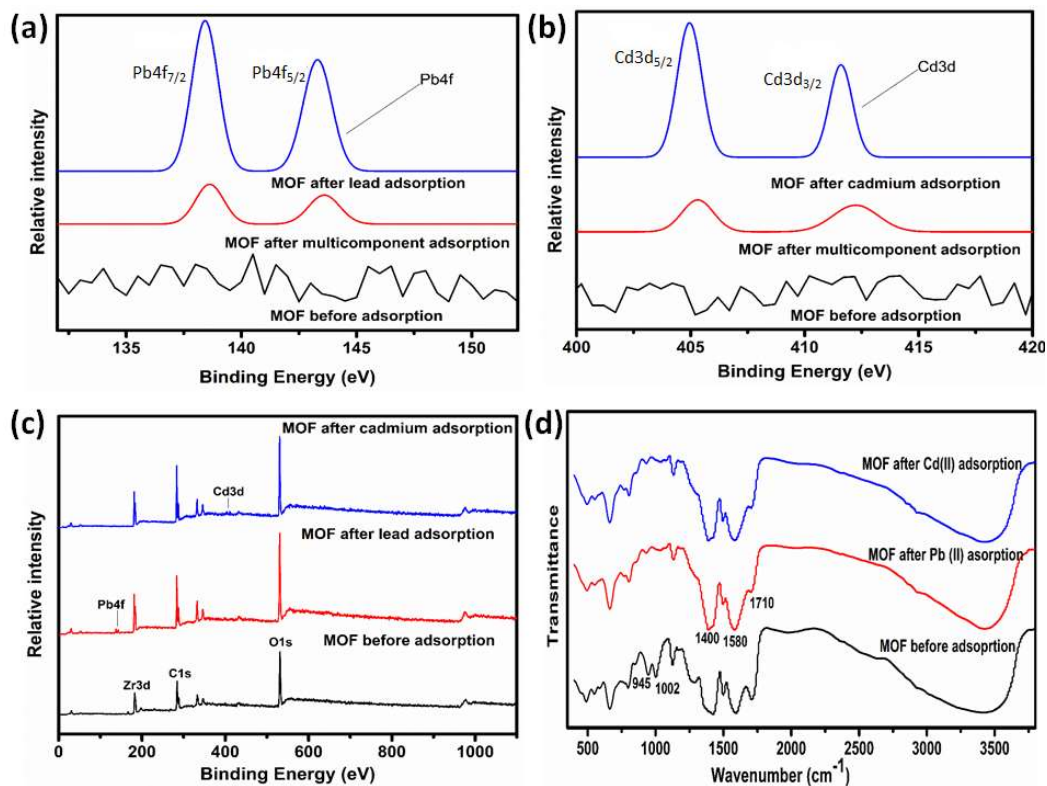
Figure 3.5. XPS analysis of MOF before and after adsorption (a) Pb 4f & (b) Cd 3d, High resolution spectra. (c) Survey XPS. (d) FTIR spectra of MOF before and after adsorption of each metal ions.

3.4.6 Effect of initial concentration

As the number of adsorbate molecules increases, the probability of interaction between adsorbate-adsorbent increases which leads to higher adsorption (Baral et al. 2009). The adsorbate concentration in the beginning governs the mass transfer resistance between adsorbate and solution phase. There always exists resistance for mass transfer from the liquid phase to solid phase and the concentration difference is inversely proportional to mass transfer resistance, hence increase in concentration in liquid phase act as driving force to reduce mass transfer resistance. A similar effect has been observed in figure 3.6., increase in concentration reduces mass transfer resistances

leading to higher q_e values. But efficiency of adsorption decreases with increasing initial concentration at fixed dosage. This is because the mass of adsorbent is constant, hence the adsorption per unit concentration is less as the number of sites available is same. The removal efficiency of MB dye is very high at low concentration and decreases steeply as the dye concentration increases, this trend is because of reduction in the number of ionic sites on the adsorbent as adsorption proceeds. For metal ions also, removal efficiency decreases but change in removal efficiency is gradual compared to dye removal. This kind of moderate change in removal efficiency is may be due to lower likeliness of interaction between metal ions and adsorbent when compared to MB dye and adsorbent.
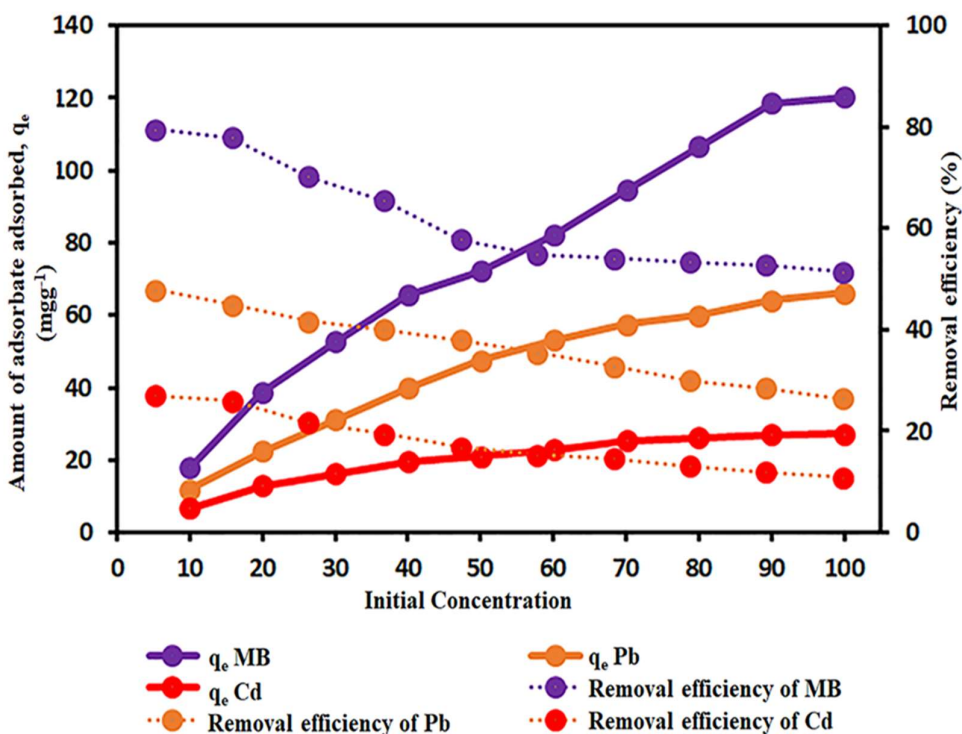
Figure 3.6. Effect of initial concentration of adsorbate on removal efficiency.

3.4.7 Adsorption isotherms

The information on how the solute particles were able to adsorb on the adsorbent is provided by adsorption isotherms (Natarajan et al. 2014). A plot of remaining adsorbate molecules in the solution and solute particles adsorbed over adsorbate at equilibrium

was constructed keeping the temperature constant. To explore and gather more information on the distribution of solute particles over adsorbent, four isotherms Langmuir, Freundlich, Redlich-Peterson and Sips models were fitted with experimental data (Table 3.2). From the isotherm curves, the information on maximum adsorption capacity, adsorption mechanism, physisorption or chemisorption, monolayer or multi-layer adsorptions were deduced.

Table3.2. Description of adsorption isotherm models and their parameters

	Isotherm	Expression	
1	Langmuir	$q_e = \dfrac{Q_o b C_e}{1 + b C_e}$	Q_o- Maximum adsorption capacity (mg g^{-1}) b- Langmuir equilibrium constant (L mg^{-1})
2	Freundlich	$q_e = K_F C_e^{\frac{1}{n}}$	K_F-Fruendlich constant (L g^{-1}) n- Fruendlich exponent
3	Redlich-Peterson	$q_e = \dfrac{K_R C_e}{1 + a_R C_e^{g}}$	K_R-Redlich-Peterson isotherm constant (L g^{-1}) a_R- Redlich-Peterson constant (L mg^{-1}) g- Redlich-Peterson model exponent
4	Sips	$q_e = \dfrac{K_s C_e^{\beta_s}}{1 + a_s C_e^{\beta_s}}$	K_s- Sips model isotherm constant (L g^{-1}) a_s- Sips model constant (L mg^{-1}) β_s- Sips model exponent

Isotherm parameters and error functions are calculated by nonlinear regression method using Microsoft excel solver. For each isotherm five error functions (Table 3.3) are calculated along with model parameters (Al-Ghouti et al. 2020). Generally lower error values and coefficient of determination near to unity indicates the best fitting isotherms. Even though isotherms were having similar coefficient of determination (R^2), the optimum isotherm was identified with lower error values as the best fitting isotherm (Figure 3.7). From the isotherm study and from the error analysis it was found out that, each adsorbate follows different isotherms. Methylene blue adsorption follows

Sips isotherm, predicting multi-layered adsorption and lead adsorption follows Langmuir isotherm.

Table 3.3. Error functions list

	Error function	Expression
1.	The Coefficient of determination	$$R^2 = \frac{\sum(q_{e,meas} - q_{e,calc})^2}{\sum(q_{e,meas} - q_{e,calc})^2 \sum(q_{e,meas} - q_{e,calc})^2}$$
2.	Nonlinear chi-square test	$$\chi^2 = \sum_{i=n}^{n} \frac{(q_{e,meas} - q_{e,calc})^2}{q_{e,meas}}$$
3.	Residual root mean square error	$$RMSE = \sqrt{\frac{1}{n-2} \sum_{i=n}^{n} (q_{e,meas} - q_{e,calc})^2}$$
4.	Marquardt's percent standard deviation	$$MPSD = 100 \sqrt{\frac{1}{n-p} \sum_{i=n}^{n} \left(\frac{q_{e,meas} - q_{e,calc}}{q_{e,meas}}\right)^2}$$
5.	Sum squares errors	$$ERRSQ = \sum_{i=1}^{n} (q_{e,meas} - q_{e,calc})^2$$

In the case of Methylene blue, the Sips exponential is 0.5790 indicating both Langmuir and Freundlich type of adsorption (Table 3.5a). For lead adsorption, both Redlich-Peterson and Sips isotherms were having higher regression coefficient values and lower error values. But the values of Redlich-Peterson exponent and Sips model exponent are more than unity, indicating both models are not suitable in explaining the adsorption process. Hence, from the experimental data, it can be concluded that adsorption of lead follows Langmuir isotherm (Table 3.5c). Whereas Cadmium adsorption was better explained by Redlich-Peterson isotherm showing both physical and chemisorption of

cadmium on adsorbent surface (Table 3.5b). The adsorption capacities were calculated from monolayer adsorption (q_m) from Langmuir equation. Dye removal capacity was quite higher than previously reports for multi solute adsorption system (Table 3.4).

Table 3.4. An overview of studies on multicomponent adsorption system and their performances

Sl No	Adsorbate	Adsorbent	Multicomponent adsorbate system	Maximum adsorption capacity mg.g^{-1}	Reference
1	MB Pb	Lignosulfonate	Pb+MB	132.6 64.9	Zhang et al. 2020
2	Cd	Fly ash	(Cu+Ni+Cd+MB)	6.36	Visa et al. 2010
3	MB Pb	Ruthenium nanoparticle-loaded activated carbon	Pb+MB	178.3 35.46	Mazaheri et al. 2015
4	Pb Cd	Mechanochemically Treated Montmorillonite /Kaolinite Clay	Pb+Cu+Zn+Cd	27.2 11.3	Kumric et al. 2013
5	Pb Cd	Ultrafine Mesoporous Magnetite Nanoparticles	Pb+Cd+Cu+Ni	85 79	Fato et al. 2019
6	MB	EDTA-modified bentonite	MB+Cu	160	De castro et al. 2018
7	MB Pb Cd	Zirconium metal-organic framework	MB+Pb+Cd	164 102 37	Presnt work

Table 3.5a. Isotherm constants and error values for nonlinear regression for Methylene blue

	Langmuir		Freundlich		Redlich-Peterson		Sips	
	Q_o	169.10	K_F	0.4590	K_R	35.284	K_s	18.552
	b	0.0538	$1/n$	21.159	a_R	1.1662	a_s	0.0426
	R2	0.9807	R2	0.9963	g	0.6145	β_s	0.5790
Methylene blue	$\chi 2$	0.1856	$\chi 2$	0.0352	R2	0.9971	R2	0.9975
	MPSD	0.5326	MPSD	0.2320	$\chi 2$	0.0279	$\chi 2$	0.02372
	RMSE	4.3545	RMSE	1.8967	MPSD	0.2208	MPSD	0.2036
	ERRSE	151.69	ERRSE	28.782	RMSE	1.6885	RMSE	1.5570
					ERRSE	22.808	ERRSE	19.395

Table 3.5b. Isotherm constants and error values for nonlinear regression for Cadmium

	Langmuir		Freundlich		Redlich-Peterson		Sips	
	Q_o	36.877	K_F	4.6531	K_R	1.3570	K_s	1.7486
	b	0.0340	$1/n$	0.4037	a_R	0.0435	a_s	0.0437
	R^2	0.9893	R^2	0.9799	g	0.9682	β_s	0.8807
Cadmium	χ^2	0.0116	χ^2	0.2209	R^2	0.9915	R^2	0.9919
	MPSD	0.4134	MPSD	0.7812	χ^2	0.0093	χ^2	0.0088
	RMSE	0.5478	RMSE	0.7531	MPSD	0.3527	MPSD	0.2463
	ERRSE	2.4014	ERRSE	4.5389	RMSE	0.5232	RMSE	0.4761
					ERRSE	0.1916	ERRSE	1.8136

Table 3.5c. Isotherm constants and error values for nonlinear regression for Lead

	Langmuir		Freundlich		Redlich-Peterson		Sips	
	Q_o	100.71	K_F	7.7564	K_R	2.4041	K_S	1.5080
	b	0.0273	$1/n$	0.5098	a_R	0.0100	a_S	0.0178
	R^2	0.9953	R^2	0.9727	g	1.1896	β_S	1.2383
Lead	χ^2	0.0202	χ^2	0.1180	R^2	0.9979	R^2	0.9981
	MPSD	0.7170	MPSD	4.1752	χ^2	0.0086	χ^2	0.0080
	RMSE	1.0734	RMSE	2.590	MPSD	0.3279	MPSD	0.1593
	ERRSE	9.2175	ERRSE	53.670	RMSE	0.7505	RMSE	0.6772
					ERRSE	3.9434	ERRSE	3.6691
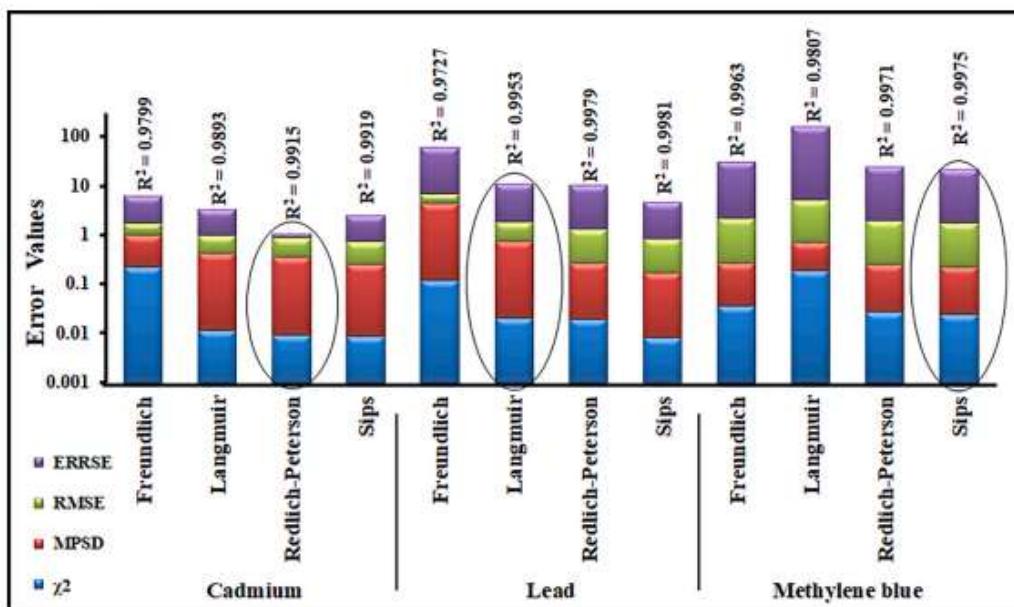
Figure 3.7. Representation of total error values and coefficient variation for each adsorbate and their isotherms

3.4.8 Kinetic modeling of the adsorption process

It is fundamental to know the kinetics of an adsorption process for predicting and designing industrial sorption systems (Subrmanyam and Das 2009). Adsorption isotherms reveal the extent of adsorption but to understand the mechanism and time required to reach this extent, it is essential to study the kinetics of adsorption.

Table 3.6. List of kinetic models

1.	Kinetic model	Expression	
2.	Pseudo first order kinetics	$q = q_e(1 - e^{-k_1 t})$	k_1-Rate of adsorption (min^{-1})
3.	Pseudo second order kinetics	$q = \dfrac{k_2 q_e^2 t}{1 + k_2 q_e t}$	k_2- Rate of adsorption (g mg^{-1} min^{-1})
4.	Elovich model	$q = \left(\dfrac{1}{\beta}\right)\ln(1 + \alpha\beta t)$	α- Initial sorption rate (mg g^{-1} min^{-1}) β-related to the extent of surface coverage and activation energy for chemisorption (g mg^{-1})
5.	Weber- moris model	$q = k_{id}\sqrt{t} + B$	k_{id}-rate coefficient (mg g^{-1} min$^{-1/2}$) B-thickness of the boundary layer

To understand the kinetics of adsorption, four different models were studied as listed in table 3.6. Usually, adsorption proceeds with four main steps (Tan and Hameed 2017).

- i) Transport in the bulk solution.
- ii) Diffusion from the bulk through the liquid film.
- iii) Diffusion of adsorbate into the adsorbent i.e. intraparticle diffusion and finally,
- iv) Chemical reaction between adsorbate and adsorbent.

The slowest of the above four steps is the rate determining step which depends on adsorbate-adsorbent properties and experimental condition. The regression coefficient value (R^2) obtained from graph is used to testfy and understand the successfulness of a kinetic model in explaining adsorption process. The experimental results along with regression coefficient values were listed in table 3.7.

Table 3.7. Kinetics parameters and coefficient of variation from experimental result

Kinetic Model	Parameters	MB	Pb	Cd
Pseudo first order kinetics	q_e(calculated) (mg g^{-1})	31.36	12.94	8.30
	k_1(min^{-1})	0.2508	0.1153	0.0774
	R^2	0.9991	0.9979	0.9914
Pseudo-Second order kinetic model	q_e(calculated) (mg g^{-1})	33.40	13.80	8.98
	k_2 (g mg^{-1} min^{-1})	0.0125	0.0144	0.0134
	R^2	0.9976	0.9994	0.9976
Elovich model	ß	0.3908	0.6803	0.7876
	α	9135.4	95.902	7.4766
	R^2	0.9998	0.9960	0.9986
Inter particle diffusion model (Weber- moris model)	k_{id} (mg g^{-1} min$^{-1/2}$)	1.451	0.6225	0.5149
	Intercept B	17.47	6.1831	2.484
	R^2	0.9516	0.9507	0.9557

q_e experimentally determined = 35.13 (mg g^{-1}) for MB, 9.05 (mg g^{-1}) for Cadmium and 13.5 (mg g^{-1}) for Lead. Test conditions; C_o=20 mg L^{-1}, pH 7, T=25 °C.

From the experimental data, methylene blue and cadmium follows Elovich model, which implies adsorption on heterogeneous system. Lead follows pseudo second model having chemisorption on homogeneous system. Intraparticle diffusion model (IPD) was also fitted with experimental results. Since the pore sizes were very narrow, it is quite difficult for the dye molecules to get adsorb inside the pores of MOF but for heavy metals being smaller can migrate through pores and adsorb (Qiu et al 2017). If kinetics is solely controlled by intraparticle diffusion model, then a plot of q vs.$\sqrt{t}$ should be linear and pass through the origin (B=0). B value corresponds to

boundary thickness. Larger the B value more will be the film diffusion resistance (Weber and Morris 1963). From the table 3.7, it can be inferring that IPD is not the rate controlling mechanism. Boundary layer diffusion seems to be the rate controlling step for MB adsorption. In case of lead and cadmium, B values were lesser compared to MB and exist two kinds of adsorption. First one with slow increase in adsorption is due to pore filling followed by surface adsorption. Introduction of hierarchical pore system in the MOF structure can reduce the resistance of intraparticle diffusion and enhance the adsorption of adsorbates by pore diffusion (Al-Jubouri et al. 2018). Such multi-level porosity in MOFs can introduced by using mixed ligand strategy (Pullen and Clever 2018) or by introducing defects in MOF (Cai and Jiang 2017).
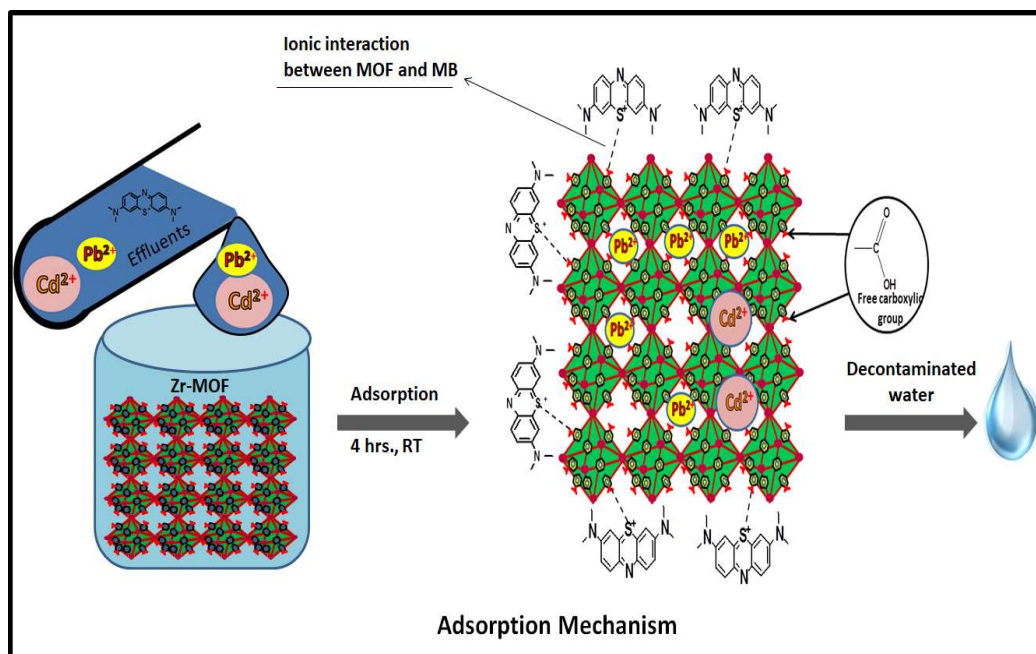
Figure 3.8. Adsorption mechanism of multiple components on Zr-MOF

3.4.9 Adsorption mechanism

From the experimental results, information regarding adsorption mechanism can be inferred and illustrated in figure 3.8. Methylene blue being bigger molecule cannot penetrate inside the pores of MOF. But due the ionic nature, it can interact strongly and adsorbs on the surface MOF. Hence, fast and maximum dye adsorption takes place. Although lead ions can make favourable adsorption due to their smaller

size and lower hydration energy but presence of dye molecules hinders the process of lead adsorption. Cadmium ions adsorbs less favourably as compared to MB and lead ions, due their bigger size and feeble interaction with the adsorbent.

3.5 ADSORBENT REUSABILITY STUDIES

The easy and effective regeneration capacity of adsorbent is an important indicator for its application in industrial process. After the adsorption, MOF was washed twice with acidified methanol (0.025 N HCl in methanol and 5 mL for 100 mg of adsorbate) by shaking 30 min at room temperature each time, dried and then used to explore the reusability of the MOF. It was found that during three cycles of studies (reused methanol from previous regenerations) the slight reduction in the dye removal efficiency of the adsorbent observed as shown in figure 3.9. This may be due to disintegration MOF structure during the washing process. From the results, it shows that the acidified methanolic treatment can be used for adsorbent regeneration with adsorbent removal efficiency after three cycle was econamical.
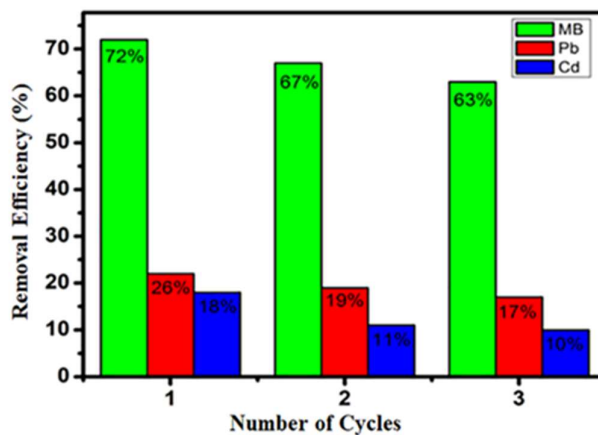
Figure 3.9. Regeneration studies of MOF adsorbent

3.6 Conclusions

Based on previous literature, here we extended the greener method for the hydrothermal synthesis of UiO-66 (COOH)$_2$ MOF using easily available zirconium chloride salt with

BETC ligand and acetic acid as modulator. Presence of water soluble acid modulator is necessary for crystal phase formation as it competes with other ligands during framework formation and alters the rate of reaction facilitating crystalline phase formation. Temperature also affects the rate of product formation, optimum temperature for hydrothermal synthesis is 130 °C. This method is environmentally benign and can be scaled up to multi gram level. Presence of free carboxylic groups in the framework amplifies the properties of MOF for wide range of applications. This metal-organic framework with free carboxyl group synthesized from 1,2,4,5-benzentetracarboxylic acid was utilized to adsorb MB dye and heavy metals simultaneously from aqueous solution. The zeta potential value at neutral pH is -7.7 mV, which reveals anionic nature of the MOF at workable pH, enhancing the ability of MOF to interact strongly and hold the adsorbate. Higher concentration of adsorbate molecule in the solution increases the probability of interaction and hence adsorption increases with increase in initial concentration. Maximum dye adsorption (up to 55%) at initial 30 min is due to ionic interaction between adsorbate-adsorbent. Size of the hydrated heavy metal ions plays important role along with functional group present in the adsorbent in increasing removal efficiency. Lead ions adsorbs favourably than cadmium because of their small sized hydrated ion and lower hydration energy. The adsorption studies showed maximum adsorption capacities per gram of adsorbent compared to earlier reports. Adsorption capacity of the adsorbent for cadmium, lead and methylene blue were found to be 37 mg g^{-1}, 100 mg g^{-1} and 169 mg g^{-1} respectively. The regeneration studies were carried out by simple washing treatment, and adsorption efficiency reduced slightly after three adsorption cycles indicating easiness of reuse. Thus, efficient green route synthesized Zr-MOF was utilized for removing MB, cadmium and lead metal ions from aqueous solution.

CHAPTER 4

SYNTHESIS AND APPLICATION OF Zr-METAL-ORGANIC FRAMEWORK FOR SIMULTANEOUS DETECTION AND RAPID ADSORPTION OF p-NITROPHENOL FROM WATER

Abstract: This chapter reports synthesis of a smart and stable zirconium-based UiO-66 type metal-organic framework from mixed ligand strategy and its structural analysis by various techniques along with its application in simultaneous detection and adsorptive removal of p-nitrophenol from the aqueous solution.

4.1 INTRODUCTION

Phenol and its allied compounds are considered to be toxic, long term exposure to high levels can cause skin, liver damage, and heart diseases (Busca et al. 2008, Zhang et al. 2012). Most of the industrial effluents from petrochemicals, drugs, coal, steel, and plastic contain phenol derivatives. The p-nitrophenol is a prime raw material in the manufacturing of paracetamol drug, used for treating pain and fever and also mixed with other drugs. It is also included in the list of most essential medicines by World Health Organization (WHO). China and India are the two biggest producers and consumers of paracetamol followed by the USA. Industrially paracetamol was synthesized by nitrating phenol followed by reduction of p-nitro group into Amine. Thus p-nitrophenol is the major pollutant coming from the paracetamol industry. Apart from this p-nitrophenol is also used in the manufacturing of fungicides and insecticides such as methyl and ethyl parathion. The presence of p-nitrophenol in the air and water can cause damage to the environment and to human health (Uberoi and Bhattachrya 1997). The p-nitrophenol is classified as a hazardous substance by United States Environmental Protection Agency (USEPA) because of its stability in the environmental condition to transport long distances and pollute groundwater resources and soil. Nose irritation, inflammation to eyes and respiratory tract and when it interacts with blood causes methemoglobinemia, these are few examples of nitrophenol exposure (Ofomaja and Unuabonah 2011, Al-asheh et al. 2004). Due to this toxicity environmental regulatory agencies fixed the allowable limit of phenol and its derivatives in drinking water to 1 ppm (Liu et al. 2014) Hence, it is very important to detect easily and remove nitrophenol from industrial effluents.

4.2 STRATEGY AND OBJECTIVES

The smart adsorbents, which can detect and adsorb pollutants simultaneously is the pressing priority in the field of environmental monitoring. Such attainment has tremendous effect on improving human health and environmental protection. Often industrial remediation operations require fast and easy detection of adsorbates to speed up the treatment cycles (Kumar et al. 2007, Pan et al. 2007). Hence a simple method needs to be developed for removal and easy detection of nitrophenol from water. Detection methods based on the fluorescence principle are of great interest because of their flexibility of operation in the solid and solution phase, short response time, high sensitivity and fluorescence-based instrumental can be made portable (Xin et al. 2012). Highly ordered porous structure and adjustable pore environment along with flexibility in the application of ligands for building frameworks made metal-organic framework materials as most desirable candidates for various applications (Kuppler et al. 2009). Due to higher surface area and the possibility of engineering the pore structure, MOFs were extensively researched for adsorption applications (Khan et al. 2013 Hasan and Jhung 2015, Li et al. 2018). The incorporation of specifically designed ligands in the framework will enhance the desirable adsorptive property (Lin et al. 2015). The present work focus on the synthesis of novel fluorescence active zirconium based UiO-66 type MOF using 1,4-Benzenedicarboxylic acid and in-house synthesized photoluminescence active ligand.

4.3. MATERIALS AND METHODS

4.3.1 Materials

1,4-Benzenedicarboxylic acid (BDC, Terephthalic acid), 4-Aminobenzoic acid were purchased from sigma Aldrich, India. Zirconium chloride, 4-Fluorobenzonitrile and Cesium fluoride, DMF and p-nitrophenol were procured from Alfa aesar, India.

4.3.2 Synthesis of trifunctional ligand (H₃ntb)

The trifunctional carboxylic ligand (H₃ntb) 4,4',4''-Nitrilotrisbenzoic acid was prepared from the slight modified reported procedure (Liou et al. 2005).1.5 g of 4-Aminobenzoic acid and 2.649 g (2 Eq) of 4-Fluorobenzonitrile along with 4.98 g of

Cesium fluoride was taken in a round bottom flask in 75 ml of DMF and refluxed for 48 hrs at 170 °C, the reaction was monitored by TLC, later DMF was evaporated and diluted with water and the product was extracted with ethyl acetate. Column purification was done by eluting with 80:20 petroleum ether and ethyl acetate solution to remove impurities. The compound obtained after purification was taken for alkaline hydrolysis and refluxed for 24 hrs with KOH and the reaction was monitored by TLC. After the reaction completion, ethanol was evaporated and acidified the reaction mixture to obtain off white solid, which was washed with water and ethanol, dried in a hot air oven at 60 °C overnight. 1H NMR (400 MHZ, [D6] DMSO, 25 °C, δ in ppm) 7.1(m, 6H, CH_2, JH,H = 8.4 Hz), δ 7.9 (m, 6H, CH_2, JH,H = 8.4 Hz), δ 12.9 (s, 3H, OH). ESI-MS: $C_{21}H_{12}NO_6$ (M+), Calculated (deprotonated) 374.07, Found- 374.15.
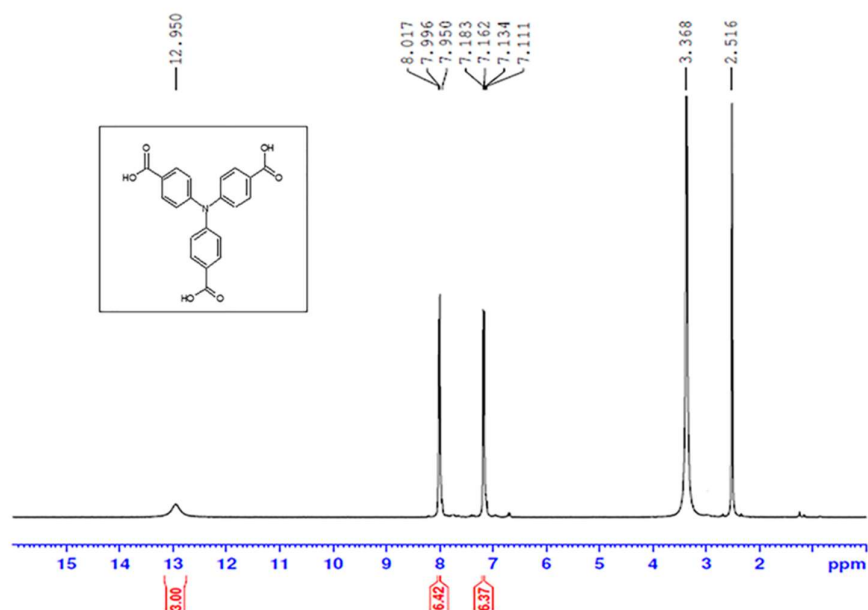
Figure 4.1. NMR spectra of in-house synthesised ligand H_3ntb

4.3.3 Synthesis of Zr-MOF

The ligand obtained from the above was alone used to synthesize the MOF but no product was obtained probably due to constrains in the geometrical arrangement for framework structure formation. Therefore, the in-house synthesised ligand (H_3ntb) was

used (10-30% replacement with BDC on mol basis) as an auxiliary ligand along with 1,4-Benzenedicarboxylic acid. The procedure is as follows, ZrCl4 0.5 g and 1,4-Benzenedicarboxylic acid 495 g and 10-30 % trifunctional synthetic ligand (H3ntb) and 1 ml concentrated HCl in 20 ml DMF in a glass vial heated to 120 °C for 24 hr to obtain powder product. Which was filtered, washed with water, acetone and dried at 60 °C overnight under vacuum (Katz et al. 2013). In each case UiO-66 MOF was formed and Powder X-Ray Diffraction (PXRD) matches well with the pattern of UiO-66 along with fluorescence activity. The products obtained are named on the basis of percent of auxiliary ligand (BDC) used (Table 4.1).

Table 4.1. Synthesis design and zeta potential along with pore size analysis of MOFs.

| MOF | Ligands | | Zeta potential | BJH pore size analysis | |
	BDC	H3tnb		Pore distribution peak	Pore volume
UiO-66 MOF-1	100 %	0 %	32.8 mV	2.43 nm	0.04973 $cm^3.g^{-1}$
UiO-66 MOF-2	90 %	10 %	25.4 mV	2.43 nm	0.05326 $cm^3.g^{-1}$
UiO-66 MOF-3	80 %	20 %	26.3 mV	2.43 nm	0.05027 $cm^3.g^{-1}$
UiO-66 MOF-4	70 %	30 %	29.5 mV	2.43 nm	0.05160 $cm^3.g^{-1}$

4.3.4 Characterization

The crystal structure of the MOF was determined by using an X-ray diffractometer (XRD, Rigaku) with monochromatic Cu-Kα radiation (λ= 0.154 nm) at a scan rate of 2° per minute in the range of 5-60. Brunauer–Emmett–Teller (BET) surface area measurements were conducted by BELSORP-minill instrument. Before the analysis, the sample was degasified for 12 h at 120 °C. Fourier Transform Infrared Spectroscopy (FTIR spectra) of the sample were recorded using Perkin Elmer spectrum 100 analyser by preparing the sample and KBr pellets. Zeta potential measurement carried out by Horiba Scientific (nanopartica) nanoparticle analyser at neutral pH. p-nitrophenol concentration was analysed by shimadzo HPLC equipped with UV-visible detector and Shim-pack GWS column (5 μm, C18). Kratos XSAM800 spectrometer equipped with Al K$_α$ source used for X-ray photoelectron spectroscopy (XPS) analysis.

4.3.5 Adsorption experiments

A batch experiments consisting of concentration of 2-20 ppm solution adsorbate and adsorbent dosage (UiO-66 MOF-2) of 0.25 g L^{-1} was taken for adsorption isotherm studies and 20 mg L^{-1} adsorbate solution was fixed for kinetics studies at 25 °C. A 1000 ppm stock solution of p-nitrophenol was prepared by deionized water and subsequent dilution were made from this solution. The concentration of the solute was analysed by HPLC instrument equipped with UV-visible detector. The mobile phase was (60+40) cm^3 (methanol + water), and the flow rate was 1.0 cm^3 min^{-1}. The temperature of the column was maintained 25 °C and the p-nitrophenol was detected at 270 nm (Liu et al. 2014). All the experiments were conducted at neutral pH. Before the adsorption studies, MOF adsorbate was dried overnight at 60 °C. The amount of adsorption at equilibrium, q_e (mg g^{-1}), was calculated by equation (4.1) (Ghosal and Gupta 2015):

$$q_e = \frac{(C_o - C_e)V}{W} \qquad (4.1)$$

Where C_o and C_e are the initial and equilibrium adsorbate concentration (mg L^{-1}) respectively. V is the volume of the solution (L) and W is the mass of dry adsorbent used (g). Kinetic experiments were similar to those of equilibrium tests. The concentrations of p-nitrophenol from the aqueous samples were measured at different time intervals. The amount of adsorption at time t, q_t (mg g^{-1}), was calculated by equation 4.2 :

$$q_t = \frac{(C_o - C_t)V}{W} \qquad (4.2)$$

4.4 RESULTS AND DISCUSSION

4.4.1 Characterization MOF

Zirconium and Terephthalic acid (1,4-Benzenedicarboxylic acid) based MOF (UiO-66) was first synthesized by Cavaka and others (Cavaka et al. 2008). Due to the high

thermal and chemical stability, this MOF was researched for numerous versatile applications (Zou and Liu 2019). Its structure was well established by a number of techniques (Valenzano et al. 2011). The inner core of UiO-66 contains six zirconium atoms forming Zr_6-octahedron. Each zirconium atom is eight-coordinated in square antiprismatic fashion with eight-oxygen atoms, where four of which from carboxylate and the other four from μ_3-O and μ_3-OH atoms. Formation of the Zr_6-Octahedron was reported earlier with monocarboxylic acids as an isolated cluster (Reza et al 1999).
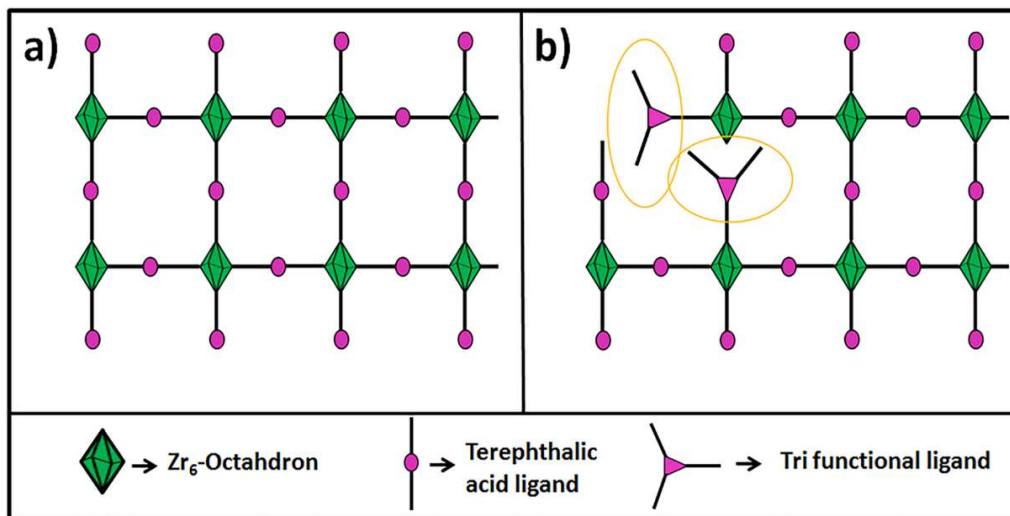
Figure 4.2. Schematic two-dimensional representation of (a) MOF formation with only BDC ligand (b) MOF formation with BDC and trifunctional ligand (For illustration purpose few of Zr_6-octahedron and Carboxylic linkages are omitted)

Terephthalic acid acts a bridge to connect this Zr_6-octahedron core-forming three-dimensional FCC structure (Figure 4.2a). Replacing the planer ligand like Terephthalic acid with trifunctional ligand (H_3ntb), which is trigonal bipyramid geometrical structure and having carboxylate groups in the twisted plane will not facilitate to produce crystalline structure because of geometrical constrain to form the framework. Hence no product obtained when ligand (H_3ntb) alone was used. To incorporate this ligand inside the framework, a mixed ligand strategy was employed and used as an auxiliary ligand with Terephthalic acid. The product obtained was crystalline and powder X-ray diffraction (PXRD) peaks confirm the FCC structure as UiO-66 along with fluorescence activity, which shows that ligand (H_3ntb) is also part

of the framework. Further to this, it can also be concluded that since not being a planer molecule when the ligand (H₃ntb) forms bonding with zirconium cluster it prevents the framework to grow further to it (Figure 4.2b). This shows that, the ligand (H₃ntb) always lies outside the framework and its likeliness of interaction with the adsorbate molecule is more (Figure 4.3).
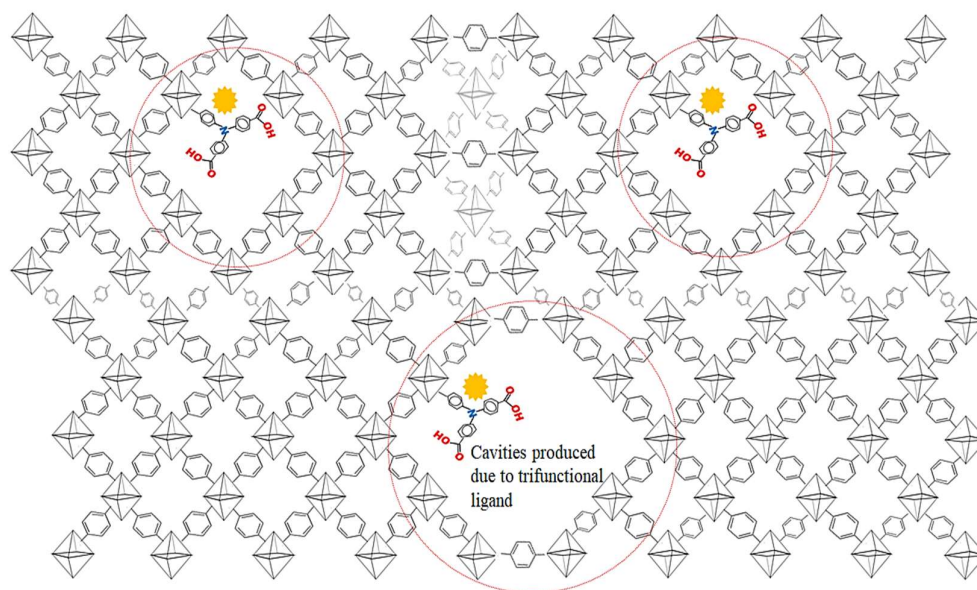
Figure 4.3. Representation of synthesised metal-organic framework with the cavities formed due to trifunctional ligand

The PXRD peaks of the synthesized MOFs are in accordance with the patterns of UiO-66, which confirms the crystal structure along with the FCC lattice (Figure 4.4a). It also clear that even with up to 30% replacement of Terephthalic acid, the formation of UiO-66 MOF structure prevails. This shows the robust nature of UiO-66 formation. Thermo gravimetric analyses were conducted to understand the effect of ligand replacement on structural stability at higher temperatures (Figure 4.4b). From the studies, it was observed that, at all concentrations of the auxiliary ligand, weight loss followed a similar kind of degradation. But as the ligand replacement increases the structural disintegration (weight loss) is more at the same temperature.
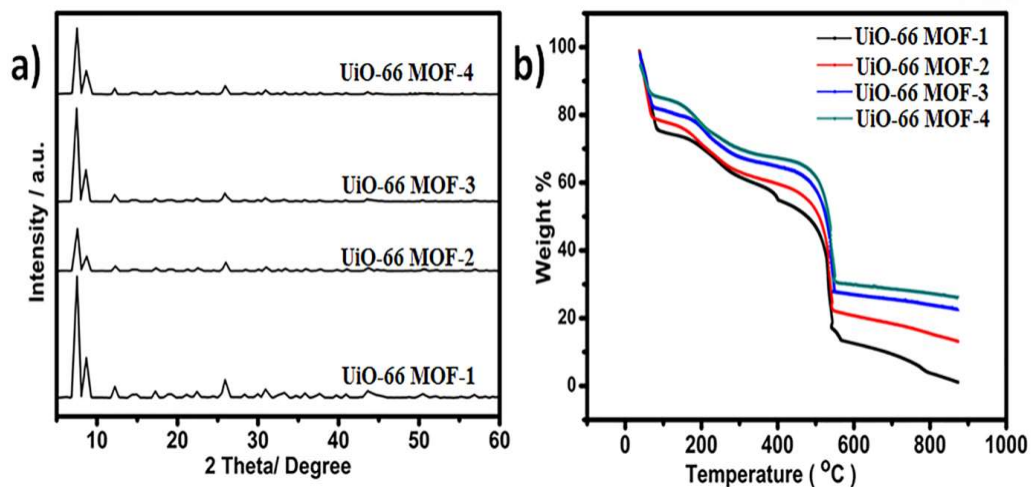
Figure 4.4. (a) PXRD spectra of synthesized MOFs (b) TGA spectra of synthesized MOFs

This behaviour of faster structural disintegration at same temperatures attributed to increases in the structural defects with the increase in trifunctional ligand concentration. Based on the TGA results UiO-66 MOF-2 was chosen for adsorption and fluorescence studies. Because among the other MOFs synthesised UiO-66 MOF-2 (with 10% BDC ligand replacement) was as stable as UiO-66 MOF-1(with only BDC ligands) in addition to displaying fluorescence activity.

The FTIR spectra (Figure 4.5) reveal the presence of a tertiary amine group in the framework at 1251 cm^{-1}. Although the signal is very weak, as the ligand concentration increases, the band starts appearing clearly (Inset of figure 4.5). Apart from this FTIR confirms the presence of regular bands of MOFs metal-carboxylic bonds. The band at 1400 cm^{-1} and 1580 cm^{-1} corresponds to carboxyl symmetric and asymmetric stretching bonded to zirconium. The band at 1511 cm^{-1} is from aromatic C=C vibration of benzene ring. The bands around 813, 750, and 550 cm^{-1} are associated with C-H vibration, O-H bending and Zr-(OC) asymmetric stretching. The bands of μ_3-O stretch and μ_3-OH stretch are appearing at 657 and 474 cm^{-1} respectively. Surface area and pore distribution were calculated by N$_2$ adsorption-desorption isotherm (Figure 4.6 (a)). The isotherm obtained is a hybrid kind of I/IV nature, indicates the presence of micro and mesopores. The existence of pore condensation was indicated by the formation of hysteresis at p/p^o =1, from this data BHJ pore distribution curve was plotted (Figure 4.6

b). BJH plots (Table 4.1) revealed a similar kind of pore distribution pattern in all the MOFs suggesting that, the addition of trifunctional ligand does not alter the internal pore structure. This also supports that the trifunctional ligands present only at the outer surface of the framework. BET surface area obtained (Inset of figure 4.6b) from N_2 isotherm decreases from UiO-66 MOF-1 to UiO-66 MOF-4 reflects that as the concentration of trifunctional ligand increases surface area decreases because of its size as compared to Terephthalic acid.

Zeta potential measurements were conducted to explore the surface charge properties of MOFs. Since the MOFs were synthesized by acid promoted procedure, it possesses positively charged surface. But the introduction of a ligand having multiple free carboxylic groups decreases this density. As a result, zeta potential values shift towards the lower side (Table 4.1). MOF synthesized from Terephthalic acid alone showed a Zeta potential of 32.6 mV whereas UiO-66 MOF-2 with 10 % trifunctional ligand loaded MOF showed 27.3 mV.
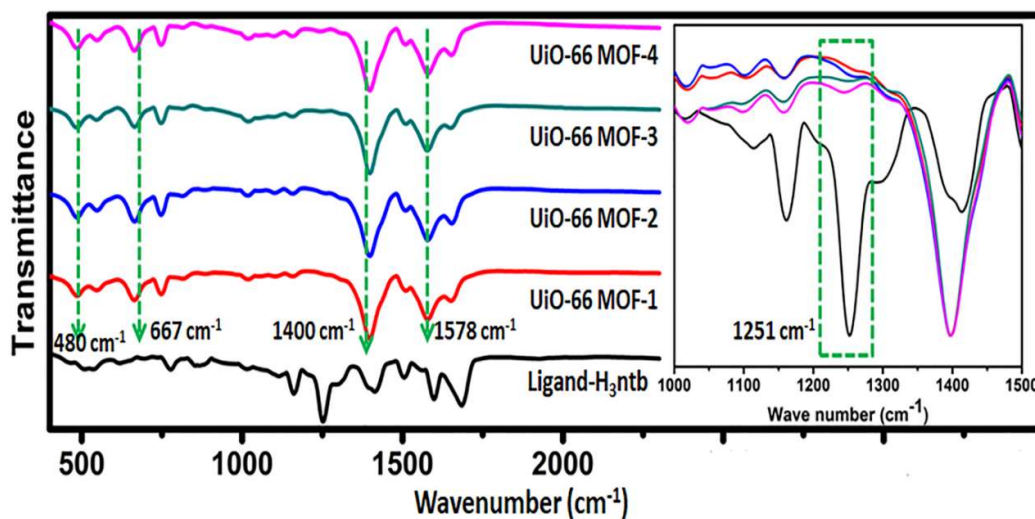
Figure 4.5. FTIR spectra of MOFs and Trifunctional ligand-H_3ntb, (inset-amine group peak)
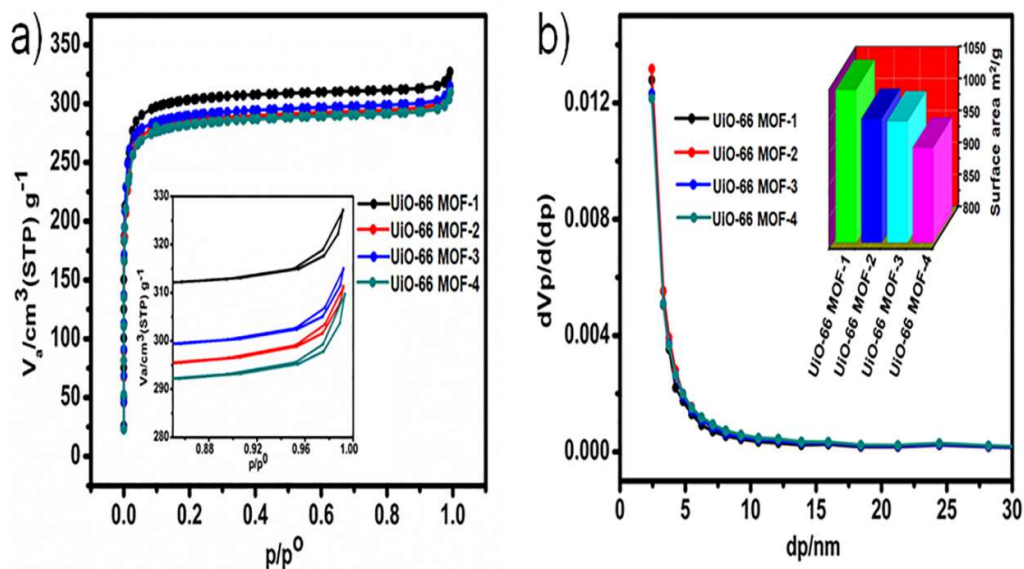
Figure 4.6. (a) N$_2$ adsorption-desorption isotherms of MOFs, (inset-hysteresis at p/p^o =1) (b) BJH pore plot of MOFs (inset-BET surface area of MOFs)

4.4.2 Photoluminescence studies

The dried MOF when dispersed in water shows strong fluorescence when excited at 297 nm (UV-visible spectra of the MOF, figure 4.7). To determine the sensing ability of the MOF, trace amount of p-nitrophenol was added to the MOF dispersed in water solution and decrease in fluorescence intensity were measured at 590 nm. To explore and to understand the potential application of MOF to detect p-nitrophenol in an aqueous solution, fluorescence quenching titrations were performed with the graduate addition of an aqueous solution of p-nitrophenol.

In the fluorescence experiment, 1 mg of UiO-66 MOF-2 (synthesised with 10% of H$_3$ntb) was dispersed in 2 ml of deionized water in a cuvette. An aqueous solution containing 1000 mg L^{-1} of p-nitrophenol was prepared in deionized water and subsequent dilution were made from this solution and used for the quenching experiments. The fluorescence response upon excitation at 297 nm was monitored in-situ after the gradual addition of p-nitrophenol solution (100 mg L^{-1}) and resultant fluorescence intensity was measured at 590 nm. As expected the addition of p-nitrophenol results in efficient and swift fluorescence quenching of 90%. In the figure

4.8(a&b) shows the changes in the intensity of fluorescence with the incremental addition of nitrophenol. The MOF was able to show prominent fluorescence response to p-nitrophenol at a concentration of as low as 34.21 μM. This clearly indicates the superior quenching ability of nitrophenol in fluorescence MOF. The Stern-Volmer plot (Figure 4.8.c) , allow us to calculate the quenching constants and to examine the quenching efficiency using the equation $\frac{I}{Io} = Ksv[A] + 1$, where I and Io are the fluorescence intensities before and after the addition of p-nitrophenol and [A] molar concentration of p-nitrophenol, Ksv quenching constant in M^{-1}.
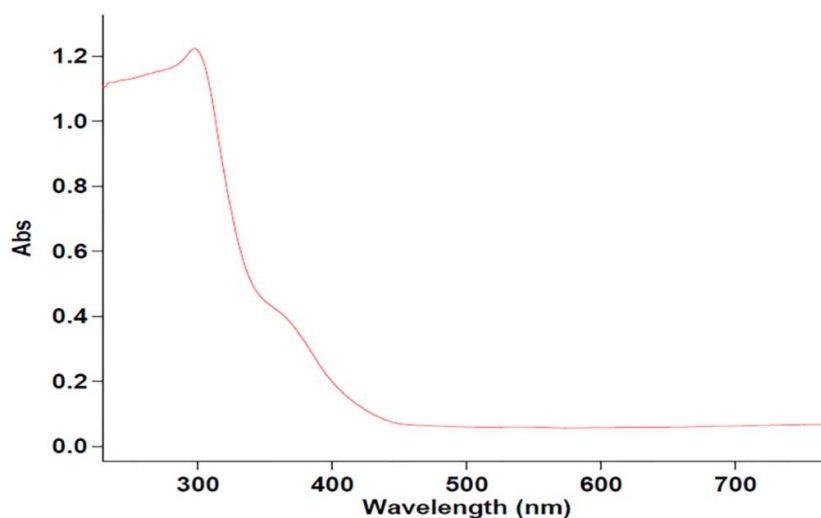
Figure 4.7. UV-vis spectra of synthesized UiO-66 MOF 2

At low concentration a linear increase can be seen in the Stern-Volmer plot but as the concentration increases, the upward bending of the curve is observed. This kind of non-linearity is due to a combination of static and dynamic quenching processes between MOF and p-nitrophenol. After fitting the Stern-Volmer plot, quenching constant 3.5297×10^4 M^{-1} obtained.

Since there is no spectral overlap between absorption spectra of p-nitrophenol and the emission spectrum of MOF, it can be concluded that, there is no resonance energy transfer mechanism that occurs in fluorescence quenching. Instead, the upward bending curve by Stern-Volmer plot indicates quenching by sphere of action mechanism, where

83

fluorophore and quencher do not actually form a ground-state complex (Melavanki et al. 2009). When the quencher p-nitrophenol molecules are adjacent to fluorescence active ligand situated at the outer layer of the framework makes it easier to establish a closely spaced fluorophore-quencher pair for quenching at the moment of excitation.
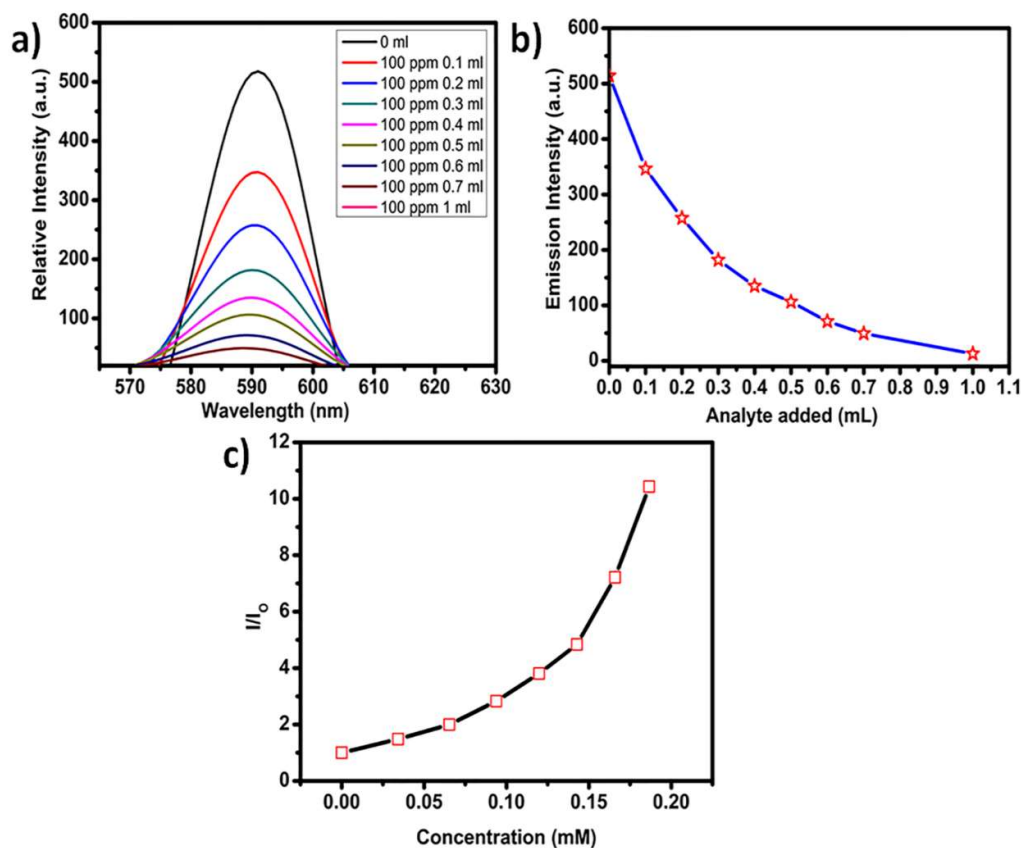
Figure 4.8. (a) Change in the fluorescence intensity of MOF on incremental addition of p-nitrophenol solution (100 ppm) (b) Decrease in fluorescence intensity on the addition of p-nitrophenol. (c) Stern-Volmer plot of p-nitrophenol added to MOF in water

4.4.3 Adsorption Isotherms

To explore and gather more information on the distribution of solute particles over adsorbent, five isotherms (Isotherm model and their parameters are given in Table 4.2), Langmuir, Freundlich, Dubinin-Radushkevich, Redlich-Peterson and Sips models were fitted with experimental data. From the isotherm analysis, the information on maximum

adsorption capacity, adsorption mechanism, physisorption or chemisorption, monolayer or multi-layer adsorptions were deduced.

Table 4.2. Description of adsorption isotherm models and their parameters.

	Isotherm	Expression	
1.	Langmuir	$q_e = \dfrac{Q_o b C_e}{1 + b C_e}$	Q_o- Maximum adsorption capacity (mg g^{-1}) b- Langmuir equilibrium constant (L mg^{-1})
2.	Freundlich	$q_e = K_F C_e^{\frac{1}{n}}$	K_F-Fruendlich constant (L g^{-1}) n- Fruendlich exponent
3.	Dubinin-Radushkevich	$q_e = q_s e^{-k_{ad}\varepsilon^2}$	q_s- Dubinin-Radushkevich model constant (mg g^{-1}) k_{ad}- Dubinin-Radushkevich model constant (mol^2 kJ^{-2}) E- mean free energy (kJ mol^{-1})
4.	Redlich-Peterson	$q_e = \dfrac{K_R C_e}{1 + a_R C_e^{g}}$	K_R-Redlich-Peterson isotherm constant (L g^{-1}) a_R- Redlich-Peterson constant (L mg^{-1}) g- Redlich-Peterson model exponent
5.	Sips	$q_e = \dfrac{K_s C_e^{\beta_s}}{1 + a_s C_e^{\beta_s}}$	K_s- Sips model isotherm constant (L g^{-1}) a_s- Sips model constant (L mg^{-1}) β_s- Sips model exponent

Isotherm parameters and error functions (Error functions and their expression are given in Table 4.3) are calculated by the nonlinear regression method using Microsoft excel, solver. For each isotherm, five sets of error functions are calculated along with model parameters. Langmuir adsorption model theoretically assumes the formation of monolayer adsorption of the sorbent molecules, occurring at a finite delocalised site of the adsorbent. Freundlich isotherm is an empirical model and extensively used for heterogeneous adsorption. Redlich-Peterson isotherm combines the Langmuir and Freundlich model and can be applied for homogenous and heterogonous adsorption systems. At high concentration the Redlich-Peterson model approaches to Freundlich model and at low concentration to Langmuir isotherm. Sips isotherm is hybrid form of Langmuir and Freundlich isotherms model and Sips model exponent gives nature of adsorption.

Dubinin-Radushkevich isotherm gives insight into whether the adsorption is physical or chemical in nature. The mean free energy (E) was calculated by the equation (4.3) below and tells the nature of adsorption.

$$E = \frac{1}{\sqrt{2k_{ad}}} \qquad (4.3)$$

The value of E < 8 kJ mol^{-1} indicates physical and 8 to 16 kJ mol^{-1} indicate chemical interaction of adsorbate with the adsorbent. The mean free energy obtained from isotherm studies was 7.68 kJ mol^{-1}, which shows the interaction is Physico-chemical in nature.

Generally, lower error values and coefficient variation near to unity indicate the best fitting isotherms. Even though isotherms were having a similar coefficient of determination (R^2), lower error values were chosen as the best fitting isotherm (Figure 4.9), hence based on these results Langmuir isotherm isotherms fit well with the experiment data (Al-ghouti et al. 2020). The Redlich-Peterson model exponent (g) value is more than to one indicating the adsorption is having Langmuir nature with monolayer formation of adsorbate molecules. Isotherm constants and error values for non-linear regression analysis obtained from experimental results are listed in table 4.4

and 4.5. XPS analysis of the adsorbent before and after adsorption was conducted to understand the mechanism of interaction between adsorbate and adsorbent. The high-resolution XPS spectra of O 1s show two peaks at 529.5 eV and 532.5 eV (Figure 4.10 a & b).

Table 4.3.   List of error functions used for isotherm evaluation.

Error function	Expression
1. The Coefficient of determination (R^2)	$R^2 = \dfrac{\Sigma(q_{e,meas}- q_{e,calc})^2}{\Sigma(q_{e,meas}- q_{e,calc})^2 \, \Sigma(q_{e,meas}- q_{e,calc})^2}$
2. Nonlinear chi-square test ($\chi 2$)	$\chi^2 = \displaystyle\sum_{i=n}^{n} \dfrac{(q_{e,meas}- q_{e,calc})^2}{q_{e,meas}}$
3. Residual root mean square error (RMSE)	$RMSE = \sqrt{\dfrac{1}{n}\displaystyle\sum_{i=n}^{n}(q_{e,meas}- q_{e,calc})^2}$
4. Marquardt's percent standard Deviation (MPSD)	$MPSD = 100\sqrt{\dfrac{1}{n-p}\displaystyle\sum_{i=n}^{n}\left(\dfrac{q_{e,meas}- q_{e,calc}}{q_{e,meas}}\right)^2}$
5. Sum squares errors (ERRSQ)	$ERRSQ = \displaystyle\sum_{i=1}^{n}(q_{e,meas}- q_{e,calc})^2$

These peaks are assigned to the Bridging linked carboxylate group and coordinated free carboxylic acid group. Hence, it confirmed the presence of free carboxylic groups from the Terephthalic acid and trifunctional ligand in the framework and they are holding firmly to the framework. The presence of a small hump at 406 eV in the after adsorption N 1s spectrum (Figure 4.10c) represents the nitro group, which is an evidence for the loading of p-nitrophenol on MOF. Apart from this, the presence of all the peaks before and after adsorption (Figure 4.10d) confirms the intactness of the framework structure during adsorption process

Table 4.4. Isotherm constants and error values for nonlinear regression for two parameter isotherms.

Langmuir	Q_o	b	R^2	χ^2	MPSD	RMSE	ERRSE
isotherm	62.48	0.0319	0.9974	0.0048	0.1727	0.2173	0.5891
Freundlich	K_F	$1/n$	R^2	χ^2	MPSD	RMSE	ERRSE
isotherm	2.416	0.7898	0.9952	0.009	0.3176	0.3677	1.0821
Dubinin-Radushkevich	q_s	k_{ad}	E	R^2	χ^2	MPSD	RMSE	ERRSE
isotherm	256.03	0.0085	7.68	0.9971	0.0054	0.192	0.29	0.655

Table 4.5. Isotherm constants and error values for nonlinear regression for three parameter isotherms.

Redlich -Peterson	K_R	a_R	g	R^2	χ^2	MPSD	RMSE	ERRSE
isotherm	1.924	0.0198	1.137	0.9974	0.0048	0.1808	0.2870	0.0.5769
Sips	K_s	a_s	β_s	R^2	χ^2	MPSD	RMSE	ERRSE
isotherm	1.887	0.0349	1.047	0.9975	0.0047	0.2366	0.2667	0.5690
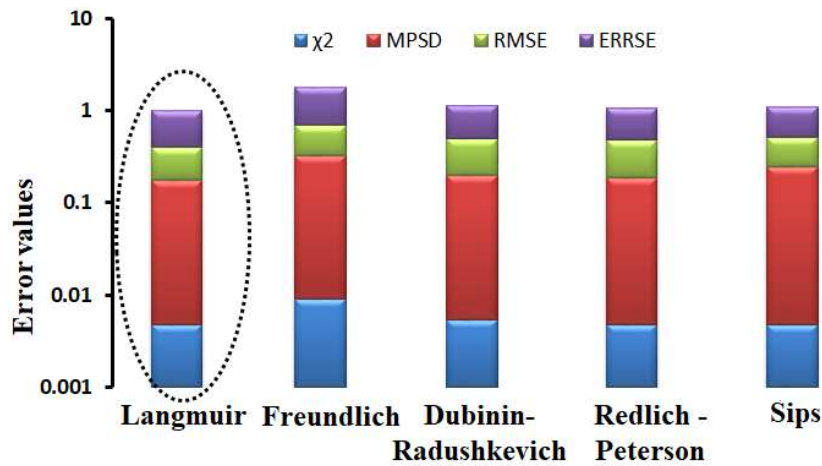
Figure 4.9. Total error values of the isotherms after non-linear fitting
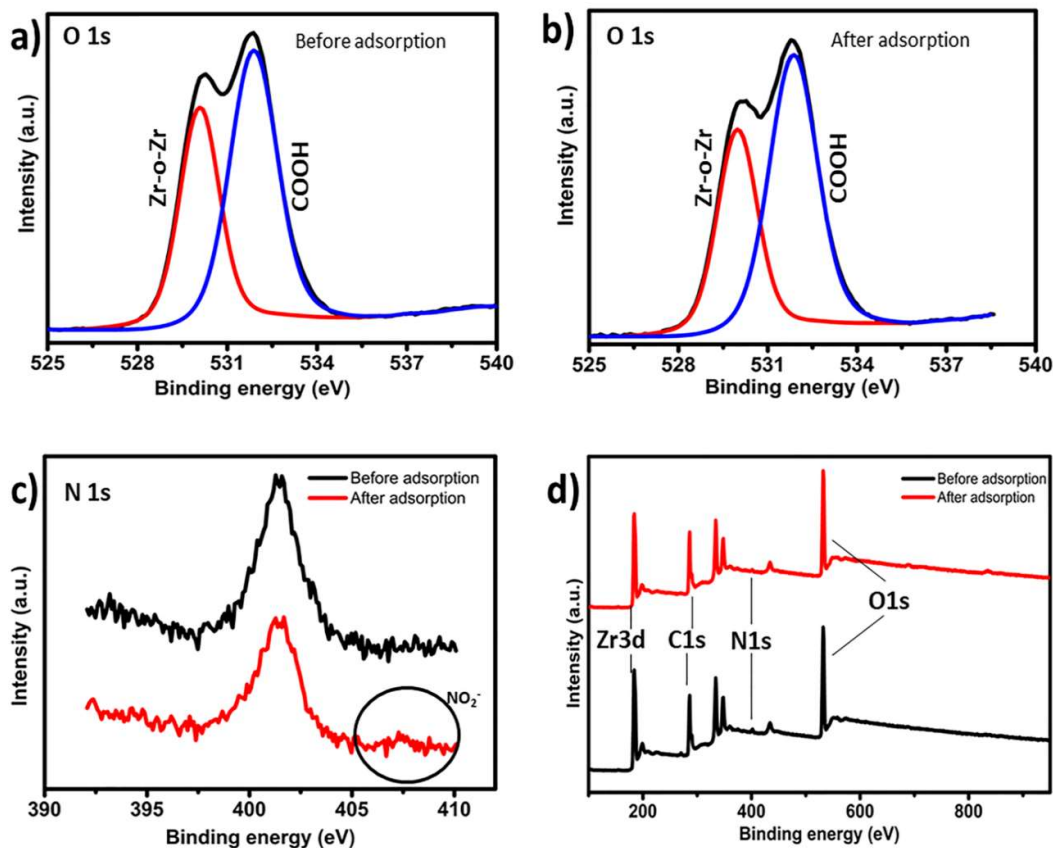
Figure 4.10. XPS analysis of MOF before and after adsorption. (a & b) O 1s, before and after adsorption high resolution spectra, (c) N 1s, high resolution spectra and (d) Survey XPS

4.4.4 Kinetic modeling of the adsorption process

To understand the kinetics process involved in the p-nitrophenol adsorption following four different models were applied to evaluate the experimental data: (1) Pseudo-first-order kinetics. (2) Pseudo-second-order kinetics, (3) Elovich model, and (4) Weber-Moris model. The model parameters were calculated by the nonlinear method using Microsoft excel, solver and coefficient of determination was used to find the best fitting model for kinetics. All the model parameters are listed in the Table 6. The experimental results (Figure 4.11) indicated that, the adsorption rate was very fast and within few minutes ($\approx$ 10 min) adsorption equilibrium was reached.

Table 4.6. List of kinetic models.

	Kinetic model	Expression		Reference
1	Pseudo first order kinetics	$q = q_e(1 - e^{-k_1 t})$	k_1-Rate of adsorption (min-1)	(Kumar, 2006)
2	Pseudo second order kinetics	$q = \dfrac{k_2 q_e^2 t}{1 + k_2 q_e t}$	k_2- Rate of adsorption (g/mg.min)	(Kumar, 2006)
3	Elovich model	$q = \left(\dfrac{1}{\beta}\right)\ln(1 + \alpha\beta t)$	α- Initial sorption rate(mg/g.min) β- related to the extent of surface coverage and activation energy for chemisorption (g/mg)	(Tan and Hameed, 2017)
4	Weber- moris model	$q = k_{id}\sqrt{t} + B$	k_{id}-rate coefficient (mg g^{-1} min$^{-1/2}$) B-thickness of the boundary layer	Weber- moris model
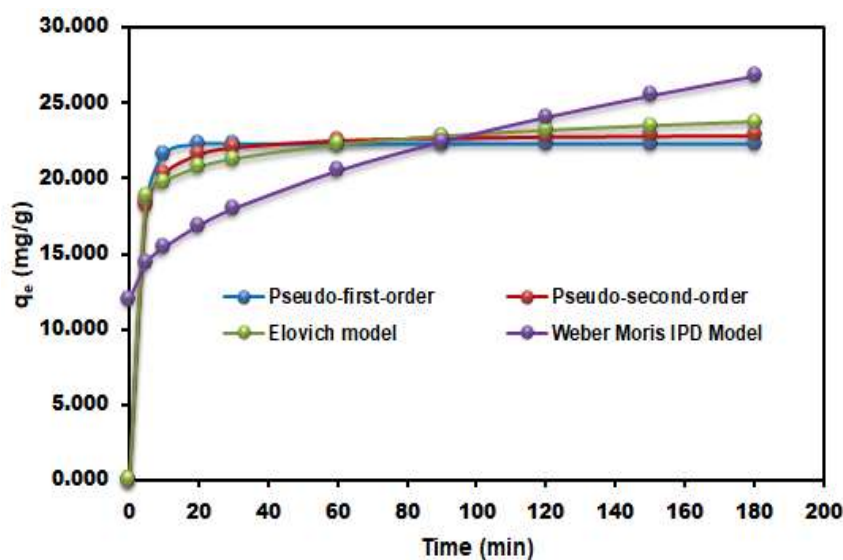
Figure 4.11. Adsorption kinetics plots of Pseudo-first/second-order, Elovich model and Weber-Morris model for p-nitrophenol adsorption

Table 4.7. Kinetics parameters and coefficient of variation from experimental result.

Kinetic Model	Parameters	Experimental results
1. Pseudo first order kinetics	q_e(calculated) (mg g^{-1})	22.3
	K_1(min^{-1})	0.3512
	R^2	0.9968
2. Pseudo-second order kinetic model	q_e(calculated) (mg g^{-1})	23.04
	K_2 (g mg^{-1} min^{-1})	0.0332
	R^2	0.9987
3. Elovich model	ß	0.734
	α	280473
	R^2	0.9997
4. Inter particle diffusion model	K_{id} (mg g^{-1}min$^{-0.5}$)	1.108
	Intercept B	11.953
	R^2	0.9523

q_e experimentally determined = 24.56 (mg g^{-1}). Test conditions; C_o=20 mg L^{-1}, pH 7, T=25°C.

From the experimental results the calculated q_e values are not consistent with the experimental q_e values, out of the four models only Pseudo second-order model was able to give nearest calculated q_e values to that of the experimental value (Table 4.7). The R^2 value of the intraparticle diffusion model was less, suggesting pore diffusion is not the rate-determining step. Both Pseudo second-order model and Elovich model fitted well with the experimental data indicating chemisorption on heterogeneous surface adsorption.

4.4.5 Mechanism of adsorption

From the experimental results, probable mechanism of adsorption has been deduced. The XPS analysis confirms the presence of similar chemical environment in the MOF before and after the adsorption. This shows there may not be an effectual chemical interaction between adsorbent and adsorbate. Instead, the following kind of mechanisms is expected (Figure 4.13).

Carboxylic groups and aromatic ring of the p-nitrophenol forms surface complexes by donor-acceptor interactions. Where carbonyl group acts as donor and aromatic rings of p-nitrophenol acts as an acceptor.

· The molecular size of p-nitrophenol is found to be 0.66 nm×0.44 nm and pore size of the synthesised MOF calculated from micropore method was 0.60 nm (Figure 10), so it is difficult for p-nitrophenol molecule to enter inside the pores of the MOF (Huang et al. 2009; Haydar et al. 2003). But at neutral pH (pKa= 7.15 at 298 K) p-nitrophenol molecules are ionized and possess a negative charge, whereas, MOF was synthesized in the presence of an acid hence, surface is positively charged. This helps in drawing p-nitrophenol molecules towards MOF resulting an assemblage of p-nitrophenol molecules in the cavities formed by the structural defects due to the presence of trifunctional ligand (H₃tnb) at the surface of the MOF.
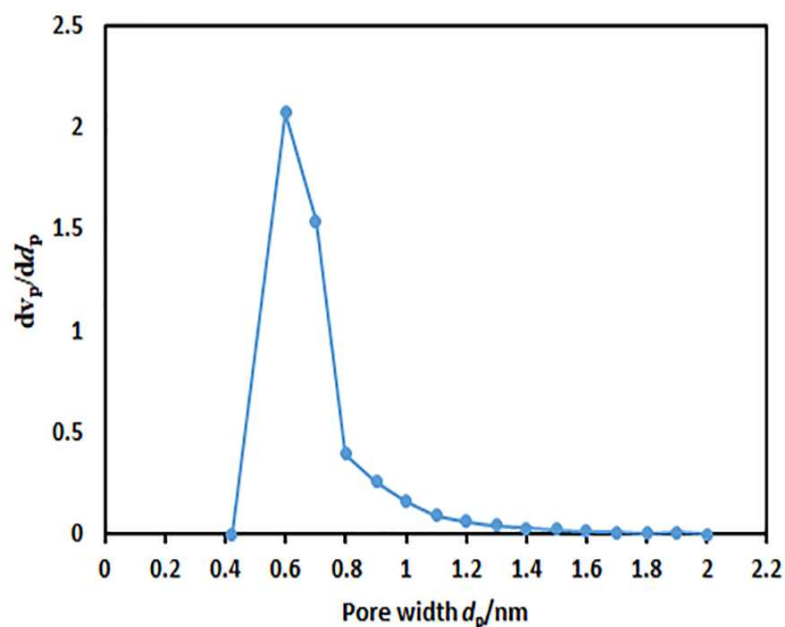
Figure 4.12. Pore volume distribution of UiO-66 MOF-2 calculated by MP method.
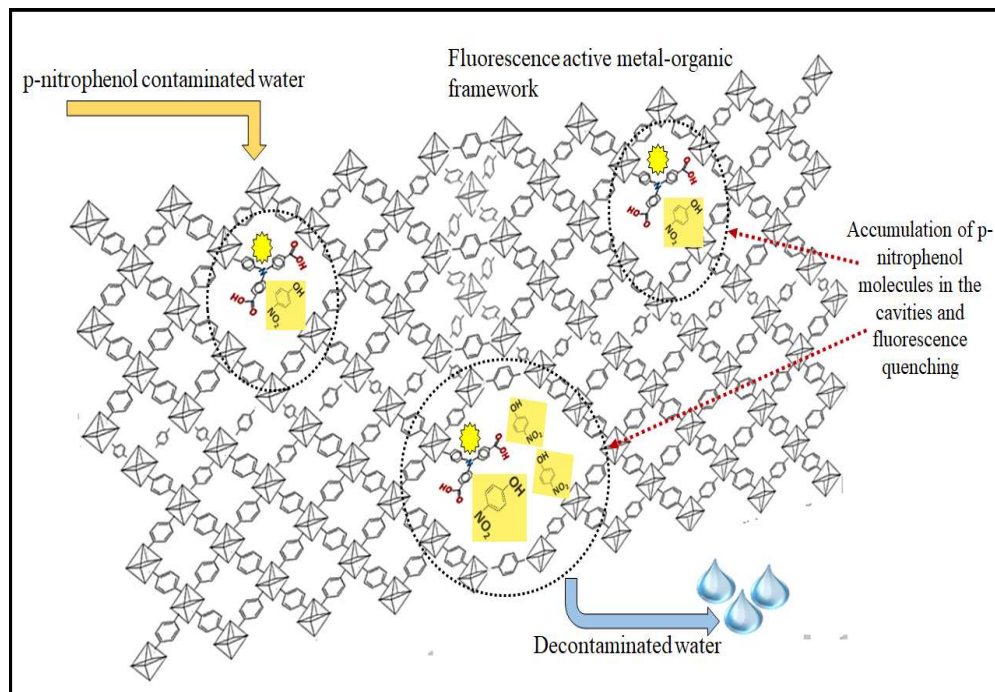
Figure 4.13. Depiction of plausible mechanism of adsorption and fluorescence quenching.

4.4.6 Real-life application of fluorescence detection and adsorption

To evaluate the efficiency of fluorescence quenching and adsorption of p-nitrophenol in real-life situations, experiments are conducted with locally available river water (Gurupura river, Dakshina Kannda, Karnataka, India). The concentration of p-nitrophenol in the water collected from the river was found to be below the detection limit (BDL), hence, p-nitrophenol was spiked in the river water at a concentration of 1000 mg L^{-1} and then used. The river sample was initially analysed for usual water quality parameters as described in table 4.8.

Batch and column adsorption trials were conducted on the p-nitrophenol solution spiked in the river water sample. For a batch adsorption study 100 mL of 100 mg L^{-1} p-nitrophenol solution was taken and 100 mg of adsorbent was added. Mixture was shaken on an orbital shaker to reach the equilibrium. Initial and final concentrations were measured by HPLC by diluting the sample 20x times (figure 4.14, HPLC

calibration graph). The amount of p-nitrophenol adsorbed was determined by equation (1). From HPLC analysis the final concentration was found to be 2.2 mg L^{-1}. This corresponds to the actual final concentration of 44 mg L^{-1}. Therefore, from equation (4.1) the amount of adsorption at equilibrium is 56 mg g^{-1}.

Table 4.8. Analysis result of the river water

Parameter	Result	Parameter	Result
pH	6.8	Silica as SiO2, ppm	8.94
Turbidity, NTU	24.4	Phosphates as PO4 ,ppm	BDL
M-alkalinity as CaCO3, ppm	22	Total Iron as Fe, ppm	1.23
Total hardness as CaCO3, ppm	84.71	Sulphates as SO4 , ppm	68.6
Calcium hardness as CaCO3, ppm	25.14	Total Solids, ppm	458
Magnesium hardness as CaCO3, ppm	59.57	Total Dissolved Solids, ppm	434
Chloride as Cl , ppm	93	Suspended Solids, ppm	24
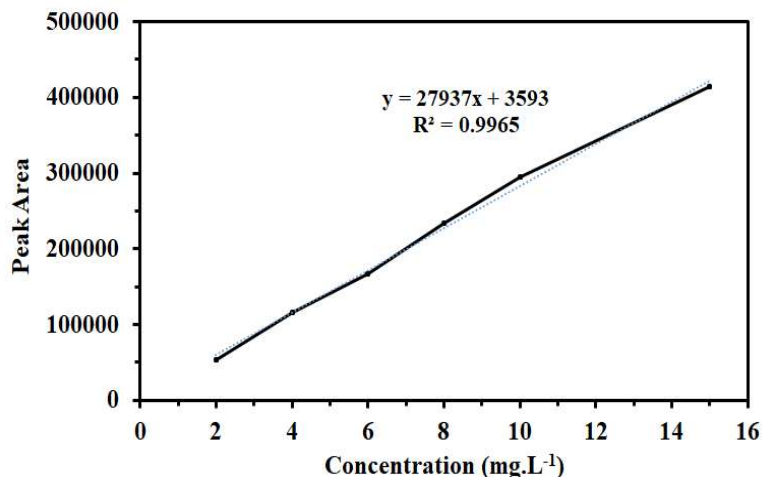
Figure 4.14. HPLC calibration curve of p-nitrophenol solution

Similarly, the column adsorption capacity was also calculated (El-Mehalmey et al. 2018). For the purpose of column adsorption studies, 100 mg of MOF was mixed with 5 g of clean and dry sand and then loaded on the column. 10 mL of 1000 mg L^{-1} of the p-nitrophenol solution prepared by using river water was passed through the column at a flow rate of 1 mL min^{-1}. The eluent was analyzed for the p-nitrophenol content by

HPLC by making 50x dilution. Exact trials were conducted on a column without the MOF content to quantify the uptake of p-nitrophenol by sand and it was found to be negligible.

From the HPLC measurements, the concentration of p-nitrophenol in the eluent was 11.4 mg L^{-1}, corresponds to the concentration of 555 mg L^{-1} in the eluent. The amount adsorbed was 455 mg.L^{-1} (4.55 mg in 10 mL) of p-nitrophenol. The column capacity was (4.55/100) *100 = 4.55 %, therefore the column can adsorb 45.5 mg of p-nitrophenol per gram of adsorbent.

The adsorptive and fluorescence quenching property of the MOF was also utilized in real-time applications. The p-nitrophenol solution prepared from the river water was used in simulating the application study. A column was prepared as before and 10 ml of the 1000 mg L^{-1} of the spike solution is passed through the column and each 0.5 mL of solution was collected separately in a vial for fluorescence study and named serially from 1 to 20.

The graph of decrease in fluorescence intensity with the addition of p-nitrophenol constructed earlier was used for the estimation of p-nitrophenol content in the eluent. The graph obtained was not linear hence, exponential fitting was done by using Microsoft excel to obtain the non-linear equation for the calculation purpose and the regression coefficient value is 0.9974 (figure 4.15 (b)), which is in good agreement with the fitting. During the course of column adsorption, fluorescence quenching was not observed until vial number twelve containing eluent. Thereafter from vial 14th complete quenching was observed, hence the vials 12th to 14th were chosen and fluorescence measurements were conducted exactly as given in section 3.2. and graph obtain represented in the below figure 4.15 (a).

From the non-linear equation the concentration of the p-nitrophenol in the 13th vial was calculated (relative intensity, y = 227.6) as below.

$$y = 497.04e^{-32.46} \quad \text{(From graph)}$$

$$since \; y = 227.6, \quad 227.6 = 497.04e^{-32.46}$$

Divide both side by 497.04, $\quad \frac{227.6}{497.04} = e^{32.46x}$
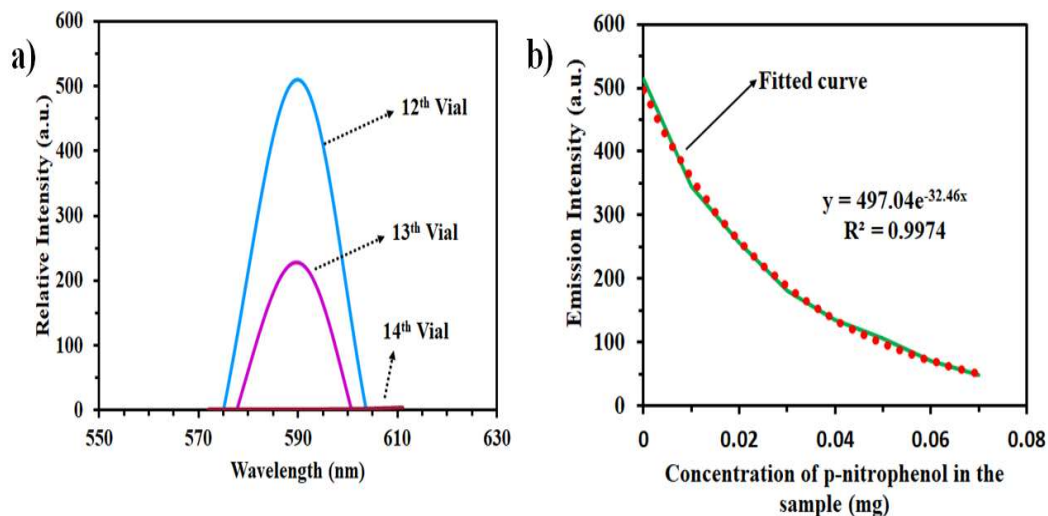
Figure 4.15. a) Decrease in fluorescence intensity after column adsorption. b) Graph of emission intensity against p-nitrophenol concentration with exponential fitting.

Taking Natural logarithm on both sides, $\quad \ln\left(\frac{227.6}{497.04}\right) = \ln(e^{-32.46x})$

$$\ln(0.4579) = -32.46x$$

$$-0.7811 = -32.46x$$

$$x = \frac{-0.7811}{-32.46}$$

$$x = 0.0240$$

Therefore, the concentration of the 13th vial is 0.0240 mg of p-nitrophenol in 0.1mL or 240 mg L^{-1}. The same solution was also tested in HPLC for p-nitrophenol content by diluting 20 times, and the result was 11.4 mg L^{-1} corresponds to 228 mg L^{-1} of final concentration. The difference between both methods was 5.2% indicates that fluorescence quenching can also be used for the detection of p-nitrophenol efficiently. Based on the experimental study, we propose the industrial application of the present work for the simultaneous use of this fluorescence active MOF for adsorption and detection of p-nitrophenol (figure 4.16). Easy detection of p-nitrophenol in the treated

water system by fluorescence quenching can be made instrumental, once detected the instruments send the signal to the control system to switch over the column automatically. This helps to run the treatment system continuously and efficiently without any retreatment.
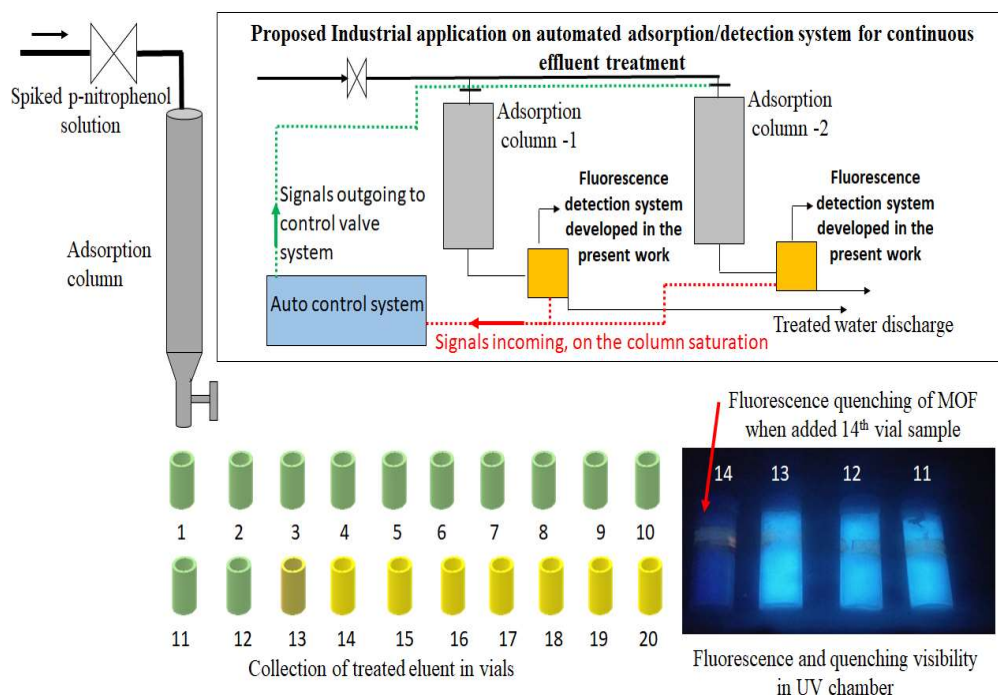
Figure 4.16. Real life column adsorption studies and proposed industrial application of the present work.

4.5 ADSORBENT REUSABILITY STUDIES

Regeneration and recycling performances of the adsorbent were examined to understand its suitability for its practical application. After adsorption and fluorescence quenching trails, 100 mg of adsorbent was treated with 10 mL of 2% Na_2CO_3 solution for 30 min. then washed with water and decanted, to this 0.1 N HCl was added and stirred for 10 min, filtered and washed with water dried in an oven at 60 °C for overnight and then reused for adsorption and quenching studies. Regeneration experiments were repeated four times (Figure 4.17) and observed that, during each cycle both the

adsorbing ability and the fluorescence property decrees gradually. This effect is attributed to the disintegration of framework structure and drifting off of the loosely bound fluorescence active ligand from the framework.
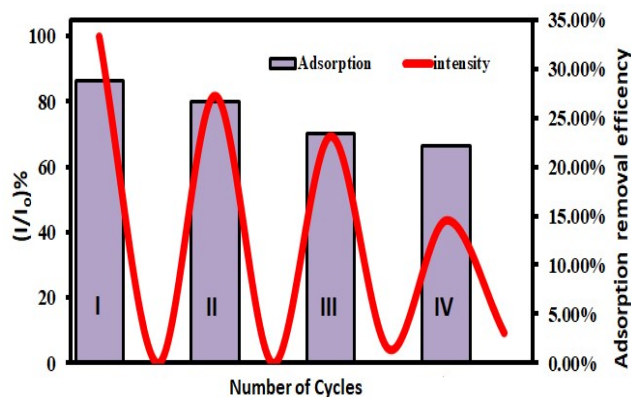
Figure 4.17. Regeneration and recycling studies of the absorbent

4.6 CONCLUSIONS

A smart and stable zirconium-based UiO-66 type metal-organic framework was successfully synthesized from mixed ligand strategy. The obtained MOF showed photoluminescence property, which was utilized for simultaneous detection and adsorptive removal of p-nitrophenol from the aqueous solution. The MOF was able to detect as low as 34.2 μM concentration of the analyte in aqueous solution at neutral pH and was able to remove rapidly (adsorption equilibrium in 10 min) p-nitrophenol from an aqueous solution. From the absorption isotherm studies, it was inferred that the adsorption obeys Langmuir isotherm and the monolayer capacity of adsorption was 62 mg.g^{-1}. The adsorption kinetic studies reveal that the mechanism follows chemisorption on the heterogeneous surface. We believe this kind of dual application property can be used effectively in effluent monitoring and treatment systems. For example, the concentration of p-nitrophenol in treated water can be detected instantaneously when the adsorption process reaches its maximum capacity and immediate switchover can save time and energy of the retreatment processes.

CHAPTER 5

CONCLUSIONS

Abstract: This chapter is the compilation of the results obtained from preceding chapters, and draws concluding remarks and future overview of the research.

5.1 SUMMARY OF THE RESEARCH WORK

In the present work, we synthesised free carboxylic acid functionalised zirconium based metal-organic framework using hydrothermal method and a fluorescence active zirconium metal-organic framework by mixed ligand strategy using solvothermal method.

- Modulated synthesis technique was utilised for the green route synthesis of free carboxylic acid functionalised metal-organic framework by hydrothermal method using acetic acid as a modulator.
- Solubility, concentration of the modulator and optimum reaction temperature played a significance role in the formation of framework during hydrothermal synthesis.
- In house synthesised ligand was utilised to synthesize a fluorescence active metal-organic framework along with Terephthalic acid.
- Powder XRD analysis was conducted to analyse the crystalline nature of the synthesised MOFs.
- FTIR analysis was carried out to confirm the functional group present in the metal- organic framework.
- TGA studies of the synthesised framework displayed the thermal stability and effect of defects on the structural integrity.
- Scanning electron microscopy and EDX analysis were performed to evaluate the surface morphology and elemental composition.
- XPS analysis was utilised to explore the nature of interaction between adsorbates and adsorbent.
- Zeta potential measurement was carried out to determine the surface charge of the MOFs.

5.1.1 Green synthesis of Zr-MOF and its application in adsorbing contaminants from aqueous solution

Synthesis of zirconium MOF by hydrothermal method using zirconium nitrate as starting material was reported earlier (Hu et al. 2015). But the reports on using zirconium chloride for the synthesis were rare and with poor reproducibility. Based on the literature, use of water soluble modulator such acetic acid influences the framework formation by altering the crystallization. The temperature also affects the MOF formation by facilitating the reaction pathway to produce more thermodynamically stable product rather than kinetically stable one. In addition, the concentration of zirconium ions further governs the crystal phase formation. As the number of metal ions increases so is the zirconium octa core nodes with BETC and acetic acid ligands. This leads more number of nuclei formation, later increases in temperature causes the replacement of acetic acid ligand with corresponding BETC ligands (Figure 5.1). The obtained MOF was analysed by various techniques to confirm the structural and functional features.

This anionic functionalised UiO-66 (COOH)$_2$ MOF was utilised in the adsorptive removal of methylene blue dye and heavy metal ions such as lead and cadmium from aqueous solution (Figure 5.2). Initial screening studies confirmed the high affinity of anionic MOF towards cationic dye at neutral pH. Hence, optimization of pH and dosage studies were conducted with respect to cationic MB dye. Later, at these optimised condition was utilised to evaluate the effect of contact time and effect of adsorbates (MB, Pb and Cd) initial concentration on adsorption. Contact time studies exhibited the higher dye adsorption at initial stages, which is due to ionic interaction between MOF and dye. When it was compared the individual and multiple adsorption trends, a competitive interaction between adsorbates to adsorb was revealed. Due to this competitive phenomenon individual adsorption of the adsorbates was always greater than its adsorption from multi solute system. Size of the hydrated metal ions control the adsorption by diffusion process. Lead ions being smaller than cadmium ion and affinity of carboxylic acid towards lead made them

to adsorb more favourably then cadmium. Presence of metal ions does not affect the MB dye adsorption because as it was adsorbed by more dominant electrostatic interaction. Overall the order selectivity of the MOF adsorbent for adsorbates is MB dye > Lead > Cadmium.
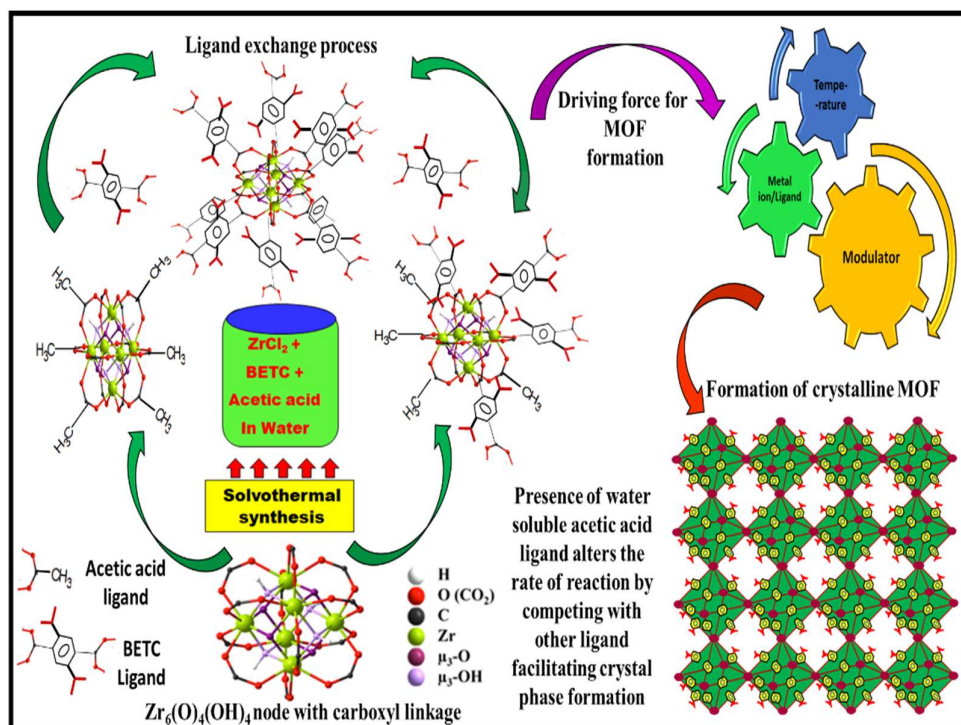
Figure 5.1. Representation of UiO-66 $(COOH)_2$ formation by modulated synthesis

As the number of solute molecules increases, the adsorption also increases due to decrease in mass transfer resistance. But as the specific sites responsible for adsorption decreases because of fixed adsorbent dosage, the increases in adsorbate concentration does not have prominent effect on adsorption. The same effect has been observed in case of MB dye adsorption causing steep decrease in adsorption as the adsorbate concentration increases. Since the affinity of MOF adsorbent towards metal ions was not high, causing gradual decreases in adsorption as the adsorbate concentration increases. Adsorption isotherm and kinetics studies were conducted to explore the mechanism behind the adsorbate-adsorbate interactions.
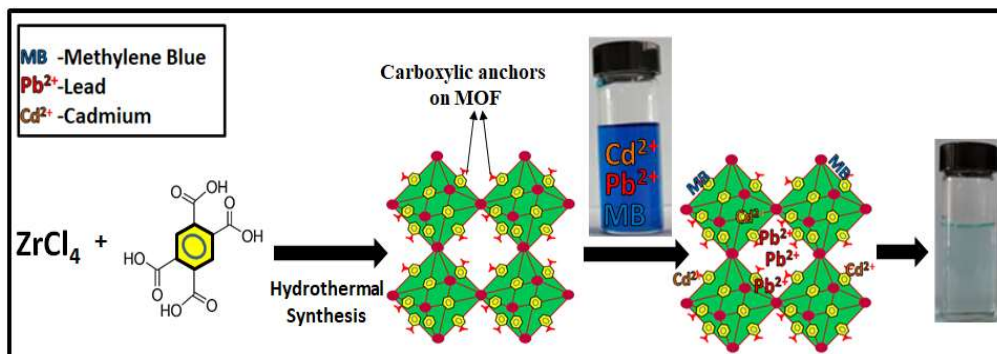
Figure 5.2 Application of UiO-66 (COOH)$_2$ for the removal of MB and heavy metal ions

5.1.2 Synthesis and application of fluorescence active zirconium MOF for nitrophenol detection and adsorption from water

Smart adsorbents which can perform dual functions are of great interest to scientific community. These adsorbents have huge benefits in terms of cost and time in environment remediation operation. Keeping in view of the above requirement a florescence MOF adsorbent was prepared by using in-house synthesised fluorescence active trifunctional carboxylic ligand, H$_3$ntb (4,4',4''-Nitrilotrisbenzoic acid) and BDC for the detection and adsorption of p-nitrophenol (Figure 5.3). The trifunctional ligand when used alone, was not able form MOF and it was confirmed by PXRD analysis. This might be due to steric constrains. Hence, mixed ligand strategy was applied. Both BDC and H$_3$ntb were used in different proportions to synthesis UiO-66 type zirconium MOFs. The obtained MOFs were analysed by PXRD, which confirms the formation UiO-66 isostructural framework. Further the MOFs were analysed by FTIR, BET surface area and TGA techniques for the functional and structural characterization. The trifunctional ligand (H$_3$ntb) ligand was not linear like BDC ligand and there is a substantial difference in structural feature between these two ligands. This has caused a distinctive bonding environment in MOF. As a result of this, the H$_3$ntb ligand is unable to build a crystal network and creates structural defects in the framework forming open pockets. These defects have negative effect on structural stability, this was confirmed by TGA studies. As the proportion of the concentration of H$_3$ntb

ligand increases during synthesis, the resulted MOF was disintegrated more at the same temperature compared other MOF having lesser H$_3$ntb ligand concentration. Therefore, the fluorescence active MOF, which was as stable as pristine UiO-66, chosen for fluorescence quenching and adsorption studies. The fluorescence quenching studies confirmed the superior quenching ability of p-nitrophenol. The Stern-Volmer plot disclosed the process of fluorescence quenching as sphere of action mechanism. The adsorption isotherm studies were conducted at neutral pH and obeys Langmuir model with maximum adsorption capacity of p-nitrophenol 62 mg g^{-1} of adsorbent. Kinetics experiment displayed a fast nature of adsorption process, reaching equilibrium in 10 min. Regeneration studies showed recycling abilities of the MOF. In a 4 cycle study, the adsorption and fluorescence activity both decreased gradually. This effect was may be due to losing off the trifunctional ligand by MOF in the washing process.
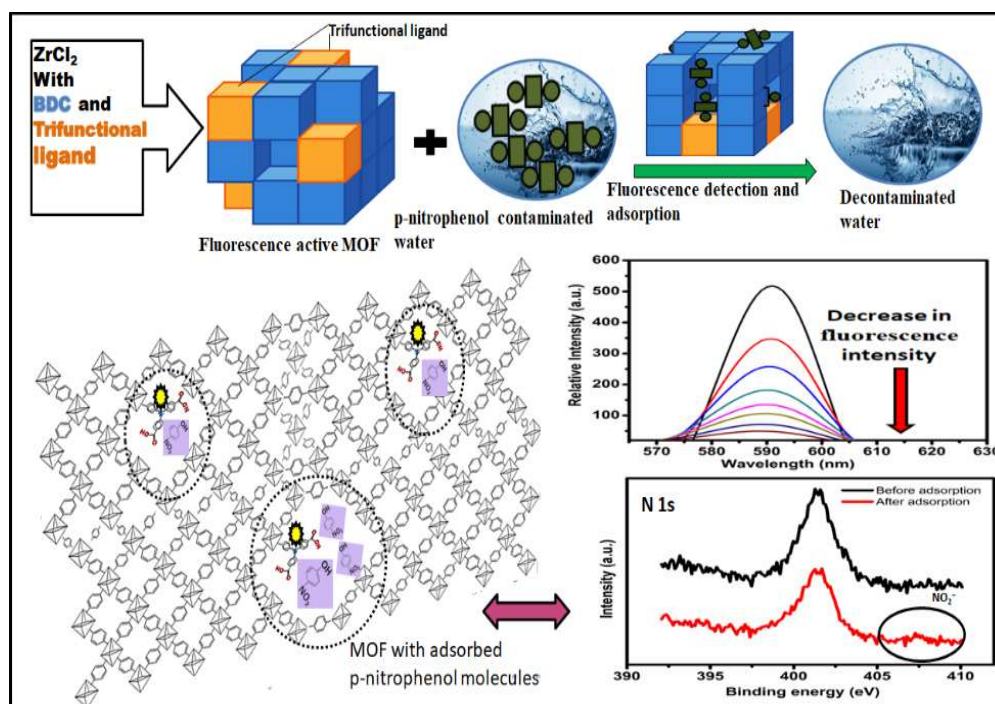
Figure 5.3. Representation of fluorescence active MOF for detection and adsorption of p-nitrophenol from aqueous solution

Further, real life application of the fluorescence active MOF was conducted using locally available river water. The results were promising and close to that of earlier performed quenching and adsorption studies indicating robustness of the MOF understudy to work in the competitive environment. In addition to this, a proposal on using this fluorescence active MOF in the remediation operation was also presented.

5.2 CONCLUSIONS

Being a most stable MOF, the zirconium based UiO-66 was researched for many applications and has become the centrepiece in the MOF domain. Along with moisture stability, tuneable porous structure and flexibility to incorporate the desired functional groups escalated the zirconium MOFs to new height in the field of material science. An environment friendly synthesis route was designed by considering easily available starting materials to build zirconium MOF with carboxylic functionalities using water as solvent. The hydrothermal synthesis of MOF using zirconium chloride was improved by using modulator and escalated temperature at 130 °C. Multi solute adsorption process was investigated and various interactions between the adsorbate and adsorbent were realised. Similarly, a smart adsorbent which adsorb and detect p-nitrophenol was developed by mixed ligand strategy and its practical applications were explored.

The following are the key findings of the proposed investigation:

- ❖ Green method for the synthesis of stable zirconium metal-organic framework having free carboxylic groups has been established.
- ❖ Smart and stable zirconium metal-organic framework is synthesised from mixed ligand strategy using in-house synthesised trifunctional ligand and benzene dicarboxylic acid ligand. The obtained MOF showed photoluminescence property imparted from its trifunctional ligand.
- ❖ The synthesised MOFs are analysed for its crystalline nature, stability, functionality, surface area and pore structure. These characterization results indicated that the strategy implied are encouraging and could be used in further developing the MOF materials.

104

❖ The zirconium metal-organic framework obtained from greener method having free functional groups used in the adsorptive removal of multi adsorbate system containing methylene blue dye, lead and cadmium metal ions. The experimental results exhibit the superior adsorbing ability of the MOF adsorbent over similar adsorbents reported.

❖ Smart MOF made of trifunctional (H_3ntb) and difunctional ligand (BDC) is utilised for the detection and adsorption of p-nitrophenol from aqueous system. The experimental results inferred that the MOF can be effectively utilised in the p-nitrophenol treatment system.

❖ The adsorbent-adsorbate systems are studied by fitting the experimental results with various adsorption isotherms. Numerous error functions are used to check the fitting ability of the adsorption isotherm equations.

5.3 FUTURE WORK

In considering the enormous advantages offered by zirconium based MOFs, further realization is required to make them suitable for practical adsorption applications. Environment friendly and low cost synthesis and fabrication of MOFs for real life applications are the main concern in the future work along with below points.

➢ Functionalization of MOF for site specific binding of hazardous material from water.

➢ Exploring the applications of MOF-composites for adsorption studies.

➢ Establishing screening methods for MOFs adsorbents to use effectively in adsorption applications.

➢ Structuring MOF adsorbents by processing of porous powders for industrial applications.

REFERENCES

Ahmed, I., Tong, M., Jun, J. W., Zhong, C.,and Jhung, S. H. (2015). "Adsorption of nitrogen-containing compounds from model fuel over sulfonated metal–organic framework: contribution of hydrogen-bonding and acid–base interactions in adsorption." *J. Phys. Chem. C*, 120(1), 407-415.

Akhbari, K., and Morsali, A. (2011). "Effect of the guest solvent molecules on preparation of different morphologies of ZnO nanomaterials from the [Zn_2 (1, 4-bdc)$_2$ (dabco)] metal-organic framework." *J. Coord. Chem.*, 64(20), 3521-3530.

Al-Asheh S, Banat F, Masad A. (2004). "Kinetics and equilibrium sorption studies of 4-nitrophenol on pyrolyzed and activated oil shale residue." *Environ. Geol.,* 45.8:1109-1117

Al-Ghouti MA, Da'ana DA. (2020). "Guidelines for the use and interpretation of adsorption isotherm models: A review." *J. Hazard. Mater.,* 393:122383

Ali, S., Zuhra, Z., Abbas, Y., Shu, Y., Ahmad, M. and Wang, Z. (2021). "Tailoring Defect Density in UiO-66 Frameworks for Enhanced Pb (II) Adsorption." *Langmuir.*, 37(46), 13602-13609.

Alvaro, M., Carbonell, E., Ferrer, B., Llabrés i Xamena, F. X., and Garcia, H. (2007). "Semiconductor Behavior of a Metal-Organic Framework (MOF)". *Chem. Eur. J,* 13(18), 5106-5112.

Ashiq, M. N., Najam-Ul-Haq, M., Amanat, T., Saba, A., Qureshi, A. M., &Nadeem, M. (2012). "Removal of methylene blue from aqueous solution using acid/base treated rice husk as an adsorbent." *Desalin. Water Treat.*, 49:376-383.

Baral, S. S., Das, N., Chaudhury, G. R., & Das, S. N. (2009). "A preliminary study on the adsorptive removal of Cr (VI) using seaweed, Hydrillaverticillata." *J. Hazard. Mater.*, 171:358-369.

Batten, S. R., Champness, N. R., Chen, X. M., Garcia-Martinez, J., Kitagawa, S., Öhrström, L., and Reedijk, J. (2013). "Terminology of metal–organic frameworks and coordination polymers (IUPAC Recommendations 2013)". *Pure Appl. Chem.*, 85(8), 1715-1724.

Boulinguiez B, Le Cloirec P, Wolbert D. (2008). "Revisiting the Determination of Langmuir Parameters□ Application to Tetrahydrothiophene Adsorption onto Activated Carbon" *Langmuir.,* 24(13):6420-6424.

Bueken, B., Van Velthoven, N., Willhammar, T., Stassin, T., Stassen, I., Keen, D. A., & De Vos, D. (2017). "Gel-based morphological design of zirconium metal–organic frameworks." *Chem. Sci.*, 8:3939-3948.

Busca G, Berardinelli S, Resini C, Arrighi L. (2008). "Technologies for the removal of phenol from fluid streams: a short review of recent developments." *J. Hazard. Mater.,* 160(2-3):265-288.

Cai, Y., Shi, D., Liu, G., Ying, Y., Cheng, Y., Wang, Y., Chen, D., Lu, J. and Zhao, D. (2020). "Polycrystalline zirconium metal-organic framework membranes supported on flexible carbon cloth for organic solvent nanofiltration." *J. Membr. Sci,* 615, 118551.

Carboni, M., Abney, C. W., Liu, S., and Lin, W. (2013). "Highly porous and stable metal–organic frameworks for uranium extraction". *Chem. Sci*, 4(6), 2396-2402.

Cavka JH, Jakobsen S, Olsbye U, Guillou N, Lamberti C, Bordiga S, Lillerud KP. (2008). "A new zirconium inorganic building brick forming metal organic frameworks with exceptional stability.*" J. Am. Chem. Soc.,* 130(42):13850-13851.

Cheetham, A. K., Férey, G., and Loiseau, T. (1999). "Open-framework inorganic materials". *Angew. Chem. Int. Ed.*, 38(22), 3268-3292.

Chen, Q., He, Q., Lv, M., Xu, Y., Yang, H., Liu, X., & Wei, F. (2015). "Selective adsorption of cationic dyes by UiO-66-NH$_2$". *Appl. Surf. Sci.*, 327, 77-85.

Chevreau, H., Devic, T., Salles, F., Maurin, G., Stock, N., and Serre, C. (2013). "Mixed-Linker Hybrid Superpolyhedra for the Production of a Series of Large-Pore Iron (III) Carboxylate Metal–Organic Frameworks". *Angew. Chem. Int. Ed.*, 52(19), 5056-5060.

Chui, S. S. Y., Lo, S. M. F., Charmant, J. P., Orpen, A. G., and Williams, I. D. (1999). "A chemically functionalizable nanoporous material [Cu_3 (TMA)$_2$ (H_2O)$_3$] n". *Science*, 283(5405), 1148-1150.

Dąbrowski A, Podkościelny P, Hubicki Z, Barczak M. (2005). "Adsorption of phenolic compounds by activated carbon— a critical review." *Chemosphere.*, 8(5):333.

Daliran, S., Ghazagh-Miri, M., Oveisi, A.R., Khajeh, M., Navalón, S., Âlvaro, M., Ghaffari-Moghaddam, M., Samareh Delarami, H. and García, H. (2020). "A pyridyltriazol functionalized zirconium metal–organic framework for selective and highly efficient adsorption of palladium." *ACS Appl. Mater. Interfaces*, 12(22), 25221-25232

Dan-Hardi, M., Serre, C., Frot, T., Rozes, L., Maurin, G., Sanchez, C., and Férey, G. (2009). "A new photoactive crystalline highly porous titanium (IV) dicarboxylate". *J. Am. Chem. Soc.*, 131(31), 10857-10859.

Das, M. C., Xu, H., Wang, Z., Srinivas, G., Zhou, W., Yue, Y. F., and Chen, B. (2011). "A Zn_4O-containing doubly interpenetrated porous metal–organic framework for photocatalytic decomposition of methyl orange". *Chem. Commun.*, 47(42), 11715-11717.

Deka, J. R., Liu, C. L., Wang, T. H., Chang, W. C., & Kao, H. M. (2014). "Synthesis of highly phosphonic acid functionalized benzene-bridged periodic mesoporous organosilicas for use as efficient dye adsorbents." *J. Hazard. Mater.*, 278:539-550.

Deng, Hexiang, Christian J. Doonan, Hiroyasu Furukawa, Ricardo B. Ferreira, John Towne, Carolyn B. Knobler, Bo Wang, and Omar M. Yaghi. (2010). "Multiple

functional groups of varying ratios in metal-organic frameworks." *Science.*, 327,5967: 846-850.

Dotto, G. L., & Pinto, L. A. A. (2011). "Adsorption of food dyes onto chitosan: Optimization process and kinetic." *Carbohydr. Polym.*, 84:231-238.

Eddaoudi, M., Moler, D. B., Li, H., Chen, B., Reineke, T. M., O'keeffe, M., and Yaghi, O. M. (2001). "Modular chemistry: secondary building units as a basis for the design of highly porous and robust metal− organic carboxylate frameworks". *Acc. Chem. Res.*, 34(4), 319-330.

El-Mehalmey, W. A., Ibrahim, A. H., Abugable, A. A., Hassan, M. H., Haikal, R. R., Karakalos, S. G., ... &Alkordi, M. H. (2018). "Metal–organic framework@ silica as a stationary phase sorbent for rapid and cost-effective removal of hexavalent chromium." *J. Mater. Chem. A.*, 6(6), 2742-2751.

Feng, D., Chung, W. C., Wei, Z., Gu, Z. Y., Jiang, H. L., Chen, Y. P., and Zhou, H. C. (2013). "Construction of ultrastable porphyrin Zr metal–organic frameworks through linker elimination". *J. Am. Chem. Soc.*, 135(45), 17105-17110.

Feng, D., Wang, K., Su, J., Liu, T. F., Park, J., Wei, Z., and Zhou, H. C. (2015). "A highly stable zeotype mesoporous zirconium metal–organic framework with ultralarge pores". *Angew. Chem. Int. Ed.*, 54(1), 149-154.

Feng, L., Wang, K. Y., Powell, J., & Zhou, H. C. (2019). "Controllable synthesis of metal-organic frameworks and their hierarchical assemblies." *Matter.,* 1(4), 801-824.

Feng, Y., Jiang, H., Li, S., Wang, J., Jing, X., Wang, Y., & Chen, M. (2013). "Metal–organic frameworks HKUST-1 for liquid-phase adsorption of uranium". *Colloids Surf. A: Physicochem. Eng. Asp.*, 431, 87-92.

Feng, Y., Yang, P., Li, Y. and Gu, J. (2020). "AgNPs-Containing Metal–Organic Frameworks for the Effective Adsorption and Immobilization of Radioactive Iodine." J. Chem. Eng. Data., 65(4), 1986-1992

Férey, G., Mellot-Draznieks, C., Serre, C., Millange, F., Dutour, J., Surblé, S., and Margiolaki, I. (2005). "A chromium terephthalate-based solid with unusually large pore volumes and surface area". *Science*, 309(5743), 2040-2042.

Foo KY, Hameed BH (2010). "Insights into the modeling of adsorption isotherm systems." Chem. Eng. J., 156(1):2-10.

Forster, P. M., Stock, N., &Cheetham, A. K. (2005). "A High-Throughput Investigation of the Role of pH, Temperature, Concentration, and Time on the Synthesis of Hybrid Inorganic–Organic Materials." *Angew. Chem. Int. Ed.*, *44*(46), 7608-7611.

Fu, Y., Sun, D., Chen, Y., Huang, R., Ding, Z., Fu, X., and Li, Z. (2012). "An Amine-Functionalized Titanium Metal–Organic Framework Photocatalyst with Visible-Light-Induced Activity for CO_2Reduction." *Angew. Chem. Int. Ed.*, 124(14), 3420-3423.

Fujishima, A., and Honda, K. (1972). "TiO_2 photoelectrochemistry and photocatalysis". *Nature*, 238(5358), 37-38.

Gable, R. W., Hoskins, B. F., and Robson, R. (1990). "A new type of interpenetration involving enmeshed independent square grid sheets. The structure of diaquabis-(4, 4′-bipyridine) zinc hexafluorosilicate". *Chem. Commun.,* (23), 1677-1678.

Ghosal PS, Gupta AK (2015). "An insight into thermodynamics of adsorptive removal of fluoride by calcined Ca–Al– (NO 3) layered double hydroxide." *RSC Adv.,* 5(128): 105889-105900.

Gomes Silva, C., Luz, I., Llabrés i Xamena, F. X., Corma, A., and García, H. (2010). "Water stable Zr–benzenedicarboxylate metal–organic frameworks as photocatalysts for hydrogen generation". *Chem. Eur. J.*, 16(36), 11133-11138.

Gupta, V. K., Mohan, D., Sharma, S., & Sharma, M. (2000). "Removal of basic dyes (rhodamine B and methylene blue) from aqueous solutions using bagasse fly ash." *Sep Sci Technol.*, 35:2097-2113.

Gürses, A., Doğar, Ç., Yalçın, M., Açıkyıldız, M., Bayrak, R., &Karaca, S. (2006). "The adsorption kinetics of the cationic dye, methylene blue, onto clay." *J. Hazard. Mater.* 131:217-228.

Gutiérrez-Serpa, A., Kundu, T., Pasán, J., Jiménez-Abizanda, A.I., Kaskel, S., Senkovska, I. and Pino, V. (2022). "Zirconium-Based Metal–Organic Framework Mixed-Matrix Membranes as Analytical Devices for the Trace Analysis of Complex Cosmetic Samples in the Assessment of Their Personal Care Product Content." *ACS Appl. Mater. Interfaces.*, 14, 3, 4510–4521.

Han, S. S., Mendoza-Cortés, J. L., and Goddard Iii, W. A. (2009). "Recent advances on simulation and theory of hydrogen storage in metal–organic frameworks and covalent organic frameworks". *Chem. Soc. Rev.*, 38(5), 1460-1476.

Haque, E., Lee, J. E., Jang, I. T., Hwang, Y. K., Chang, J. S., Jegal, J.,and Jhung, S. H. (2010). "Adsorptive removal of methyl orange from aqueous solution with metal-organic frameworks, porous chromium-benzenedicarboxylates". *J. Hazard. Mater*, 181(1), 535-542.

Hasan Z, Jhung SH (2015). "Removal of hazardous organics from water using metal-organic frameworks (MOFs): plausible mechanisms for selective adsorptions." J. *Hazard. Mater.,* 283:329-339.

Hasan, Z., Choi, E. J., and Jhung, S. H. (2013). "Adsorption of naproxen and clofibric acid over a metal–organic framework MIL-101 functionalized with acidic and basic groups." *Chem. Eng. J.*, 219, 537-544.

Hausdorf, S., Baitalow, F., Seidel, J., and Mertens, F. O. (2007). "Gaseous species as reaction tracers in the solvothermal synthesis of the zinc oxide terephthalate MOF-5". *J. Phys. Chem.,* 111(20), 4259-4266.

Haydar S, Ferro-Garcıa MA, Rivera-Utrilla J, Joly JP. (2003). "Adsorption of p-nitrophenol on an activated carbon with different oxidations." *Carbon*., 41(3):387-395.

He, J., Wang, J., Chen, Y., Zhang, J., Duan, D., Wang, Y., and Yan, Z. (2014). "A dye-sensitized Pt@ UiO-66 (Zr) metal–organic framework for visible-light photocatalytic hydrogen production". *Chem. Commun.*, 50(53), 7063-7066.

Ho, Y. S. (2006). "Review of second-order models for adsorption systems." *J. Hazard. Mater.,* 136:681-689.

Horie, K., Barón, M., Fox, R.B., He, J., Hess, M., Kahovec, J., Kitayama, T., Kubisa, P., Maréchal, E., Mormann, W. and Stepto, R.F.T. (2004). "Definitions of terms relating to reactions of polymers and to functional polymeric materials (IUPAC Recommendations 2003)." *Pure Appl. Chem*., 76(4),889-906.

Hoskins, B. F., and Robson, R. (1989). "Infinite polymeric frameworks consisting of three dimensionally linked rod-like segments". *J. Am. Chem. Soc*, 111(15), 5962-5964.

Howarth, A. J., Katz, M. J., Wang, T. C., Platero-Prats, A. E., Chapman, K. W., Hupp, J. T., and Farha, O. K. (2015). "High Efficiency Adsorption and removal of selenate and selenite from water using metal–organic frameworks". *J. Am. Chem. Soc*, 137(23), 7488-7494.

Hu Q, Zhang Z. (2019). "Application of Dubinin–Radushkevich isotherm model at the solid/solution interface: a theoretical analysis." *J. Mol. Liq.,* 277:646-648.

Hu, Z., Peng, Y., Kang, Z., Qian, Y., & Zhao, D. (2015). "A modulated hydrothermal (MHT) approach for the facile synthesis of UiO-66-type MOFs." *Inorg. Chem.*, *54*(10), 4862-4868.

Huang J, Yan C, Huang K. (2009). "Removal of p-nitrophenol by a water-compatible hypercrosslinked resin functionalized with formaldehyde carbonyl groups and XAD-4 in aqueous solution: A comparative study." *J. Colloid Interface Sci.,* 243:2-45.

Huang, L., He, M., Chen, B., & Hu, B. (2018). "Magnetic Zr-MOFs nanocomposites for rapid removal of heavy metal ions and dyes from water". *Chemosphere*, 199, 435-444.

Huang, L., He, M., Chen, B., and Hu, B. (2016). "A mercapto functionalized magnetic Zr-MOF by solvent-assisted ligand exchange for Hg^{2+} removal from water". *J. Mater. Chem. A.*, 4(14), 5159-5166.

Huang, L., He, M., Chen, B., and Hu, B. (2016). "A mercapto functionalized magnetic Zr-MOF by solvent-assisted ligand exchange for Hg^{2+} removal from water." *.J. Mater. Chem. A.*, 4(14), 5159-5166.

Jain, N., Bhargava, A., &Panwar, J. (2014). "Enhanced photocatalytic degradation of methylene blue using biologically synthesized "protein-capped" ZnO nanoparticles." *Chem. Eng. J.*, 243:549-555.

Jia, X., Zhang, B., Chen, C., Fu, X. and Huang, Q. (2021). "Immobilization of chitosan grafted carboxylic Zr-MOF to porous starch for sulfanilamide adsorption." *Carbohydr. Polym.*, 253.117305.

Juan-Alcañiz, J., Gascon, J., and Kapteijn, F. (2012). "Metal–organic frameworks as scaffolds for the encapsulation of active species: state of the art and future perspectives". *J. Mater. Chem.*, 22(20), 10102-10118.

Jun, J. W., Tong, M., Jung, B. K., Hasan, Z., Zhong, C., and Jhung, S. H. (2015). "Effect of central metal ions of analogous metal–organic frameworks on adsorption of organoarsenic compounds from water: plausible mechanism of adsorption and water purification". *Chem. Eur. J*, 21(1), 347-354.

Karim, Z., Mathew, A. P., Grahn, M., Mouzon, J., &Oksman, K. (2014). "Nanoporous membranes with cellulose nanocrystals as functional entity in chitosan: removal of dyes from water." *Carbohydr. Polym*, 112:668-676.

Katz MJ, Brown ZJ, Colón YJ, Siu PW, Scheidt KA, Snurr RQ, Hupp JT, Farha OK. (2013). "A facile synthesis of UiO-66, UiO-67 and their derivatives.*" Chem Commun.,* 49(82): 9449-9451.

Ke, F., Qiu, L. G., Yuan, Y. P., Peng, F. M., Jiang, X., Xie, A. J., and Zhu, J. F. (2011). "Thiol-functionalization of metal-organic framework by a facile coordination-based postsynthetic strategy and enhanced removal of Hg^{2+} from water". *J. Hazard. Mater*, 196, 36-43.

Khan NA, Hasan Z, Jhung SH. (2013). "Adsorptive removal of hazardous materials using metal-organic frameworks (MOFs): a review." *J. Hazard. Mater.,* 244:444-456.

Kim, M., & Cohen, S. M. (2012). "Discovery, development, and functionalization of Zr (iv)-based metal–organic frameworks." CrystEngComm., 14(12), 4096-4104.

Kitagawa, S., Kitaura, R., and Noro, S. I. (2004). "Functional porous coordination polymers". Angew. Chem. Int. Ed, 43(18), 2334-2375.

Kondo, M., Yoshitomi, T., Matsuzaka, H., Kitagawa, S., and Seki, K. (1997). "Three-Dimensional Framework with Channeling Cavities for Small Molecules: $\{[M_2(4, 4'\text{-bpy})_3 (NO3)_4]\cdot xH_2O\}$ n (M□ Co, Ni, Zn)". *Angew. Chem. Int. Ed*, 36(16), 1725-1727.

Kumar A, Kumar S, Kumar S, Gupta DV. (2007). "Adsorption of phenol and 4-nitrophenol on granular activated carbon in basal salt medium: equilibrium and kinetics." *J. Hazard. Mater.,* 147(1-2):155-166.

Kumar KV (2006). "Linear and non-linear regression analysis for the sorption kinetics of methylene blue onto activated carbon." *J. Hazard. Mater.*, 137(3):1538-1544.

Kuppler RJ, Timmons DJ, Fang QR, Li JR, Makal TA, Young MD, Yuan D, Zhao D, Zhuang W, Zhou HC. (2009). "Potential applications of metal-organic frameworks." *Coord. Chem. Rev.,* 253: 3042.

LaMer, V. K., & Dinegar, R. H. (1950). "Theory, production and mechanism of formation of monodispersed hydrosols." *J. Am. Chem. Soc.*, 72(11), 4847-4854.

Langmuir I (1916). "The constitution and fundamental properties of solids and liquids. Part I. Solids*." J. Am. Chem. Soc.*, 38(11), 2221-2295.

Lanigan, R. S., and Yamarik, T. A. (2001). "Final report on the safety assessment of EDTA, calcium disodium EDTA, diammonium EDTA, dipotassium EDTA, disodium EDTA, TEA-EDTA, tetrasodium EDTA, tripotassium EDTA, trisodium EDTA, HEDTA, and trisodium HEDTA". *Int J Toxicol*, 21, 95-142.

Lee, J., Farha, O. K., Roberts, J., Scheidt, K. A., Nguyen, S. T., and Hupp, J. T. (2009). "Metal–organic framework materials as catalysts". *Chem. Soc. Rev.*, 38(5), 1450-1459.

Li J, Wang X, Zhao G, Chen C, Chai Z, Alsaedi A, Hayat T, Wang X (2018). "Metal–organic framework-based materials: superior adsorbents for the capture of toxic and radioactive metal ions." *Chem. Soc. Rev.,* 47(7): 2322.

Li, H., Eddaoudi, M., Groy, T. L., and Yaghi, O. M. (1998). "Establishing microporosity in open metal− organic frameworks: gas sorption isotherms for Zn

(BDC) (BDC= 1, 4-benzenedicarboxylate)". *J. Am. Chem. Soc.*, 120(33), 8571-8572.

Li, H., Eddaoudi, M., O'Keeffe, M., and Yaghi, O. M. (1999). "Design and synthesis of an exceptionally stable and highly porous metal-organic framework". *Nature*, 402(6759), 276-279.

Li, J., Wu, Y. N., Li, Z., Zhang, B., Zhu, M., Hu, X., and Li, F. (2014). "Zeolitic imidazolate framework-8 with high efficiency in trace arsenate adsorption and removal from water". *J. Phys. Chem. C*, 118(47), 27382-27387.

Li, J., Wu, Y. N., Li, Z., Zhu, M., and Li, F. (2014). "Characteristics of arsenate removal from water by metal-organic frameworks (MOFs)". *Wat Sci Tech*, 70(8), 1391-1397.

Li, L., Wang, S., Chen, T., Sun, Z., Luo, J.,and Hong, M. (2012). "Solvent-Dependent Formation of Cd (II) Coordination Polymers Based on a C_2-Symmetric Tricarboxylate Linker." *Cryst. Growth Des.*,12(8), 4109-4115.

Liang, Weibin, Hubert Chevreau, Florence Ragon, Peter D. Southon, Vanessa K. Peterson, and Deanna M. D'Alessandro. (2014) "Tuning pore size in a zirconium–tricarboxylate metal–organic framework." *CrystEngComm* 16,29: 6530-6533.

Libralato, G., Ghirardini, A. V., and Avezzù, F. (2010). "Seawater ecotoxicity of monoethanolamine, diethanolamine and triethanolamine". *J. Hazard. Mater.*, 176(1), 535-539.

Lin KY, Chen SY, Jochems AP. (2015). "Zirconium-based metal organic frameworks: Highly selective adsorbents for removal of phosphate from water and urine." *Mater. Chem. Phys.,* 160: 168-176.

Liou GS, Hsiao SH, Su TH. (2005). "Synthesis, luminescence and electrochromism of aromatic poly (amine–amide) s with pendent triphenylamine moieties." *J. Mater. Chem.,* 15(18): 1812-1820.

Liu B, Yang F, Zou Y, Peng Y. (2014). "Adsorption of phenol and p-nitrophenol from aqueous solutions on metal–organic frameworks: effect of hydrogen bonding." *J. Chem. Eng. Data.,* 59(5): 1476-1482.

Liu, X., Demir, N.K., Wu, Z. and Li, K. (2015). "Highly water-stable zirconium metal–organic framework UiO-66 membranes supported on alumina hollow fibers for desalination." *J. Am. Chem. Soc*., 137(22), 6999-7002.

Long, J. R., & Yaghi, O. M. (2009). "The pervasive chemistry of metal–organic frameworks." *Chem. Soc. Rev.*, *38*(5), 1213-1214.

Lv, G., Liu, J., Xiong, Z., Zhang, Z., & Guan, Z. (2016). "Selectivity adsorptive mechanism of different nitrophenols on UiO-66 and UiO-66-NH$_2$ in aqueous solution". *J. Chem. Eng. Data*, 61(11), 3868-3876.

Lv, S. W., Liu, J. M., Ma, H., Wang, Z. H., Li, C. Y., Zhao, N., & Wang, S. (2019). "Simultaneous adsorption of methyl orange and methylene blue from aqueous solution using amino functionalized Zr-based MOFs". *Microporous Mesoporous Mater.*, 282, 179-187.

M. Kandiah, M. H. Nilsen, S. Usseglio, S.Jakobsen, U. Olsbye, M. Tilset, C. Larabi,E. A. Quadrelli, F. Bonino and K. P.Lillerud.(2010). "Synthesis and stability of tagged UiO-66 Zr-MOF." *Chem. Mater.*, 22, 6632–6640.

M. Kim, J. F. Cahill, K. A. Prather and S. M. Cohen. (2011). "Postsynthetic modification at orthogonal reactive sites on mixed, bifunctional metal–organic frameworks." *Chem. Commun*., 47,7629–7631.

M. Kim, J. F. Cahill, Y. Su, K. A. Prather and S. M. Cohen. (2012). "Evidence for stereoelectronic effects in ligand exchange reactions on Au25 nanoclusters." *Chem. Sci*., 2012, 3,126–130.

M. Kim, S. J. Garibay and S. M. Cohen. (2011). "Microwave-Assisted Cyanation of an Aryl Bromide Directly on a Metal− Organic Framework." *Inorg. Chem.*,50, 729–731.

Ma, L., Abney, C., and Lin, W. (2009). "Enantioselective catalysis with homochiral metal–organic frameworks". *Chem. Soc. Rev.*, 38(5), 1248-1256.

Mahata, P., Prabu, M., andNatarajan, S. (2008). "Role of temperature and time in the formation of infinite− M− O− M− linkages and isolated clusters in MOFs: a few illustrative examples". *InorgChem*, 47(19), 8451-8463.

Matrosov, E. I., Goryunov, E. I., Baulina, T. V., Goryunova, I. B., Petrovskii, P. V., and Nifant'ev, E. E. (2010). "First complexes of N-diphenylphosphorylureas with actinides and lanthanides: Synthesis and structure". *Dokl. Chem.* 432, 1, 136-139

Melavanki RM, Kusanur RA, Kadadevaramath JS, Kulakarni MV. (2009). "Quenching mechanisms of 5BAMC by aniline in different solvents using Stern–Volmer plots." *J. Lumin.,* 129(11): 1298-1303.

Mohammadi, A. A., Alinejad, A., Kamarehie, B., Javan, S., Ghaderpoury, A., Ahmadpour, M., & Ghaderpoori, M. (2017). "Metal-organic framework Uio-66 for adsorption of methylene blue dye from aqueous solutions". *Int. J. Environ. Sci. Technol.*, 14(9), 1959-1968.

Morris, W., Volosskiy, B., Demir, S., Gándara, F., McGrier, P. L., Furukawa, H., and Yaghi, O. M. (2012). "Synthesis, structure, and metalation of two new highly porous zirconium metal–organic frameworks". *Inorg Chem.*, 51(12), 6443-6445.

Motegi H, Yano K, Setoyama N, Matsuoka Y, Ohmura T, Usuki A. (2017). "A facile synthesis of UiO-66 systems and their hydrothermal stability." *J. Porous Mater.,* 24(5): 1327-1333.

Murray, L. J., Dincă, M., and Long, J. R. (2009). "Hydrogen storage in metal–organic frameworks". *Chem. Soc. Rev*, 38(5), 1294-1314.

Nagarkar, S. S., Desai, A. V., Samanta, P., & Ghosh, S. K. (2015). "Aqueous phase selective detection of 2, 4, 6-trinitrophenol using a fluorescent metal–organic framework with a pendant recognition site". *Dalton Trans.*, 44(34), 15175-15180.

Nagarkar, Sanjog S., Aamod V. Desai, and Sujit K. Ghosh. (2014). "A fluorescent metal–organic framework for highly selective detection of nitro explosives in the aqueous phase." *Chem. Commun.*, 50, 64: 8915-8918.

Natarajan, S., Mahata, P., &Sarma, D. (2012). "The relevance of metal organic frameworks (MOFs) in inorganic materials chemistry." *J. Chem. Sci.*, *124*(2), 339-353.

Natarajan, T. S., Bajaj, H. C., &Tayade, R. J. (2014). "Preferential adsorption behavior of methylene blue dye onto surface hydroxyl group enriched TiO2 nanotube and its photocatalytic regeneration." *J. Colloid Interface Sci.*, 433:104-114.

Nebaghe KC, El Boundati Y, Ziat K, Naji A, Rghioui L, Saidi M. (2016). "Comparison of linear and non-linear method for determination of optimum equilibrium isotherm for adsorption of copper (II) onto treated Martil sand." *Fluid Ph. Equilibria.,* 430:188-194.

Ofomaja AE, Unuabonah EI. (2011). "Adsorption kinetics of 4-nitrophenol onto a cellulosic material, mansonia wood sawdust and multistage batch adsorption process optimization." *Carbohydr. Polym.,* 83(3): 1192-1200.

Pan B, Du W, Zhang W, Zhang X, Zhang Q, Pan B, Lv L, Zhang Q, Chen J. (2007). "Improved adsorption of 4-nitrophenol onto a novel hyper-cross-linked polymer." *Environ. Sci. Technol* 41(14): 5057-5062.

Perry Iv, J. J., Perman, J. A., and Zaworotko, M. J. (2009). "Design and synthesis of metal–organic frameworks using metal–organic polyhedra as supermolecular building blocks". *Chem. Soc. Rev*, 38(5), 1400-1417.

Petit, C., and Bandosz, T. J. (2012). "Exploring the coordination chemistry of MOF–graphite oxide composites and their applications as adsorbents". *Dalton Trans.*, 41(14), 4027-4035.

Pu, S., Xu, L., Sun, L., and Du, H. (2015). "Tuning the optical properties of the zirconium–UiO-66 metal–organic framework for photocatalytic degradation of methyl orange". *Inorg. Chem. Commun.*, 52, 50-52.

Qiu, J., Feng, Y., Zhang, X., Jia, M., & Yao, J. (2017). "Acid-promoted synthesis of UiO-66 for highly selective adsorption of anionic dyes: Adsorption performance and mechanisms." *J. Colloid Interface Sci.*, 499:151-158.

Ragon, F., Campo, B., Yang, Q., Martineau, C., Wiersum, A. D., Lago, A., & Taulelle, F. (2015). "Acid-functionalized UiO-66 (Zr) MOFs and their evolution after intra-framework cross-linking: structural features and sorption properties." *J. Mater. Chem. A*, 3:3294-3309.

Railey, P., Song, Y., Liu, T. and Li, Y. (2017). "Metal organic frameworks with immobilized nanoparticles: Synthesis and applications in photocatalytic hydrogen generation and energy storage." *Mater. Res. Bull.*, 96,385-394.

Redlich OJ, Peterson DL. (1959). "A useful adsorption isotherm." *J. Phys. Chem. A.,* 63(6):1024-1024.

Reza MY, Matsushima H, Koikawa M, Nakashima M, Tokii T. (1999). "Synthesis and crystal structure of a novel hexanuclear Zr (IV) complex with 1, 10-phenanthroline including carboxylato, hydroxo, and oxo bridging." *Polyhedron.,* 12(16): 2001-2004.

Saadi R, Saadi Z, Fazaeli R, Fard NE. (2015). "Monolayer and multilayer adsorption isotherm models for sorption from aqueous media." *Korean J. Chem. Eng.,* 32(5):787-799.

Schaate, A., Roy, P., Godt, A., Lippke, J., Waltz, F., Wiebcke, M., and Behrens, P. (2011). "Modulated synthesis of Zr-based metal–organic frameworks: from nano to single crystals". *Chem. Eur. J*, 17(24), 6643-6651.

Sha, Z., and Wu, J. (2015). "Enhanced visible-light photocatalytic performance of BiOBr/UiO-66 (Zr) composite for dye degradation with the assistance of UiO-66". *RSC Adv.*, 5(49), 39592-39600.

Sips R. (1948). "On the structure of a catalyst surface." *J. Chem. Phys*., 16(5):490-495.

Sohoni, S., Sridhar, R., and Mandal, G. (1991). "The effect of grinding aids on the fine grinding of limestone, quartz and Portland cement clinker". *Powder Technol*, 67(3), 277-286.

Stock, N., & Biswas, S. (2012). "Synthesis of metal-organic frameworks (MOFs): routes to various MOF topologies, morphologies, and composites." *Chem. Rev.,* 112(2), 933-969.

Stott, W. T., Radtke, B. J., Linscombe, V. A., Mar, M. H., and Zeisel, S. H. (2004). "Evaluation of the potential of triethanolamine to alter hepatic choline levels in female B6C3F1 mice". *Toxicol. Sci*, 79(2), 242-247.

Subramanyam, B., & Das, A. (2009). "Study of the adsorption of phenol by two soils based on kinetic and isotherm modeling analyses." *Desalination.*, 249:914-921.

Sun, D. T., Peng, L., Reeder, W. S., Moosavi, S. M., Tiana, D., Britt, D. K., ...& Queen, W. L. (2018). "Rapid, Selective Heavy Metal Removal from Water by a Metal–Organic Framework/PolydopamineComposite." *ACS Cent. Sci.*, *4*(3), 349-356.

Sýkora, V., Pitter, P., Bittnerová, I., and Lederer, T. (2001). "Biodegradability of ethylenediamine-based complexing agents". *Water Res*, 35(8), 2010-2016.

Tan KL, Hameed BH. (2017). "Insight into the adsorption kinetics models for the removal of contaminants from aqueous solutions." *J Taiwan Inst Chem Eng.,* 74:25-48.

Tan, K., Nijem, N., Canepa, P., Gong, Q., Li, J., Thonhauser, T., andChabal, Y. J. (2012). "Stability and hydrolyzation of metal organic frameworks with paddle-wheel SBUs upon hydration".*Chem. Mater.,*24(16), 3153-3167.

Tanabe, K. K., and Cohen, S. M. (2011). "Post synthetic modification of metal–organic frameworks—a progress report." *Chem. Soc. Rev.*, 40(2), 498-519.

Tong, M., Liu, D., Yang, Q., Devautour-Vinot, S., Maurin, G., andZhong, C. (2013). "Influence of framework metal ions on the dye capture behavior of MIL-100 (Fe, Cr) MOF type solids." *J. Mater.Chem., A*, 1(30), 8534-8537.

Tranchemontagne, D. J., Mendoza-Cortés, J. L., O'Keeffe, M., and Yaghi, O. M. (2009). "Secondary building units, nets and bonding in the chemistry of metal–organic frameworks". *Chem. Soc. Rev.*, 38(5), 1257-1283.

Tsuruoka, T., Furukawa, S., Takashima, Y., Yoshida, K., Isoda, S., and Kitagawa, S. (2009). "Nanoporous nanorods fabricated by coordination modulation and oriented attachment growth". *Angew. Chem. Int. Ed*, 48(26), 4739-4743.

Uberoi V, Bhattacharya SK. (1997). "Toxicity and degradability of nitrophenols in anaerobic systems." *Water Environ. Res.,* 69(2): 146-156.

Vadivelan, V., & Kumar, K. V. (2005). "Equilibrium, kinetics, mechanism, and process design for the sorption of methylene blue onto rice husk." *J. Colloid Interface Sci.*, 286:90-100.

Valenzano L, Civalleri B, Chavan S, Bordiga S, Nilsen MH, Jakobsen S, Lillerud KP, Lamberti C. (2011). "Disclosing the complex structure of UiO-66 metal organic framework: a synergic combination of experiment and theory*." Chem. Mater.,* 36(1):35-41.

Vinod, V. P., &Anirudhan, T. S. (2003). "Adsorption behaviour of basic dyes on the humic acid immobilized pillared clay." *Water Air Soil Pollut.*, 150:193-217.

Vu, T. A., Le, G. H., Dao, C. D., Dang, L. Q., Nguyen, K. T., Nguyen, Q. K., and Lee, G. D. (2015). "Arsenic removal from aqueous solutions by adsorption using novel MIL-53 (Fe) as a highly efficient adsorbent".   *RSC Adv.*, 5(7), 5261-5268.

Wang, C., Liu, X., Chen, J. P., and Li, K. (2015). "Superior removal of arsenic from water with zirconium metal-organic framework UiO-66". *Sci. Rep.*, 5.

Wang, K., Gu, J., & Yin, N. (2017). "Efficient removal of Pb (II) and Cd (II) using NH2-functionalized Zr-MOFs via rapid microwave-promoted synthesis." *Ind. Eng. Chem. Res., 56*(7), 1880-1887.

Weber Jr WJ, Morris JC. (1963). "Kinetics of adsorption on carbon from solution." J. *San-it. Eng. Div. Am. Soc. Civ. Engrs.,* 89:31-59.

Wee, L. H., Bajpe, S. R., Janssens, N., Hermans, I., Houthoofd, K., Kirschhock, C. E., and Martens, J. A. (2010). "Convenient synthesis of Cu_3 (BTC) 2 encapsulated Keggin heteropolyacid nanomaterial for application in catalysis". *Chem. Commun.*, 46(43), 8186-8188.

Work, W. J., Horie, K., Hess, M., and Stepto, R. F. T. (2004). "Definition of terms related to polymer blends, composites, and multiphase polymeric materials (IUPAC Recommendations 2004)". *Pure Appl. Chem*, 76(11), 1985-2007.

Xin Y, Wang Q, Liu T, Wang L, Li J, Fang Y. (2012). "A portable and autonomous multichannel fluorescence detector for on-line and in situ explosive detection in aqueous phase*." Lab Chip.,* 12(22): 4821-4828.

Xu, W. T., Ma, L., Ke, F., Peng, F. M., Xu, G. S., Shen, Y. H., and Yuan, Y. P. (2014). "Metal–organic frameworks MIL-88A hexagonal microrods as a new photocatalyst for efficient decolorization of methylene blue dye". *Dalton Trans.*, 43(9), 3792-3798.

Yaghi, O. M., Richardson, D. A., Li, G., Davis, C. E., and Groy, T. L. (1994). "Open-framework solids with diamond-like structures prepared from clusters and metal-organic building blocks". In *MRS Proc.,* Cambridge University Press.,371,15

Yagub, M. T., Sen, T. K., Afroze, S., &Ang, H. M. (2014). "Dye and its removal from aqueous solution by adsorption: a review." *Adv. Colloid Interface Sci.*, 209:172-184.

Yakovenko, A. A., Wei, Z., Wriedt, M., Li, J. R., Halder, G. J., and Zhou, H. C. (2014). "Study of Guest Molecules in Metal–Organic Frameworks by Powder X-ray Diffraction: Analysis of Difference Envelope Density". *Cryst. Growth Des.*, 14(11), 5397-5407.

Yang, J. M. (2017). "A facile approach to fabricate an immobilized-phosphate zirconium-based metal-organic framework composite (UiO-66-P) and its activity in the adsorption and separation of organic dyes". *J. Colloid Interface Sci.*, 505, 178-185.

Yang, Q., Vaesen, S., Ragon, F., Wiersum, A. D., Wu, D., Lago, A., ...& Jobic, H. (2013). "A water stable metal–organic framework with optimal features for CO2 capture." *Angew. Chem. Int. Ed.*, *52*(39), 10316-10320.

Z. Fang, B. Bueken, D. E. De Vos and R. A. Fischer. (2015). "Defect-engineered metal–organic frameworks." *Angew. Chem., Int. Ed.*, 2015, 54, 7234–7254

Zeng, L., Guo, X., He, C., and Duan, C. (2016). "Metal–Organic Frameworks: Versatile Materials for Heterogeneous Photocatalysis". *ACS Catal.*, 6(11), 7935-7947.

Zhang A, Wang N, Zhou J, Jiang P, Liu G (2012). "Heterogeneous Fenton-like catalytic removal of p-nitrophenol in water using acid-activated fly ash." *J. Hazard. Mater.,* 201:68-73.

Zhang, C., Ai, L., and Jiang, J. (2014). "Graphene hybridized photoactive iron terephthalate with enhanced photocatalytic activity for the degradation of Rhodamine B under visible light". *Ind. Eng. Chem. Res.*, 54(1), 153-163.

Zhang, T. and, & Lin, W. (2014). "Metal–organic frameworks for artificial photosynthesis and photocatalysis". *Chem. Soc. Rev*, 43(16), 5982-5993.

Zhang, Y., Zhao, X., Huang, H., Li, Z., Liu, D., and Zhong, C. (2015). "Selective removal of transition metal ions from aqueous solution by metal–organic frameworks." *RSC Adv*., 5(88), 72107-72112.

Zhang, Yutian, Xudong Zhao, Hongliang Huang, Zhengjie Li, Dahuan Liu, and Chongli Zhong. (2015). "Selective removal of transition metal ions from aqueous solution by metal–organic frameworks." *RSC Adv*., 5(88): 72107-72112.

Zhao, J., Dong, W. W., Wu, Y. P., Wang, Y. N., Wang, C., Li, D. S., and Zhang, Q. C. (2015). "Two (3, 6)-connected porous metal–organic frameworks based on linear trinuclear $[Co_3 (COO)_6]$ and paddlewheel dinuclear $[Cu_2 (COO)_4]$ SBUs: gas adsorption, photocatalytic behaviour, and magnetic properties". *J. Mater. Chem. A*, 3(13), 6962-6969.

Zhu, X., Li, B., Yang, J., Li, Y., Zhao, W., Shi, J., and Gu, J. (2014). "Effective adsorption and enhanced removal of organophosphorus pesticides from aqueous solution by Zr-based MOFs of UiO-67". *ACS Appl. Mater. Interfaces*, 7(1), 223-231.

Zhu, Xiangyang, Bing Li, Jian Yang, Yongsheng Li, Wenru Zhao, Jianlin Shi, and Jinlou Gu. (2015). "Effective adsorption and enhanced removal of organophosphorus pesticides from aqueous solution by Zr-based MOFs of UiO-67." *ACS Appl. Mater. Interfaces*., 7(1): 223-231.

Zou D, Liu D. (2019). "Understanding the modifications and applications of highly stable porous frameworks via UiO-66." *Mater. Today Chem.,* 12:139-165.

PUBLICATIONS

1. Nimbalkar, M.N. and Bhat, B.R., (2019). "Facile green synthesis of zirconium based metal-organic framework having carboxylic anchors." Mater. Today: Proc., 9, .522-527.

2. Nimbalkar, M.N. and Bhat, B.R., (2021). "Simultaneous adsorption of methylene blue and heavy metals from water using Zr-MOF having free carboxylic group." J. Environ. Chem. Eng., 9(5), 106216.

3. Madhu N Nimbalkar and Badekai Ramachandra Bhat (2022). "Simultaneous Detection and Adsorption of p-nitrophenol from Water using Zr-metal-organic Framework"- Under Review.

4. Madhu N Nimbalkar and Badekai Ramachandra Bhat (2022). **"Current aspects of zirconium MOFs for the adsorption of various contaminants from aqueous solution"**- Communicated.

CONFERENCES

1. Madhu N Nimbalkar and Badekai Ramachandra Bhat (2018). "Facile green synthesis of zirconium based metal-organic framework having carboxylic anchors" International Conference on Green Methods for Separation Purification and Nanomaterial Synthesis, 24-25 April, Jain University, Bangalore.

2. Madhu N Nimbalkar and Badekai Ramachandra Bhat (2018). "The effect of anionic functionalised MOF on adsorptive removal of methylene blue from aqueous solution" 37thAnnualnational Conference of Indian council of chemist 12-14 December NITK, Mangalore.

3. Madhu N Nimbalkar and Badekai Ramachandra Bhat (2019)" Simultaneous removal of methylene blue and heavy metals from water using Zr-MOF having free carboxylic group". 2nd International conference on Nanoscience and Nanotechnology 29th November to 1st December, Vellore institute of technology, Vellore.

4. Madhu N Nimbalkar and Badekai Ramachandra Bhat (2021). "Simultaneous Detection and Adsorption of P-nitrophenol from Water using Zr-metal-organic Framework". Two Days International Conference on advances in chemical and environmental engineering (acee-2021) 16th-17th December, 2021 NIT-Raipur.

CURRICULUM VITAE

MADHU N NIMBALKAR

PRESENT ADDRESS:

Kasturi Nilaya

(Near Honnakatte Circle)

Honnakatte

Kulai, Mangalore-575019

Mobile: +91 9663397922,

nimbalkar.madhu@gmail.com

ACADEMIC QUALIFICATIONS

DOCTER OF PHILOSOPHY (Ph.D.) July 2015 – July 2022, Under the guidance **of Prof. Badekai Ramachandra Bhat.**, at Department of Chemistry, National Institute of Technology Karnataka, Surathkal, India. Title of the thesis – "**Synthesis and Investigation of Zirconium Metal-Organic Frameworks for Adsorption Application**".

MASTER OF SCIENCE IN INDUSTRIAL CHEMISTRY (M.Sc.), June 2005-June 2007, at Department of Industrial Chemistry, Kuvempu University, Shankaraghatta, Shimoga, Karnataka, India.

Grade secured- O (75.4%)

BACHELOR OF SCIENCE (B.Sc.) [Physics, Chemistry, Industrial Chemistry], June 2002- June 2005 at Sahyadri science college, Shimoga, Karnataka, India. Grade secured- A (72.5%)

REAEARCH EXPERIENCE

Research Scholar, Department of Chemistry, National Institute of Technology Karnataka, Surathkal, India.

- Design and synthesis functionalized zirconium metal-organic frameworks.
- Synthesis of N, O donor ligands and preparation zirconium metal-organic frameworks using in-house synthesized ligands.
- Study of the structure of the synthesized ligand and metal-organic frameworks by various analytical techniques.
- Study of the detection and adsorption of hazardous materials by using synthesized zirconium metal-organic frameworks.

PROFESSIONAL EXPERIENCE

Deputy Manager, Quality control and Technical service, July 2012 to till date
Mangalore Chemicals and Fertilizers, Mangalore.
- Managing quality control lab activities of the chemical fertilizers (Urea, Diammonium phosphate and Specialty fertilizers) and allied products such as Ammonium Bicarbonate, Sulfuric acid, Sulphonated Naphthalene formaldehyde polymer.
- Responsible for the role of the technical manager of ISO 17025:2017 accredited lab.
- Coordinating for the implementation of ISO 14001, ISO 45001 and ISO 22000 standards.
- Coordinating with marketing department for any customer queries.
- Scheduling and Ensuring the maintenance, calibration and safe working condition of lab Instruments.

Development Specialist in Cementitious Product Range, June-2010 to June 2012
Fosroc Technology Centre, Bangalore-Global R&D Centre for Fosroc Construction Chemicals group.
- To develop new cost effective Grinding aids for clinker, slag and Limestone grinding.
- Study of cement hydration using isothermal calorimeter and developing novel accelerator and retarder for cement.

- Formulation of Grinding aids as per the requirement, such as early strength enhancer for blended PPC and PSC cement.
- Formulation of different Cementitious product like Grouts, Repair products, flooring products with organic and inorganic additives to obtain desired properties like flow, strength, shrinkage, setting time etc.
- Carried out various test on cement as per the standards ASTM, BS and DIN.

Scientist in Medicinal Chemistry Division, June 2007-June 2010.

Syngene international Limited Subsidiary company of Biocon India ltd, Bangalore

- Synthesis of novel organic molecules which are potent drug precursors, as per the procedure.
- Carried out synthesis in milligram to kilogram scale and purification by using column chromatography and other techniques.
- To find new scheme for the synthesis by doing literature survey when given procedure is not working.
- Experience of using sensitive reagents and reactions.

PRESENTATIONS AT CONFERENCES

- Madhu N Nimbalkar and Badekai Ramachandra Bhat (2018). "Facile green synthesis of zirconium based metal-organic framework having carboxylic anchors" International Conference on Green Methods for Separation Purification and Nanomaterial Synthesis, 24-25 April, Jain University, Bangalore.
- Madhu N Nimbalkar and Badekai Ramachandra Bhat (2018). "The effect of anionic functionalized MOF on adsorptive removal of methylene blue from aqueous solution" 37thAnnualnational Conference of Indian council of chemist 12-14 December NITK, Mangalore.
- Madhu N Nimbalkar and Badekai Ramachandra Bhat (2019)" Simultaneous removal of methylene blue and heavy metals from water using Zr-MOF having free carboxylic group". 2nd International conference on Nanoscience and

Nanotechnology 29th November to 1st December, Vellore institute of technology, Vellore.

- Madhu N Nimbalkar and Badekai Ramachandra Bhat (2021). "Simultaneous Detection and Adsorption of P-nitrophenol from Water using Zr-metal-organic Framework". Two Days International Conference on advances in chemical and environmental engineering (acee-2021) 16th-17th December, 2021 NIT-Raipur.

RESEARCH JOURNALS

- Nimbalkar, M.N. and Bhat, B.R., (2019). "Facile green synthesis of zirconium based metal-organic framework having carboxylic anchors." Mater. Today: Proc., 9, .522-527.
- Nimbalkar, M.N. and Bhat, B.R., (2021). "Simultaneous adsorption of methylene blue and heavy metals from water using Zr-MOF having free carboxylic group." J. Environ. Chem. Eng., 9(5), 106216.
- Madhu N Nimbalkar and Badekai Ramachandra Bhat (2021). "Simultaneous Detection and Adsorption of p-nitrophenol from Water using Zr-metal-organic Framework"- Under Review.

PROFESSIONAL SKILLS

- Hands-on Experience in handling and usage of HPLC, GC, AAS, SKALAR auto analyzer, UV-visible spectrometers, Calorimeter, Particle size analyzer, Universal testing machine.
- Characterization of chemical compounds by using NMR, LC-MS, GC-MS, FTIR Spectroscopy and XRD.
- Language-Fluent in oral and written English, Kannada.
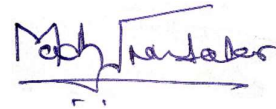- Computer-Microsoft windows, word, excel, outlook and use of internet.

PERSONAL DETAILS

Name	: Madhu N Nimbalkar
Father Name	: Nagaraja Rao
Date of Birth	: 01 April 1984
Sex	: Male
Nationality	: Indian
Marital status	: Married
Permanent address	: Tevare chatnna halli
	Gondi chatnna halli, post
	Shimoga (Dist.)-577216
	Karnataka, India.

DECLARATION

I hereby declare that the above information furnished is true to the best of my knowledge

Place: Mangalore

Date: 10 August 2022   Madhu N Nimbalkar